

Figure 11-2 Motor and load torque interaction with a rigid coupling.

$$\frac{d}{dt} \omega_m = \frac{T_J}{J_{eq}} \quad (11-4)$$

where the net torque  $T_J = T_{em} - T_L$  and the equivalent combined inertia  $J_{eq} = J_M + J_L$ .

Eq. 11-4 shows that the net torque is the quantity that causes acceleration, which in turn leads to changes in speed and position. Integrating the acceleration  $\alpha(t)$  with respect to time,

$$\text{Speed } \omega_m(t) = \omega_m(0) + \int_0^t \alpha(\tau) d\tau \quad (11-5)$$

where  $\omega_m(0)$  is the speed at  $t=0$  and  $\tau$  is a variable of integration. Further integrating  $\omega_m(t)$  in Eq. 11-5 with respect to time yields

$$\theta_m(t) = \theta_m(0) + \int_0^t \omega_m(\tau) d\tau \quad (11-6)$$

where  $\theta_m(0)$  is the position at  $t = 0$ , and  $\tau$  is again a variable of integration. Eqs. 11-4 through 11-6 indicate that torque is the fundamental variable for controlling speed and position. Eqs. 11-4 through 11-6 can be represented in a block-diagram form, as shown in Fig. 11-2b.

### 11-2-2 Power and Energy in Rotational Systems

In the rotational system shown in Fig. 11-3, if a net torque  $T$  causes the cylinder to rotate by a differential angle  $d\theta_m$ , the differential work done is

$$dW = T d\theta_m \quad (11-7)$$

If this differential rotation takes place in a differential time  $dt$ , the power can be expressed as

$$p = \frac{dW}{dt} = T \frac{d\theta_m}{dt} = T \omega_m \quad (11-8)$$

where  $\omega_m = d\theta_m / dt$  is the angular speed of rotation.

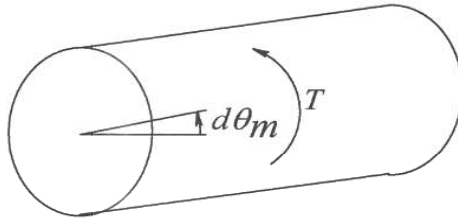


Figure 11-3 Torque, work and power.

### 11-2-3 Electrical Analogy

An analogy with electrical circuits can be very useful when analyzing mechanical systems. A commonly used analogy, though not a unique one, is to relate mechanical and electrical quantities as shown in Table 11-1.

Table 11-1 Torque-Current Analogy

Mechanical System	Electrical System
Torque (T)	Current (i)
Angular speed ( $\omega_m$ )	Voltage (v)
Angular displacement ( $\theta_m$ )	Flux linkage ( $\psi$ )
Moment of inertia (J)	Capacitance (C)

For the mechanical system shown in Fig. 11-2a, Fig. 11-4 shows the electrical analogy, where torques are represented by current sources. Inertias are represented by capacitors, from its node to a reference (ground) node, and the two capacitors representing the two inertias are combined to result in a single equivalent capacitor.

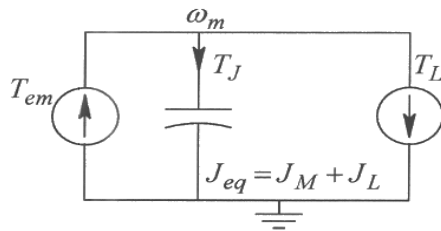


Figure 11-4 Electrical Analogy.

## 11-3 INTRODUCTION TO ELECTRIC MACHINES AND THE BASIC PRINCIPLES OF OPERATION

Electric machines, as motors, convert electrical power input into mechanical output, as shown in Fig. 11-5. Machines may be operated solely as generators, but they also enter the generating mode when slowing down (during regenerative braking) where the power flow is reversed. In this section, we will briefly look at the basic structure and the fundamental principles of the electromagnetic interactions that govern their operation.

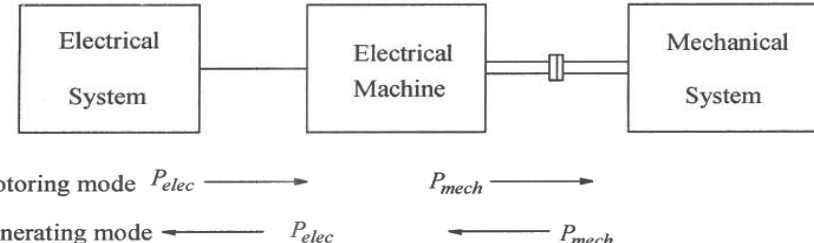


Figure 11-5 Electric machine as an energy converter.

There are two basic principles that govern electric machines' operation to convert between electric energy and mechanical work:

- 1) A force is produced on a current-carrying conductor when it is subjected to an *externally-established* magnetic field.
- 2) An emf is induced in a conductor moving in a magnetic field.

### 11-3-1 Electromagnetic Force

Consider a conductor of length  $\ell$  in Fig. 11-6a. The conductor is carrying a current  $i$  and is subjected to an *externally-established* magnetic field of a uniform flux-density  $B$  perpendicular to the conductor length. A force  $f_{em}$  is exerted on the conductor due to the electromagnetic interaction between the external magnetic field and the conductor current. The magnitude of this force  $f_{em}$  is given as

$$\underline{f_{em}} = \underbrace{B}_{[N]} \underbrace{i}_{[T]} \underbrace{\ell}_{[m]} \quad (11-9)$$

As shown in Fig. 11-6a, the direction of the force is perpendicular to the directions of both  $i$  and  $B$ . To obtain the direction of this force, we will superimpose the flux lines produced by the conductor current, which are shown in Fig. 11-6a. The flux lines add up on the right side of the conductor and subtract on the left side, as shown in Fig. 11-6b. Therefore, the force  $f_{em}$  acts *from the higher concentration of flux lines to the lower concentration*, that is, from right to left in this case.

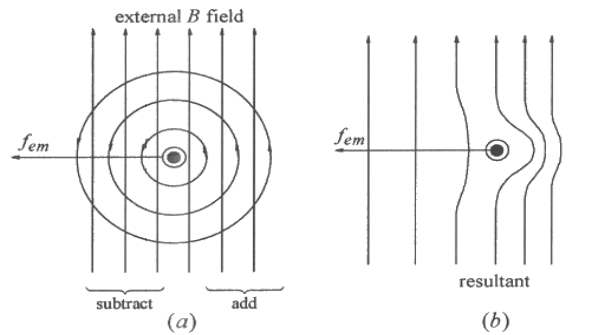


Figure 11-6 Electric force on a current-carrying conductor in a magnetic field.

### 11-3-2 Induced EMF

In Fig. 11-7a, a conductor of length  $\ell$  is moving to the right at a speed  $u$ . The  $B$ -field is uniform and is perpendicularly directed into the paper plane. The magnitude of the induced emf at any instant of time is then given by

$$\underline{e} = \frac{B}{[V]} \frac{l}{[T]} \frac{u}{[m][m/s]} \quad (11-10)$$

The polarity of the induced emf can be established as follows: due to the conductor motion, the force on a charge  $q$  (positive, or negative in the case of an electron) within the conductor can be written as

$$f_q = q(\mathbf{u} \times \mathbf{B}) \quad (11-11)$$

where the speed and the flux density are shown by bold letters to imply that these are vectors and their cross product determines the force. Since  $\mathbf{u}$  and  $\mathbf{B}$  are orthogonal to each other, as shown in Fig. 11-7b, the force on a positive charge is upward. Similarly, the force on an electron will be downwards. Thus, the upper end will have a positive potential with respect to the lower end. This induced emf across the conductor is independent of the current that would flow if a closed path were to be available (as would normally be the case). With the current flowing, the voltage across the conductor will be the induced-emf  $e(t)$  in Eq. 11-10 minus the voltage drops across the conductor resistance and inductance.

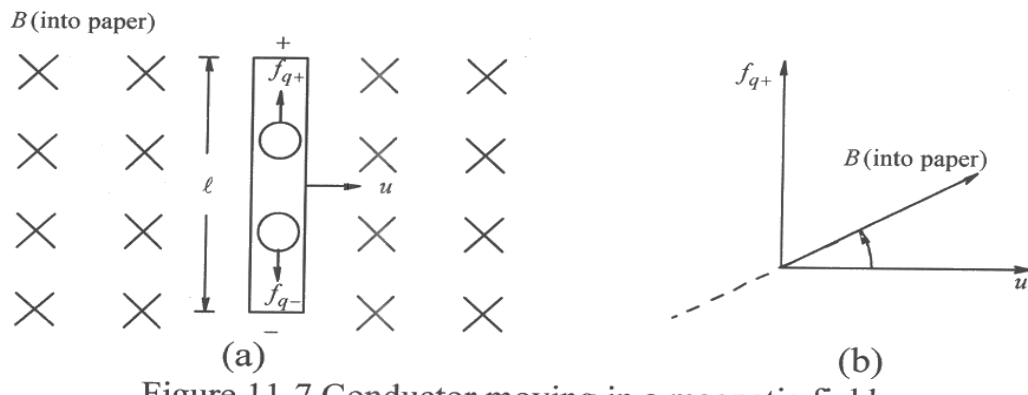


Figure 11-7 Conductor moving in a magnetic field.

### 11-3-3 Basic Structure

Based on the above basic principles, all machines have a stationary part, called the stator, and a rotating part, called the rotor, separated by an air gap, thereby allowing the rotor to rotate freely on a shaft, supported by bearings. This is shown by the cross-section of the machine in Fig. 11-8a, where the stator is firmly affixed to a foundation to prevent it from turning.

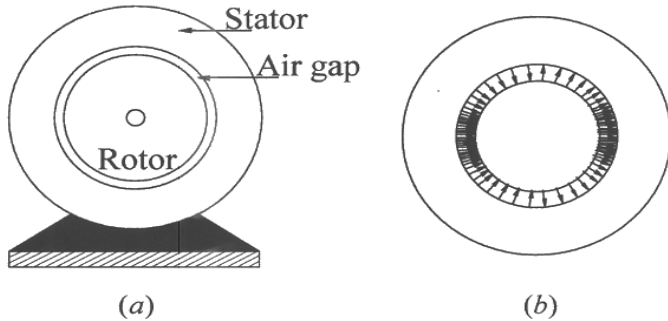


Figure 11-8 Cross-section of the machine seen from one side.

In electric machines, a magnetic field is produced either by permanent magnets or by windings that are supplied currents to produce radial flux-lines through the air gap, as shown in Fig. 11-8b. In order to require small ampere-turns to create flux lines crossing the air gap, both the rotor and the stator are made up of high permeability ferromagnetic materials and the length of the air gap is kept as small as possible. In machines with ratings under 10  $kW$  in ratings, a typical length of the air gap is about 1  $mm$ , which is shown highly exaggerated for ease of drawing.

In the next sections, we will briefly examine commonly used machines: dc, permanent-magnet ac, and induction.

#### 11-4 DC MOTORS

DC motors were widely used in the past for all types of applications, and they continue to be used in applications to control speed and position. There are two designs of dc machines: stators consisting of either permanent magnets or a field winding. The power-processing units can also be classified into two categories: switch-mode power converters that operate at a high switching frequency as discussed in the next Chapter 12, or line-commutated, thyristor converters, which are discussed later in Chapter 14. In this chapter, our focus will be on small servo-drives, which usually consist of permanent-magnet motors supplied by switch-mode power electronic converters.

##### 11-4-1 Structure of DC Machines

Fig. 11-9 shows a cut-away view of a dc motor. It shows a permanent-magnet stator, a rotor that carries a winding, a commutator, and the brushes. In dc machines, the stator establishes a uniform flux  $\phi_f$  in the air gap in the radial direction (the subscript “ $f$ ” is for field). If permanent magnets like those shown in Fig. 11-9 are used, the air gap flux density established by the stator remains constant. A field winding whose current can be varied can be used to achieve an additional degree of control over the air gap flux density.

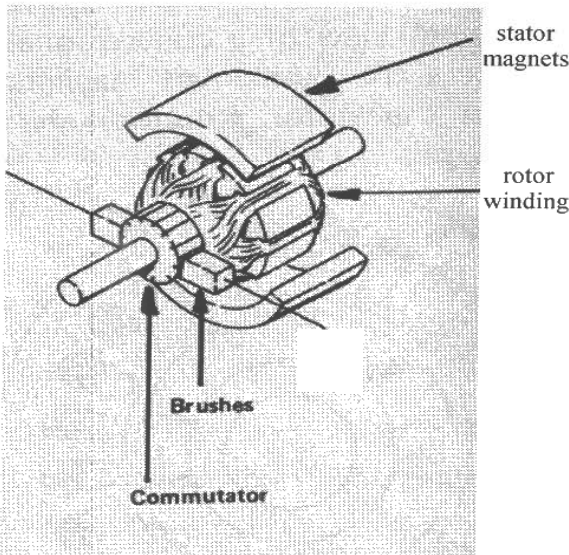


Figure 11-9 Exploded view of a dc motor; source: Engineering Handbook by Electro-Craft Corp.

As shown in Fig. 11-9, the rotor slots contain a winding, called the armature winding, which handles electrical power for conversion to (or from) mechanical power at the rotor shaft. In addition, there is a commutator affixed to the rotor. On its outer surface, the commutator contains copper segments, which are electrically insulated from each other by means of mica or plastic. The coils of the armature winding are connected to these commutator segments so that a stationary dc source can supply voltage and current to the rotating commutator by means of stationary carbon brushes which rest on top of the commutator. The wear due to the mechanical contact between the commutator and the brushes requires periodic maintenance, which is the main drawback of dc machines.

#### 11-4-2 Operating Principles of DC Machines

As Fig. 11-10 pictorially shows, the commutator and the brushes in dc machines act as a “mechanical rectifier” and convert a dc current  $i_a$  supplied by a stationary dc source into a current that changes direction in the armature coil every half revolution of the rotor.

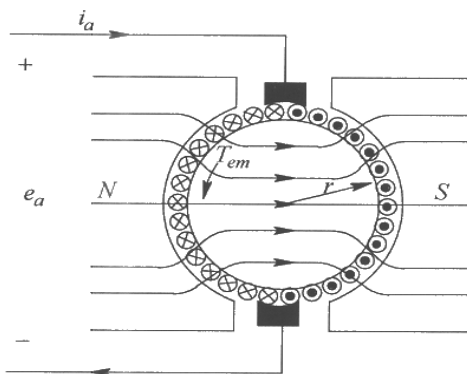


Figure 11-10 DC machine schematic representation.

All conductors under a stator pole have currents in the same direction but the current direction reverses when the conductors reach the other pole. This is needed so that the forces produced on each conductor are in the same direction and add up to yield the total torque. Similarly, all conductors under a pole have induced emfs of the same polarity, which changes in polarity every half revolution of the rotor when the conductors reach the other pole.

The above description shows that the magnitude and the direction of the electromagnetic torque depend on the armature current  $i_a$ . Therefore, in a permanent-magnet dc machine, the electromagnetic torque produced by the machine is linearly related to a machine torque-constant  $k_T$ , which is unique to a given machine and is specified in its data sheets

$$T_{em} = k_T i_a \quad (11-12)$$

Similarly, the induced emf  $e_a$  depends only on the rotational speed  $\omega_m$ , and can be related to it by a voltage-constant  $k_E$ , which is unique to a given machine and specified in its data sheets

$$e_a = k_E \omega_m \quad (11-13)$$

Equating the mechanical power ( $\omega_m T_{em}$ ) to the electrical power ( $e_a i_a$ ), the torque-constant  $k_T$  and the voltage-constant  $k_E$  are exactly the same numerically in MKS units

$$k_T = k_E \quad (11-14)$$

Reversing the Torque Direction. The direction of the armature current  $i_a$  determines the direction of currents through the conductors. Therefore, the direction of the electromagnetic torque produced by the machine also depends on the direction of  $i_a$ . This explains, how a dc machine while rotating in a forward or reverse direction can be made to go from motoring mode (where the speed and torque are in the same direction) to its generator mode (where the speed and torque are in the opposite direction) by reversing the direction of  $i_a$ .

Reversing the Direction of Rotation. Applying a reverse-polarity dc voltage to the armature terminals makes the armature current flow in the opposite direction. Therefore, the electromagnetic torque is reversed, reversing the direction of rotation and the polarity of induced emfs in conductors, which depends on the direction of rotation.

Four-Quadrant Operation. The above discussion shows that a dc machine can easily be made to operate as a motor or as a generator in forward or reverse direction of rotation.

### 11-4-3 DC-Machine Equivalent Circuit

It is convenient to discuss a dc machine in terms of its equivalent circuit of Fig. 11-11, which shows conversion between electrical and mechanical power. The armature current  $i_a$  produces the electromagnetic torque  $T_{em} (= k_T i_a)$ , represented by a dependent current-source necessary to rotate the mechanical load at a speed  $\omega_m$ . Across the armature terminals, the rotation at the speed of  $\omega_m$  induces a voltage, called the back-emf  $e_a (= k_E \omega_m)$ , represented by a dependent voltage-source.

On the electrical side, the applied voltage  $v_a$  overcomes the back-emf  $e_a$  and causes the current  $i_a$  to flow. Recognizing that there is a voltage drop across both the armature winding resistance  $R_a$  (which includes the voltage drop across the carbon brushes) and the armature winding inductance  $L_a$ , we can write the equation of the electrical side as

$$v_a = e_a + R_a i_a + L_a \frac{di_a}{dt} \quad (11-15)$$

On the mechanical side, the electromagnetic torque produced by the motor overcomes the mechanical-load torque  $T_L$  to produce acceleration:

$$\frac{d\omega_m}{dt} = \frac{1}{J_{eq}} (T_{em} - T_L) \quad (11-16)$$

where  $J_{eq}$  is the total effective value of the combined inertia of the dc machine and the mechanical load.

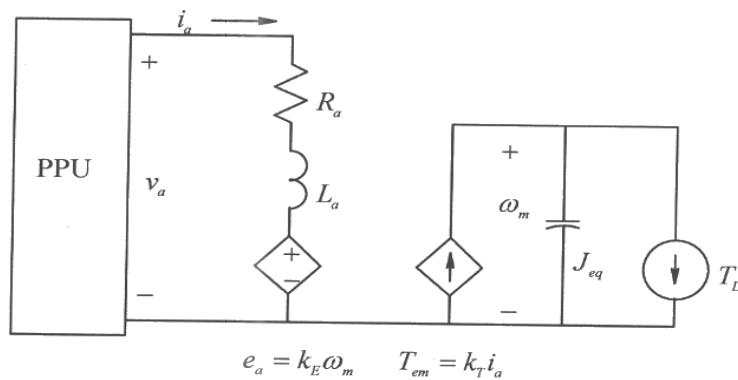


Figure 11-11 DC motor equivalent circuit.

### 11-4-4 Torque-Speed Characteristics

Note that the electric and the mechanical systems are coupled. The torque  $T_{em}$  in the mechanical system (Eq. 11-12) depends on the electrical current  $i_a$ . The back-emf  $e_a$  in the electrical system (Eq. 11-13) depends on the mechanical speed  $\omega_m$ . The electrical

power absorbed from the electrical source by the motor is converted into mechanical power and vice versa. In a dc steady state, with a voltage  $V_a$  applied to the armature terminals, and a load-torque  $T_L$  being supplied to the load, the equivalent circuit is as shown in Fig. 11-12a, where the inductance  $L_a$  (not shown) in the electrical portion and the capacitance (shown dotted) representing  $J_{eq}$  in the mechanical portion of the circuit do not play a role in dc steady state. Hence, in Fig. 11-12

$$I_a = \frac{T_{em} (= T_L)}{k_T} \quad (11-17)$$

$$\omega_m = \frac{E_a}{k_E} = \frac{V_a - R_a I_a}{k_E} = \frac{V_a - R_a (T_{em} / k_T)}{k_E} \quad (11-18)$$

Based on Eqs. 11-17 and 11-18, the steady state torque-speed characteristics for various values of  $V_a$  are plotted in Fig. 11-12b.

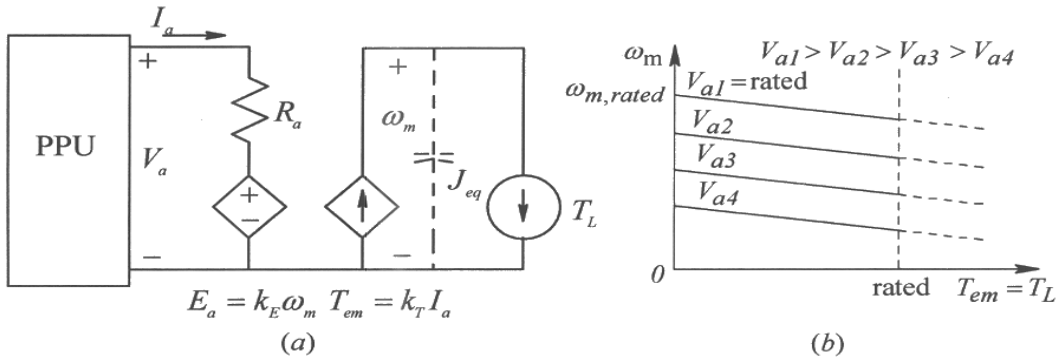


Figure 11-12 DC motor in the dc steady state.

## 11-5 PERMANENT-MAGNET AC MACHINES

We will now study an important class of ac drives, namely sinusoidal-waveform, permanent-magnet ac (PMAC) drives, which are used in applications where a high efficiency and a high power density are required in controlling the speed and position. In trade literature, they are also called "brushless dc" drives. We will examine these machines for speed and position control applications, usually in small ( $< 10 \text{ kW}$ ) power ratings, where these drives have three-phase ac stator windings and the rotor has dc excitation in the form of permanent magnets. In such drives, the stator windings of the machine are supplied by controlled currents, which require a closed-loop operation, as shown in the block diagram of Fig. 11-13. The discussion of PMAC drives also lends itself to the analysis of line-connected synchronous machines, which are used in very large ratings in the central power plants of utilities to generate electricity.

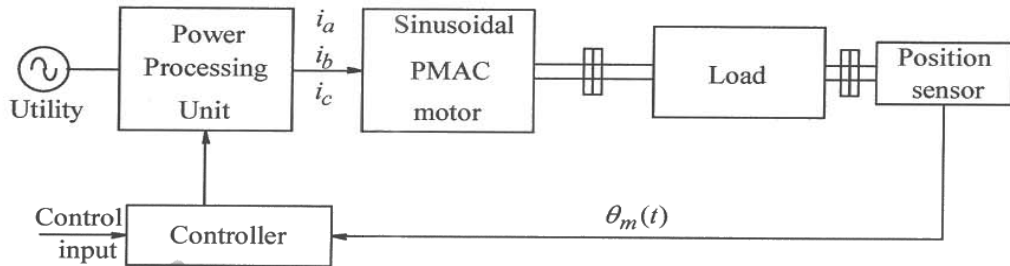


Figure 11-13 Block diagram of the closed loop operation of a PMAC drive.

### 11-5-1 The Basic Structure of Permanent-Magnet AC Machines

We will consider 2-pole machines, like the one shown schematically in Fig. 11-14a. This analysis can be generalized to  $p$ -pole machines where  $p > 2$ . The stator contains three-phase, wye-connected windings shown in the cross-section of Fig. 11-14a, each of which produce a sinusoidally-distributed flux-density distribution in the air gap, when supplied by a current.

### 11-5-2 Principle of Operation

The permanent-magnet pole pieces mounted on the rotor surface are shaped to ideally produce a sinusoidally-distributed flux density in the air gap. The rotor flux-density distribution (represented by a vector  $\vec{B}_r$ ) peaks at an angle  $\theta_m(t)$  with respect to the  $a$ -axis of phase winding  $a$ , as shown in Fig. 11-14b. As the rotor turns, the entire rotor-produced flux density distribution in the air gap rotates with it and “cuts” the stator-winding conductors and produces emf in phase windings that are sinusoidal functions of time. In the ac steady state, these voltages can be represented by phasors.

Considering phase-a as the reference in Fig. 11-14b, the induced voltage in it due to the rotor flux cutting it can be expressed as

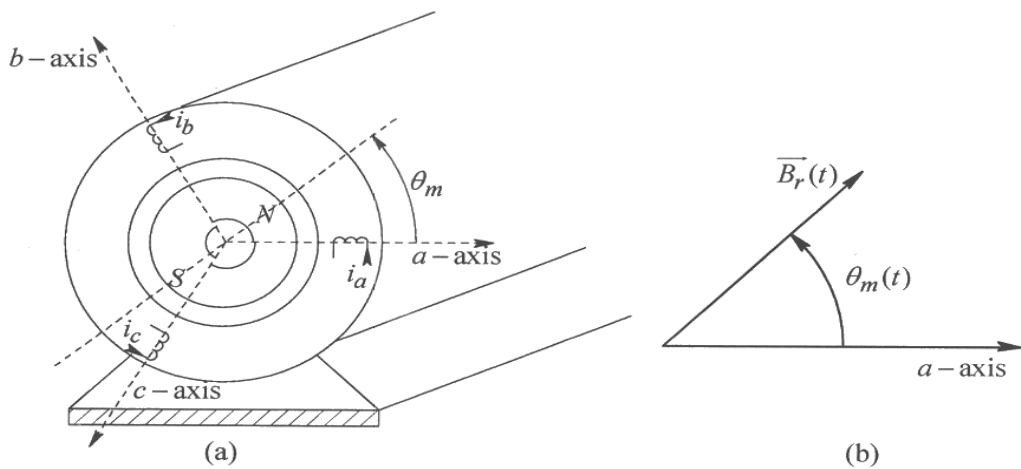


Figure 11-14 Two-pole PMAC machine.

$$\bar{E}_{ma} = E_{rms} \angle 0^0 \quad (11-19)$$

It should be noted that the induced voltage in phase-a peaks when the rotor-flux peak in Fig. 11-14 is pointing downward,  $90^\circ$  before it reaches the phase-a magnetic axis. Since the flux produced by the permanent magnets on the rotor is constant, the rms magnitude of the induced voltage in each stator phase is linearly related to the rotational speed  $\omega_m$  by a per-phase voltage-constant  $k_{E, phase}$

$$E_{rms} = k_{E, phase} \omega_m \quad (11-20)$$

An important characteristic of the machines under consideration is that they are supplied through a current-regulated power-processing unit shown in Fig. 11-13, which controls the currents  $i_a$ ,  $i_b$ , and  $i_c$  supplied to the stator at any instant of time. To optimize such that the maximum torque-per-ampere is produced, each phase current in ac steady state is controlled in phase with the induced voltage. Therefore, with the voltage expressed in Eq. 11-19, the current in ac steady state is

$$\bar{I}_a = I_{rms} \angle 0^0 \quad (11-21)$$

In ac steady state, accounting all three-phases, the input electric power, supplied by the current in opposition to the induced back-emf, equals the mechanical output power. Using Eqs. 11-19 through 11-21

$$T_{em} \omega_m = 3 \underbrace{\left( k_{E, phase} \omega_m \right)}_{E_{rms}} I_{rms} \quad (11-22)$$

The torque contribution of each phase can be written as

$$T_{em,1-phase} = \frac{T_{em}}{3} = k_{E, phase} I_{rms} \quad (11-23)$$

In Eq. 11-23, the constant that relates the rms current to the per-phase torque is the per-phase torque-constant  $k_{T, phase}$ . Therefore, similar to that in dc machines, in MKS units

$$k_{T, phase} = k_{E, phase} \quad (11-24)$$

At this point, we should note that PMAC drives constitute a class, which we will call *self-synchronous* motor drives, where the term “*self*” is added to distinguish these machines from the conventional synchronous machines. The reason for this is as follows: in PMAC drives, the stator phase currents are synchronized to the mechanical position of the rotor such that, for example, the current into phase-a, in order to be in phase with the induced-emf, peaks when the rotor-flux peak is pointing downward,  $90^\circ$  before it reaches

the phase-a magnetic axis. This explains the necessity for the rotor-position sensor, unless the rotor position is mathematically computed by sensed voltages and currents.

### 11-5-3 Mechanical System of PMAC Drives

The electromagnetic torque acts on the mechanical system connected to the rotor, and the resulting speed  $\omega_m$  can be obtained from the equation below:

$$\frac{d\omega_m}{dt} = \frac{T_{em} - T_L}{J_{eq}} \quad \Rightarrow \quad \omega_m(t) = \omega_m(0) + \frac{1}{J_{eq}} \int_0^t (T_{em} - T_L) \cdot d\tau \quad (11-25)$$

where  $J_{eq}$  is the combined motor-load inertia and  $T_L$  is the load torque, which may include friction. The rotor position  $\theta_m(t)$  is

$$\theta_m(t) = \theta_m(0) + \int_0^t \omega_m(\tau) \cdot d\tau \quad (11-26)$$

where  $\theta_m(0)$  is the rotor position at time  $t=0$ .

### 11-5-4 PMAC Machine Equivalent Circuit

Similar to a dc machine, it is convenient to discuss a PMAC machine in terms of its equivalent circuit of Fig. 11-15a, which shows conversion between electrical and mechanical power. In the ac steady state, using phasors, the current  $\bar{I}_a$  is ensured to be in phase with the phase-a induced voltage  $\bar{E}_{ma}$  by the feedback control. The phase currents produce the total electromagnetic torque  $T_{em} (= 3k_{T, \text{phase}} I_{rms})$ , represented by a dependent current-source, necessary to rotate the mechanical load at a speed  $\omega_m$ . The induced back-emf  $\bar{E}_{ma} = E_{rms} \angle 0^\circ$ , whose rms magnitude is linearly proportional to the speed of rotation  $\omega_m$ , is represented by a dependent voltage-source.

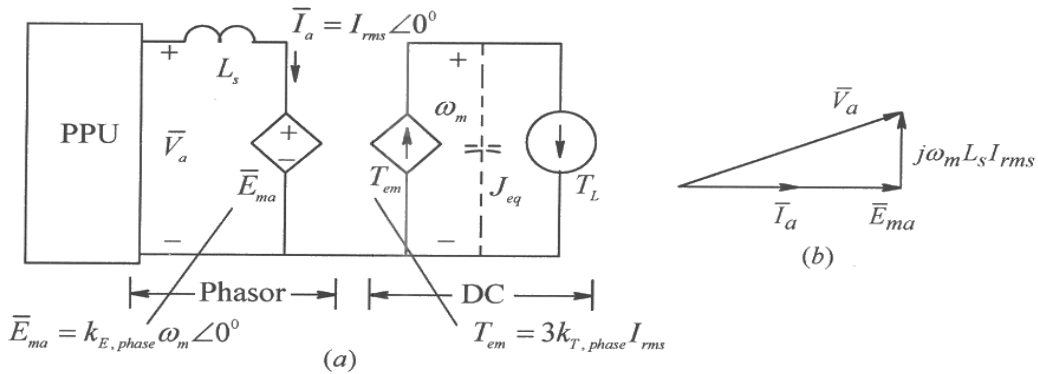


Figure 11-15 Equivalent circuit diagram and the phasor diagram of PMAC (2 pole).

On the electrical side, the applied voltage  $\bar{V}_a$  in Fig. 11-15a overcomes the back-emf  $\bar{E}_{ma}$  and causes the current  $\bar{I}_a$  to flow. The frequency of the phasors in Hz equals  $\omega_m / (2\pi)$

in a 2-pole PMAC machines. There is a voltage drop across both the per-phase stator winding resistance  $R_s$  (neglected here) and a per-phase inductance  $L_s$ , which is the sum of the leakage inductance caused by the leakage flux of the stator winding, and the effect of the combined flux produced by the currents flowing in the stator phases. On the mechanical side in Fig. 11-15a in steady state, the capacitance representing  $J_{eq}$  in the mechanical portion of the circuit is of no effect, and  $T_{em} = T_L$ .

Note that the electric and the mechanical systems are coupled. In the electrical system, the back-emf  $\bar{E}_{ma}$  magnitude (Eq. 11-20) depends on the mechanical speed  $\omega_m$ . In the mechanical system, the torque  $T_{em}$  (Eq. 11-23) depends on the magnitude of the electrical current  $\bar{I}_a$ , which depends on the load torque being demanded of the machine. The electrical power absorbed from the electrical source by the motor is converted into mechanical power and vice versa. The phasor diagram, neglecting  $R_s$ , is shown in Fig. 11-15b.

### 11-5-5 PMAC Torque-Speed Characteristics

In PMAC machines, the speed is independent of the electromagnetic torque developed by the machine, as shown in Fig. 11-16a, and depends on the frequency of voltages and currents applied to the stator phases of the machine.

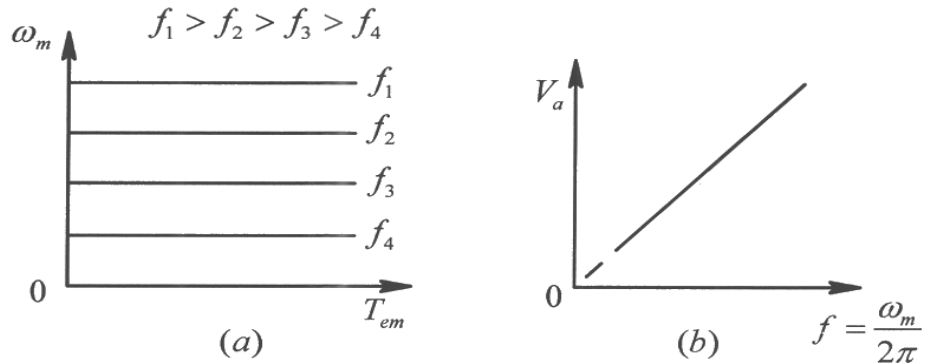


Figure 11-16 Torque-speed characteristics and the voltage versus frequency in PMAC.

In the per-phase equivalent circuit of Fig. 11-15a and the phasor diagram of Fig. 11-15b, the back-emf is proportional to the speed  $\omega_m$ . Similarly, since the electrical frequency is linearly related to  $\omega_m$ , the voltage drop across  $L_s$  is also proportional to  $\omega_m$ . Therefore, neglecting the per-phase stator winding resistance  $R_s$ , in the phasor diagram of Fig. 11-15b, the voltage phasors are all proportional to  $\omega_m$ , requiring that the per-phase voltage magnitude that the power-processing unit needs to supply is proportional to the speed  $\omega_m$ , as plotted in Fig. 11-16b. This relationship between the voltage and speed shown in Fig. 11-16b is approximate. A substantially higher voltage, called the voltage boost,

above that indicated by the dotted line, is needed at very low speeds, where the voltage drop across the stator winding resistance  $R_s$  becomes substantial at higher torque loading, and hence cannot be neglected.

### 11-5-6 The Controller and the Power-Processing Unit (PPU)

As shown in the block diagram of Fig. 11-13, the task of the controller is to dictate the switching in the power-processing unit, such that the desired currents are supplied to the PMAC motors. The reference torque signal is generated from the outer speed and position loops discussed in Chapter 13. The rotor position  $\theta_m$  is measured by the position sensor connected to the shaft. Knowing the torque constant  $k_{T,phase}$  allows us to calculate the rms value of the reference current from Eq. 11-23. Knowing the current rms value and  $\theta_m$  allows the reference currents for the three phases to be calculated, which the PPU delivers at any instant of time.

## 11-6 INDUCTION MACHINES

Induction motors with squirrel-cage rotors are the workhorses of industry because of their low cost and rugged construction. When operated directly from line voltages (a 50- or 60-Hz utility input at essentially a constant voltage), induction motors operate at a nearly constant speed. However, by means of power electronic converters, it is possible to vary their speed efficiently.

### 11-6-1 Structure of Induction Machines

The stator of an induction motor consists of three-phase windings, distributed in the stator slots. These three windings are displaced by  $120^\circ$  in space with respect to each other, as shown by their axes in Fig. 11-17a.

The rotor, consisting of a stack of insulated laminations, has electrically conducting bars of copper or aluminum inserted (molded) through it, close to the periphery in the axial

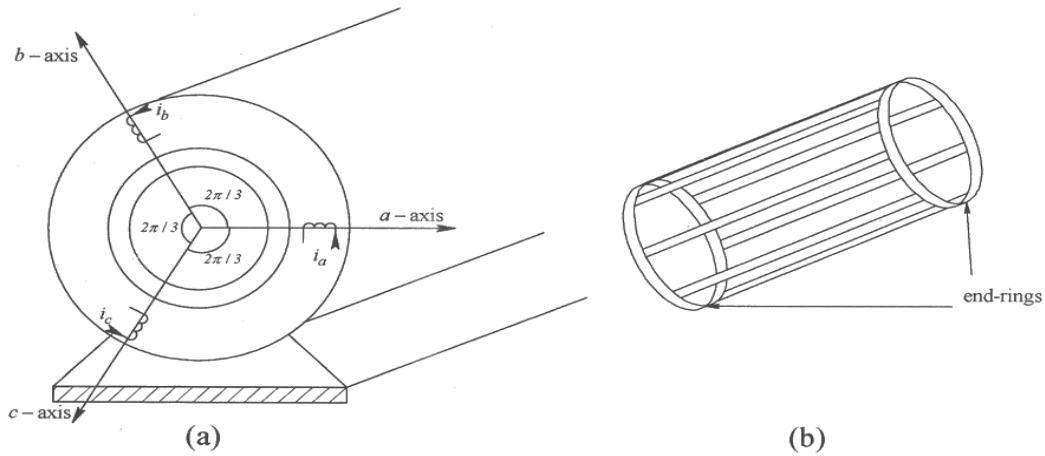


Figure 11-17 (a) Three-phase stator; (b) squirrel-cage rotor.

direction. These bars are electrically shorted at each end of the rotor by electrically conducting end-rings, thus producing a conducting cage-like structure, as shown in Fig. 11-17b. Such a rotor, called a squirrel-cage rotor, has a low cost, and rugged nature.

### 11-6-2 Principles of Induction Motor Operation

Figure 11-18a shows the stator windings whose voltages are shown in the phasor diagram of Fig. 11-18b, where the frequency of the applied line-voltages to the motor is  $f$  in Hz, and  $V_{rms}$  is the magnitude in rms

$$\bar{V}_a = V_{rms} \angle 0^\circ, \quad \bar{V}_b = V_{rms} \angle -120^\circ, \quad \text{and} \quad \bar{V}_c = V_{rms} \angle -240^\circ \quad (11-27)$$

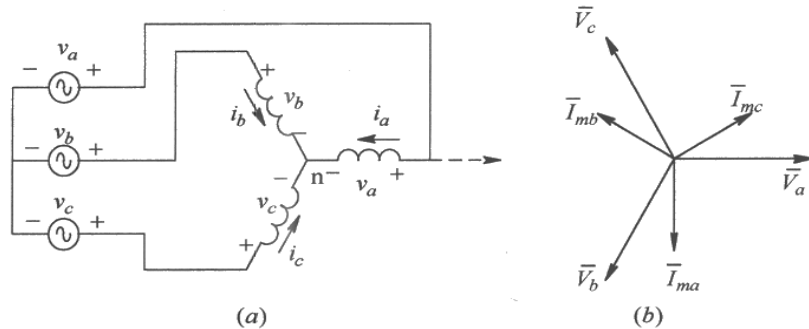


Figure 11-18 Induction machine: applied voltages and magnetizing currents.

By Faraday's law, the applied stator voltages given in Eq. 11-27 establish a rotating flux-density distribution in the air gap by drawing magnetizing currents of rms value  $I_m$ , which are shown in Fig. 11-18b:

$$\bar{I}_{ma} = I_m \angle -90^\circ, \quad \bar{I}_{mb} = I_m \angle -210^\circ, \quad \text{and} \quad \bar{I}_{mc} = I_m \angle -330^\circ \quad (11-28)$$

As these currents vary sinusoidally with time, the combined flux-density distribution in the air gap produced by these currents rotates at a synchronous speed  $\omega_{syn}$ , where

$$\omega_{syn} = 2\pi f \quad \left( \omega_{syn} = \frac{2\pi f}{p/2} \quad \text{for a } p\text{-pole machine} \right) \quad (11-29)$$

The rotor in an induction motor turns (due to the electromagnetic torque developed, as will be discussed shortly) at a speed  $\omega_m$  in the same direction as the rotation of the air gap flux-density distribution, such that  $\omega_m < \omega_{syn}$ . Therefore, there is a relative speed between the flux-density distribution rotating at  $\omega_{syn}$  and the rotor conductors at  $\omega_m$ . This relative speed, that is the speed at which the rotor is "slipping" with respect to the rotating flux-density distribution, is called the slip speed:

$$\text{slip speed} \quad \omega_{slip} = \omega_{syn} - \omega_m \quad (11-30)$$

By Faraday's Law ( $e = B \ell u$ ), voltages are induced in the rotor bars at the slip frequency due to the relative motion between the flux-density distribution and the rotor, where the slip frequency  $f_{\text{slip}}$  in terms of the frequency  $f$  of the stator voltages and currents is

$$\text{slip frequency } f_{\text{slip}} = \frac{\omega_{\text{slip}}}{\omega_{\text{syn}}} f \quad (11-31)$$

Since the rotor bars are shorted at both ends, these induced bar voltages cause slip-frequency currents to flow in the rotor bars. The rotor-bar currents interact with the flux-density distribution established by the stator-applied voltages, and the result is a net electromagnetic torque  $T_{\text{em}}$  in the same direction as the rotor's rotation.

The sequence of events in an induction machine to meet the load torque demand is as follows: At essentially no load, an induction machine operates nearly at the synchronous speed that depends on the frequency of applied stator voltages (Eq. 11-29). As the load torque increases, the motor slows down, resulting in a higher value of slip speed. Higher slip speed results in higher voltages induced in the rotor bars and hence higher rotor-bar currents. Higher rotor-bar currents result in a higher electromagnetic torque to satisfy the increased load-torque demand.

Neglecting second-order effects, the air gap flux is totally determined by the applied stator voltages. Hence, the air gap flux produced by the rotor-bar currents is nullified by the additional currents drawn by the stator windings, which are in addition to the magnetizing currents in Eq. 11-28.

### 11-6-3 Per-Phase Equivalent Circuit of Induction Machines

In this balanced three-phase sinusoidal steady state analysis, we will neglect second-order effects such as the stator winding resistance and leakage inductance, and the rotor circuit leakage inductance. As shown in Fig. 11-19a for phase-a in this per-phase circuit,  $\bar{V}_a$  and so on are applied at a frequency  $f$ , which results in magnetizing currents to establish the air gap flux-density distribution in the air gap, represented as flowing through a magnetizing inductance  $L_m$ . The voltage magnitude and frequency are such that the magnitude of the flux-density distribution in the air gap is at its rated value and this distribution rotates counter-clockwise at the desired  $\omega_{\text{syn}}$  (Eq. 11-29) to induce a back-emf in the stationary stator phase windings such that

$$\bar{V}_a = \bar{E}_{ma} = k_{E, \text{phase}} \omega_{\text{syn}} \angle 0^\circ \quad (11-32)$$

where,  $k_{E, \text{phase}}$  is the machine per-phase voltage-constant.

Next, we will consider the effect of the rotor-bar currents. The rotor-bar currents result in additional stator currents (in addition to the magnetizing current), which can be represented on a per-phase basis by a current  $\bar{I}'_{ra}$  in-phase with the applied voltage (since the rotor-circuit leakage inductance is ignored), as shown in Fig. 11-19a

$$\bar{I}'_{ra} = I'_{ra} \angle 0^\circ \quad (11-33)$$

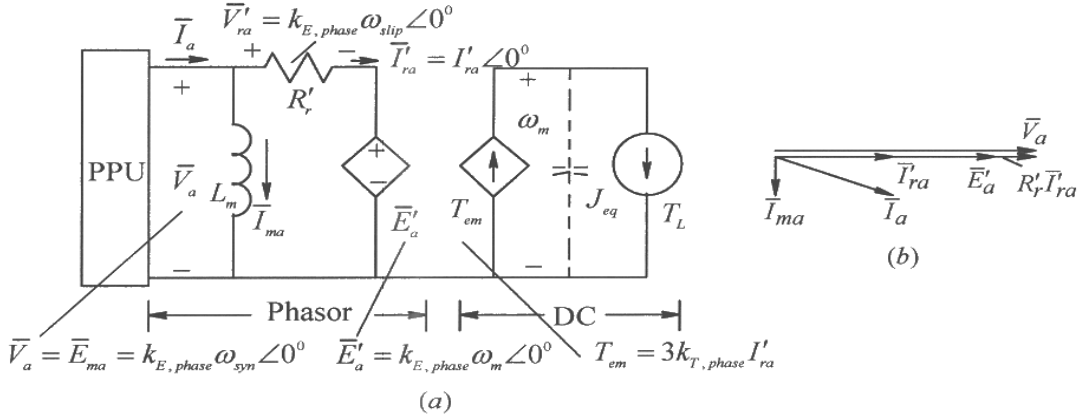


Figure 11-19 Induction motor equivalent circuit and phasor diagram.

The flux-density distribution (although produced differently than in PMAC machines) interacts with these stator currents, just like in PMAC machines, and hence the per-phase torque-constant equals the per-phase voltage constant

$$k_{T, phase} = k_{E, phase} \quad (11-34)$$

The per-phase torque can be expressed as

$$T_{em, phase} = k_{T, phase} I'_{ra} \quad (11-35)$$

This torque at a mechanical speed  $\omega_m$  results in per-phase electromagnetic power that gets converted to mechanical power, where using Eqs. 11-34 and 11-35

$$P_{em, phase} = \omega_m T_{em, phase} = \omega_m k_{E, phase} I'_{ra} \quad (11-36)$$

In Eq. 11-36,  $(\omega_m k_{E, phase})$  can be considered the back-EMF  $\bar{E}'_a$ , just like in the DC and the PMAC machines, as shown in Fig. 11-19a

$$\bar{E}'_a = \omega_m k_{E, phase} \angle 0^\circ \quad (11-37)$$

In the rotor-circuit, the voltages induced depend on the slip-speed  $\omega_{slip}$ , and overcome the  $IR$  voltage drop in the rotor bar resistances. The rotor-bar resistances, and the voltage drop and the power losses in them, are represented in the per-phase equivalent circuit of

Fig. 11-19a by a voltage drop across an equivalent resistance  $R'_r$ . Using the Kirchhoff's voltage law in Fig. 11-19a,

$$\bar{V}'_{ra} = \underbrace{k_{E, \text{phase}} \omega_{\text{syn}} \angle 0^0}_{\bar{E}_{ma}} - \underbrace{k_{E, \text{phase}} \omega_m \angle 0^0}_{\bar{E}'_a} = k_{E, \text{phase}} \omega_{\text{slip}} \angle 0^0 \quad (11-38)$$

Hence,

$$I'_{ra} = \left( \frac{k_{E, \text{phase}}}{R'_r} \right) \omega_{\text{slip}} \quad (11-39)$$

Using Eqs. 11-34, 11-36 and 11-39, the combined torque of all three phases is

$$T_{em} = \frac{P_{em}}{\omega_m} = \underbrace{\left( 3 \frac{k_{T, \text{phase}}^2}{R'_r} \right)}_{k_{T, \omega_{\text{slip}}}} \omega_{\text{slip}} \quad (11-40)$$

where  $k_{T, \omega_{\text{slip}}}$  in the above equation is a machine constant that shows that the torque produced is linearly proportional to the slip speed. Using Eqs. 11-30 and 11-40,

$$\omega_m = \omega_{\text{syn}} - \frac{T_{em}}{k_{T, \omega_{\text{slip}}}} \quad (11-41)$$

Based on Eq. 11-41, the torque-speed characteristics are shown in Fig. 11-20a for various applied frequencies to the stator. The stator voltage as function of frequency is shown in Fig. 11-20b to maintain the peak of the flux-density distribution at its rated value. The relationship between the voltage and the synchronous speed or  $f$  shown in Fig. 11-20b is approximate. It needs a substantially higher voltage than indicated (shown dotted) at very low frequencies where the voltage drop across the stator winding resistance  $R_s$  becomes substantial at higher torque loading, and hence cannot be neglected.

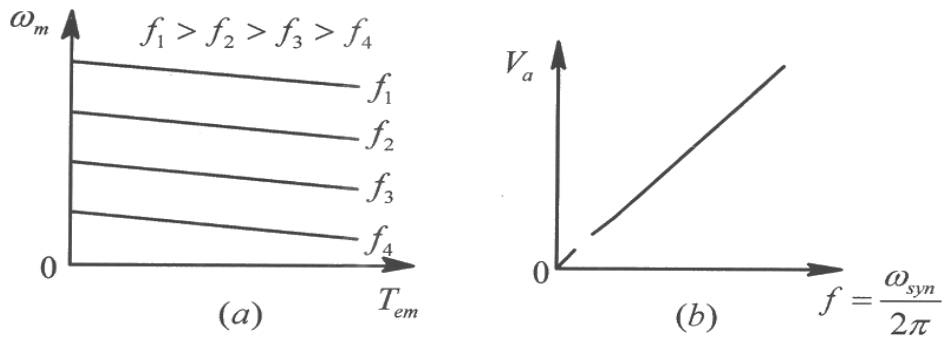


Figure 11-20 Induction motors: Torque-speed characteristics and voltage vs. frequency.

## 11-7 SUMMARY

The discussion above shows the requirements of three common types of machines supplied through power-electronics based power processing units in steady state.

## REFERENCE

1. N. Mohan, *Electric Drives: An Integrative Approach*, year 2003 Edition, MNPERE, Minneapolis, [www.MNPERE.com](http://www.MNPERE.com).
2. N. Mohan, *Advanced Electric Drives: Analysis, Modeling and Simulation using Simulink*, year 2001 Edition, MNPERE, Minneapolis, [www.MNPERE.com](http://www.MNPERE.com).

## PROBLEMS

### Mechanical Systems

- 11-1 A constant torque of  $5 \text{ Nm}$  is applied to an unloaded motor at rest at time  $t = 0$ . The motor reaches a speed of  $1800 \text{ rpm}$  in  $4 \text{ s}$ . Assuming the damping to be negligible, calculate the motor inertia.
- 11-2 In an electric-motor drive similar to that shown in Fig. 11-2a, the combined inertia is  $J_{eq} = 5 \times 10^{-3} \text{ kg} \cdot \text{m}^2$ . The load torque is  $T_L = 0.05 \text{ kg} \cdot \text{m}^2$ . Draw the electrical equivalent circuit and plot the electromagnetic torque required from the motor to bring the system linearly from rest to a speed of  $100 \text{ rad/s}$  in  $4 \text{ s}$ , and then to maintain that speed.
- 11-3 Plot the power required in Problem 11-2.

### DC Motors

- 11-4 A permanent-magnet dc motor has the following parameters:  $R_a = 0.35\Omega$  and  $k_E = k_T = 0.5$  in MKS units. For a torque of up to  $8 \text{ Nm}$ , plot its steady state torque-speed characteristics for the following values of  $V_a$ :  $100V$ ,  $75V$ , and  $50V$ .
- 11-5 Consider the dc motor of Problem 11-4 whose moment-of-inertia  $J_m = 0.02 \text{ kg} \cdot \text{m}^2$ . Its armature inductance  $L_a$  can be neglected for slow changes. The motor is driving a load of inertia  $J_L = 0.04 \text{ kg} \cdot \text{m}^2$ . The steady state operating speed is  $300 \text{ rad/s}$ . Calculate and plot the terminal voltage  $v_a(t)$  that is required to bring this motor to a halt as quickly as possible, without exceeding the armature current of  $12 \text{ A}$ .

### Permanent-Magnet AC Motors

- 11-6 In a three-phase, 2-pole, brushless-dc motor, the torque constant  $k_T = 0.5 \text{ Nm/A}$ . Calculate the phase currents if the motor is to produce a counter-clockwise torque of  $5 \text{ Nm}$ .

- 11-7 In a 2-pole, three-phase (PMAC) brushless-dc motor drive, the torque constant  $k_T$  and the voltage constant  $k_E$  are 0.5 in *MKS* units. The synchronous inductance is *15 mH* (neglect the winding resistance). This motor is supplying a torque of *3 Nm* at a speed of *3,000 rpm* in a balanced sinusoidal steady state. Calculate the per-phase voltage across the power-processing unit as it supplies controlled currents to this motor.

### Induction Motors

- 11-8 Consider an induction machine that has 2 poles and is supplied by a rated voltage of *208 V* (line-to-line, rms) at the frequency of *60 Hz*. It is operating in steady state and is loaded to its rated torque. Neglect the stator leakage impedance and the rotor leakage flux. The per-phase magnetizing current is *4.0 A* (rms). The current drawn per-phase is *10 A* (rms) and is at an angle of *23.56 degrees* (lagging). Calculate the per-phase current if the mechanical load decreases so that the slip speed is one-half that of the rated case.
- 11-9 In Problem 11-8, the rated speed (while the motor supplies its rated torque) is *3475 rpm*. Calculate the slip speed  $\omega_{slip}$ , and the slip frequency  $f_{slip}$  of the currents and voltages in the rotor circuit.
- 11-10 In Problem 11-9, the rated torque supplied by the motor is *8 Nm*. Calculate the torque constant, which linearly relates the torque developed by the motor to the slip speed.
- 11-11 A three-phase, *60-Hz*, 4-pole, *440-V* (line-line, rms) induction-motor drive has a full-load (rated) speed of *1746 rpm*. The rated torque is *40 Nm*. Keeping the air gap flux-density peak constant at its rated value, (a) plot the torque-speed characteristics (the linear portion) for the following values of the frequency  $f$  : *60 Hz, 45 Hz, 30 Hz, and 15 Hz*. (b) This motor is supplying a load whose torque demand increases linearly with speed, such that it equals the rated torque of the motor at the rated motor speed. Calculate the speeds of operation at the four values of frequency in part (a).
- 11-12 In the motor drive of Problem 11-11, the induction motor is such that while applied the rated voltages and loaded to the rated torque, it draws *10.39 A* (rms) per-phase at a power factor of *0.866* (lagging).  $R_s = 1.5\Omega$ . Calculate the voltages corresponding to the four values of the frequency  $f$  to maintain  $\hat{B}_{ms} = \hat{B}_{ms, \text{rated}}$ .

# Chapter 12

## SYNTHESIS OF DC AND LOW-FREQUENCY SINUSOIDAL AC VOLTAGES FOR MOTOR DRIVES AND UPS

### 12-1 INTRODUCTION

Motor drives (ac and dc) are important application areas of power electronics with market value of tens of billions dollars annually, as described in Chapter 1. Uninterruptible power supplies (UPS) are a special case of ac motor drives in discussing the role of power electronics, and will be briefly discussed in section 12-6 in this chapter.

In motor drive applications, the voltage-link structure of Fig. 1-16, repeated in Fig. 12-1, is used, where our emphasis will be to discuss how the load-side converter with the dc voltage as an input synthesizes dc or low-frequency sinusoidal voltage outputs. Functionally, this converter operates as a linear amplifier, amplifying a control signal, dc in case of dc-motor drives, and ac in case of ac-motor drives. The power flow through this converter should be reversible.

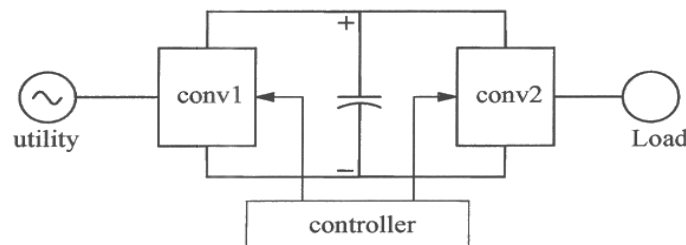


Figure 12-1 Voltage-link system.

These converters consist of bi-directional switching power-poles discussed earlier, two in case of dc-motor drives and three in ac motor drives, as shown in Figs. 12-2a and b.

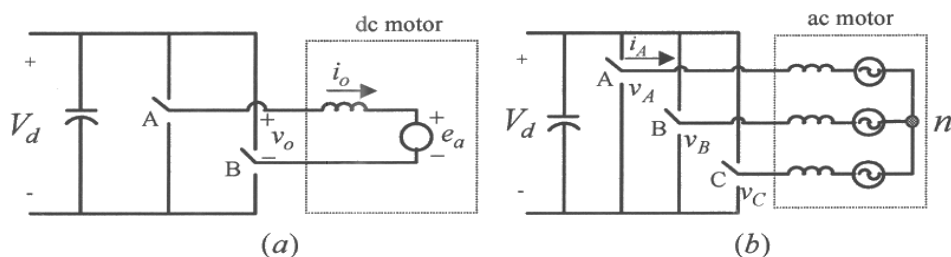


Figure 12-2 Converters for dc and ac motor drives.

## 12-2 SWITCHING POWER-POLE AS THE BUILDING BLOCK

To synthesize dc or low-frequency sinusoidal ac outputs, these converters consist of the switching power-pole shown in Fig. 12-3a with the bi-directional current capability, which was introduced in Chapter 3. It consists of a parallel combination of Buck and Boost converters, as shown in Fig. 12-3b, where the two transistors are controlled by complimentary gate signals. This implementation and the complimentary gating of transistors allow a continuous bi-directional power and current capability as discussed below, and hence ideally a discontinuous conduction mode does not exist. The average representation by an ideal transformer is shown in Fig. 12-3c.

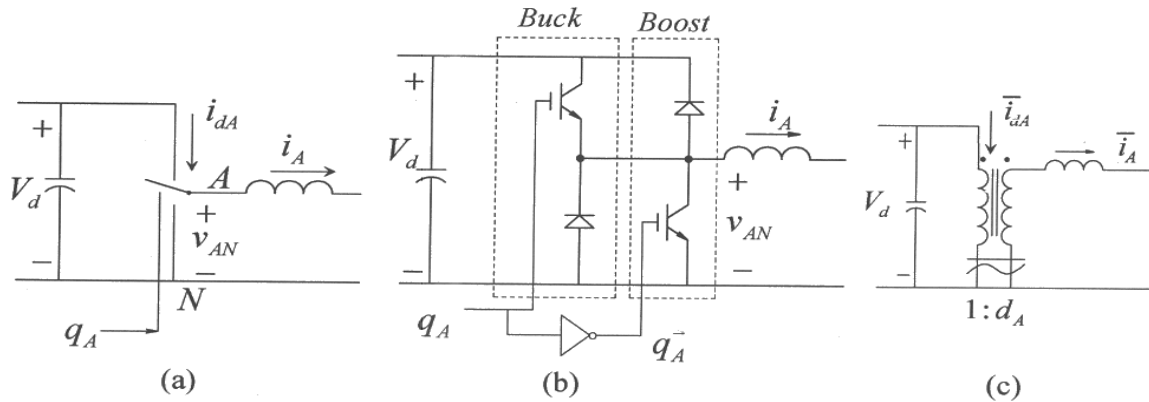


Figure 12-3 Bi-directional switching power-pole.

### 12-2-1 Pulse-Width-Modulation (PWM) of the Bi-Directional Switching Power-Pole

It is clear from the discussion of the switching power-poles that the output voltages of these poles at the current-port are always of a positive polarity. However, the output voltages of converters for motor drives must be reversible in polarity. This is achieved as shown in Fig. 12-2 by the differential output between two switching power-poles in dc-motor drives, and between any two of the three power-poles in ac motor drives.

The average representation of a switching power-pole is shown in Fig. 12-4a. In each switching pole, the output voltage at the current-port includes a dc offset of  $V_d/2$  (that corresponds to the duty-ratio  $d_A$  equal to 0.5). To synthesize a low-frequency sine wave, for example, varying the duty-ratio sinusoidally around 0.5, the average output voltage varies sinusoidally around  $V_d/2$ , as shown in Fig. 12-4b. The average output voltage can range from 0 and  $V_d$ . In the differential output between two power-poles in converters for dc drives, and between any two of the three poles for ac drives, shown in Fig. 12-2a and b, the dc offset is neutralized as will be discussed in the following sections in this chapter.

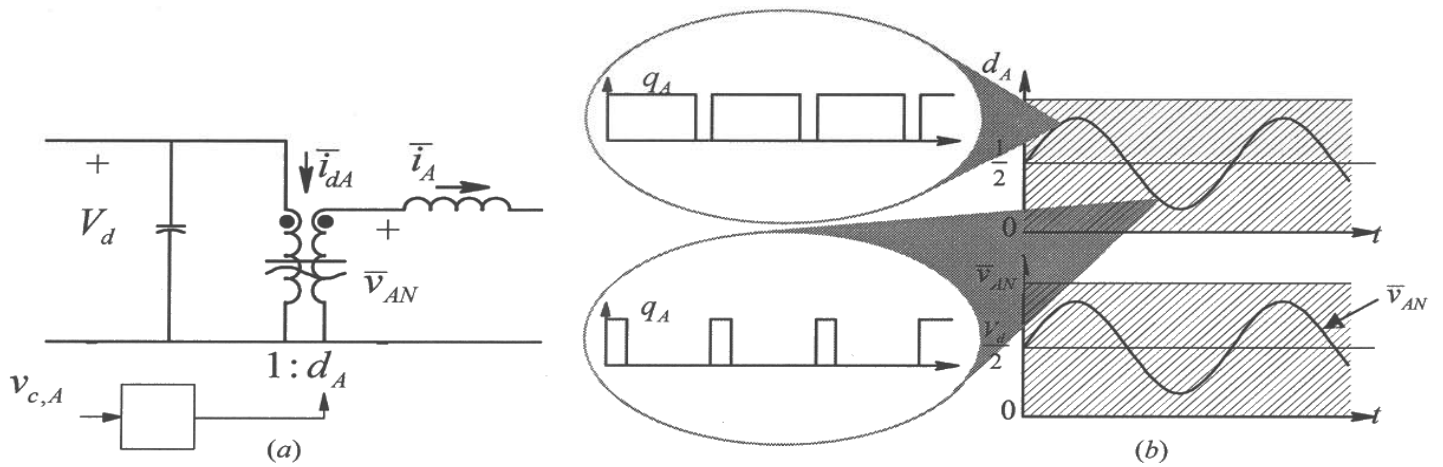


Figure 12-4 Varying the duty-ratio around 0.5 varies  $\bar{v}_{AN}$  around  $V_d/2$ .

In motor drives, to generate the switching function  $q_A$ , a triangular-waveform signal  $v_{tri}$  is used for comparison in the PWM-IC, as shown in Fig. 12-5a, where the peak value  $\hat{V}_{tri}$  is kept constant and the frequency of the triangular waveform establishes the switching frequency  $f_s$ .

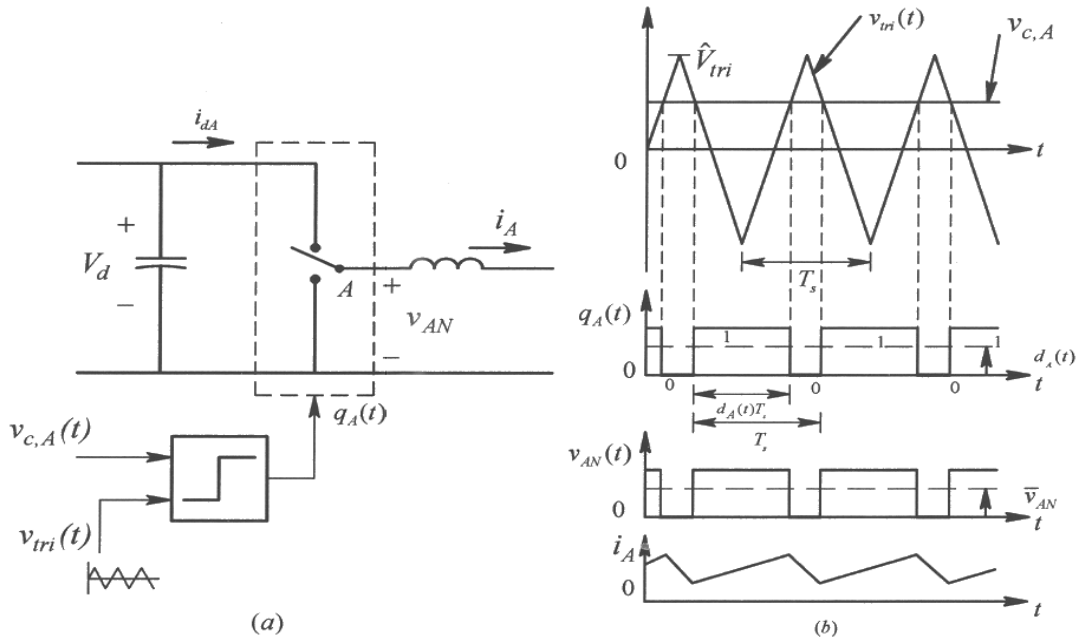


Figure 12-5 Switching power-pole and its voltage and current waveforms.

The resulting switching-signal waveforms are shown in Fig. 12-5b. The duty-ratio  $d_A$ , obtained by comparison of these linear waveforms, can be derived by considering two values of the control signal  $v_{c,A}$ :  $\hat{V}_{tri}$  results in  $d_A$  to equal 1, and  $(-\hat{V}_{tri})$  results in  $d_A$  to equal 0. Linearly interpolating between these two values, the expression for  $d_A$  can be written as

$$d_A(t) = 0.5 + 0.5 \frac{v_{c,A}(t)}{\hat{V}_{tri}} \quad (0 < d_A < 1) \quad (12-1)$$

which shows that it consists of two terms – a dc offset of 0.5 and a term that is linearly proportional to the control voltage  $v_{c,A}(t)$ . Therefore, the average output voltage of the power-pole can be written as

$$\bar{v}_{AN}(t) = d_A(t)V_d = \underbrace{0.5V_d}_{dc\ offset} + \underbrace{0.5 \frac{V_d}{\hat{V}_{tri}} v_{c,A}(t)}_{k_{pole}} \quad (12-2)$$

where  $0.5V_d$  is the dc offset and  $k_{pole}$  is the gain by which the control signal is amplified to produce the output voltage. The average representation of the pulse-width-modulated switching power-pole is shown Fig. 12-6.

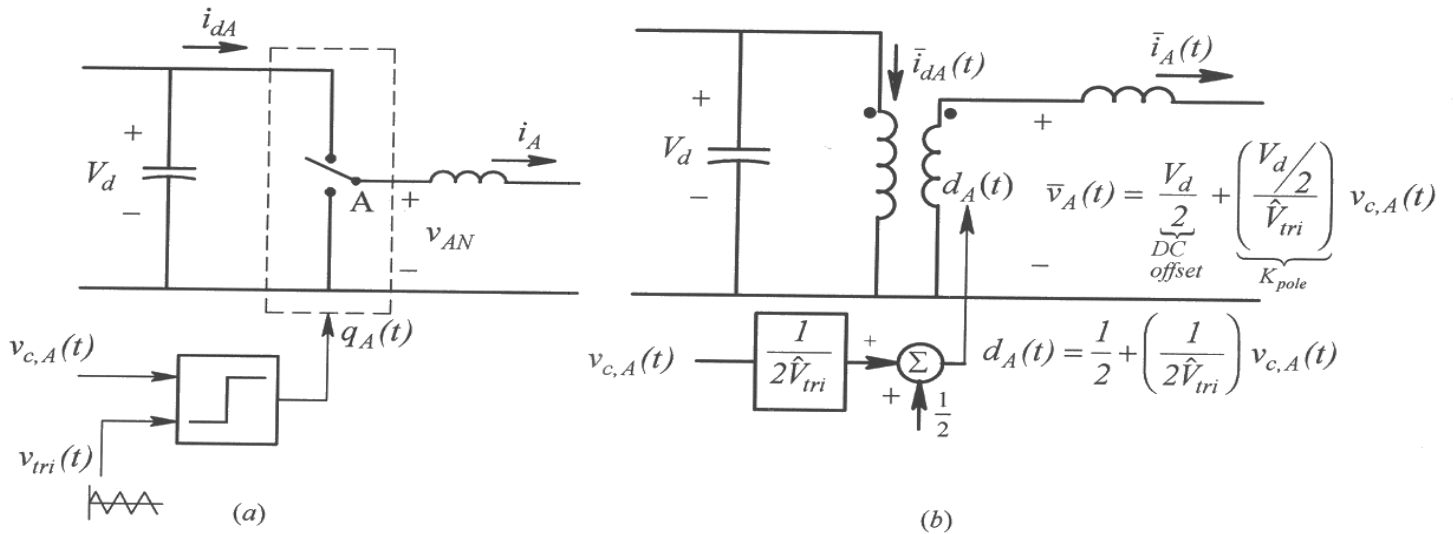


Figure 12-6 Average representation of the pulse-width-modulated power-pole.

### 12-2-3 Harmonics in the PWM Waveforms $v_A$ and $i_{dA}$

Although only their average values are of interest, we must recognize that the voltage  $v_A$  and the current  $i_{dA}$  contain harmonics in addition to their intended average values. Fourier analysis of these waveforms shows that they contain components at frequencies at the multiples of the switching frequency  $f_s$ , with sidebands located at the multiples of the frequency  $f_1$  being synthesized by the switching power-pole. These harmonic frequencies can be expressed as follows, where  $k_1$  and  $k_2$  are constants, which can take on values 1, 2, 3, and so on:

$$f_h = k_1 f_s \pm \underbrace{k_2 f_1}_{\text{sidebands}} \quad (12-3)$$

This harmonic analysis is graphically shown in Fig. 12-7, which highlights the importance of selecting a high switching frequency. Clearly, the harmonic components in  $v_A$  at frequencies  $f_h$  given by Eq. 12-3 are undesirable but also unavoidable in a switching power-pole. However, the minimum value in  $f_h$  depends on  $f_s$ , and by selecting a high switching frequency, all the harmonic frequencies are pushed to the correspondingly high values. At these high values, the series inductance at the current-port becomes very effective in ensuring that the current  $i_A$  has a small ripple in spite of the pulsating  $v_A$ . Similarly, the high-frequency components in  $i_{dA}$  are filtered by a relatively small capacitor across the voltage-port. For this reason in modern power electronic systems, it is typical to use switching frequencies a few hundred kHz in dc-dc converters at low power, and a few tens of kHz in converters for motor drives up to a few hundred kW.

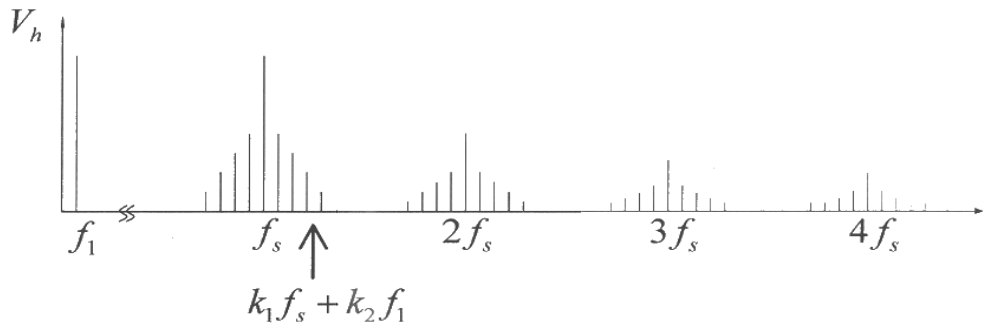


Figure 12-7 Harmonics in the switching power-pole.

### 12-3 DC-MOTOR DRIVES

In dc-motor drives as shown by Fig. 12-8a, the dc motor is controlled by the dc voltage  $v_o$  applied to its terminals. The converter consists of two bi-directional switching power-poles, which are pulse-width-modulated. Allowing the power (and hence the current) through this converter to be bi-directional facilitates the machine to operate both in motor and as well in its generator mode, in either direction of rotation, as shown in Fig. 12-8b in terms of average terminal quantities. Motoring-mode in the forward direction rotation is represented by quadrant 1 with positive voltage and current. While rotating in the forward direction, this machine can be slowed down by making the machine go into its generator mode in which the power flow reverses, as shown by quadrant 2 with a positive voltage and a negative current. Motoring in the reverse direction of rotation requires voltage and current both negative, corresponding to quadrant 3. While rotating in the reverse direction, the generator-mode in quadrant 4 slows down the machine.

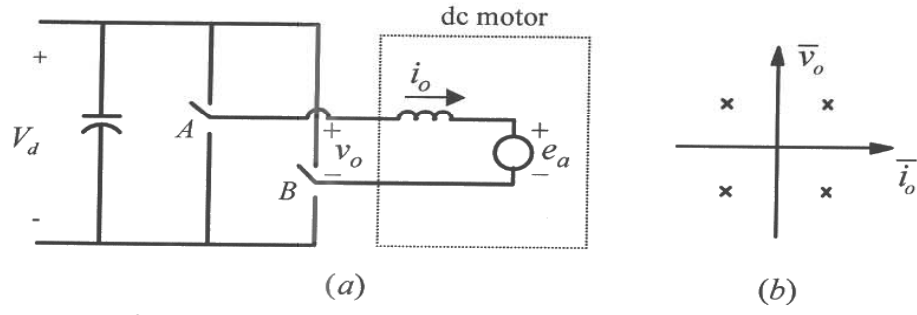


Figure 12-8 DC-motor four-quadrant operation.

In dc-motor drives, as shown in Fig. 12-9a, the control voltage  $v_c(t)$  produced by the feedback controller is applied as  $v_{c,A}(t)$ , equal to  $v_c(t)$ , to produce the switching function  $q_A(t)$  for pole-*A*. The control voltage for pole-*B* is negative of the control voltage for pole-*A*:  $v_{c,B}(t) = -v_c(t)$ . The average representation of the two poles is shown in Fig. 12-9b and the switching waveforms are shown in Fig. 12-9c. Using Eq. 12-1

$$\bar{v}_{AN}(t) = d_A(t)V_d = 0.5V_d + 0.5\frac{V_d}{\hat{V}_{tri}}v_c(t) \quad (12-4)$$

$$\bar{v}_{BN}(t) = d_B(t)V_d = 0.5V_d - 0.5\frac{V_d}{\hat{V}_{tri}}v_c(t) \quad (12-5)$$

$$\bar{v}_o(t) = \bar{v}_{AN}(t) - \bar{v}_{BN}(t) = \underbrace{\frac{V_d}{\hat{V}_{tri}}}_{k_{pwm}} v_c(t) \quad (12-6)$$

where  $k_{pwm}$  is the gain by which the control voltage is amplified by this switch-mode converter to apply the voltage at the terminals of this dc machine. This output voltage can be controlled in a range from  $(-V_d)$  to  $V_d$ . Thus, a four-quadrant converter is realized by using two-poles, each of which is capable of a two-quadrant operation.

The total average dc-side current is the sum of the average dc-side currents of each pole in Fig. 12-9b:

$$\bar{i}_d(t) = \bar{i}_{dA} + \bar{i}_{dB} = d_A(t)\bar{i}_A(t) + d_B(t)\bar{i}_B(t) \quad (12-7)$$

Using the values of the duty-ratios of the two poles, and recognizing the directions with which the currents are defined,

$$i_A(t) = -i_B(t) = i_o(t) \quad (12-8)$$

Thus, using Eq. 12-1 to achieve  $d_A$  and  $d_B$  in terms of  $v_c(t)$  and substituting them in Eq. 12-7 along with the currents from Eq. 12-8:

$$\bar{i}_d(t) = \frac{v_c(t)}{\hat{V}_{tri}} \bar{i}_o(t) \quad (12-9)$$

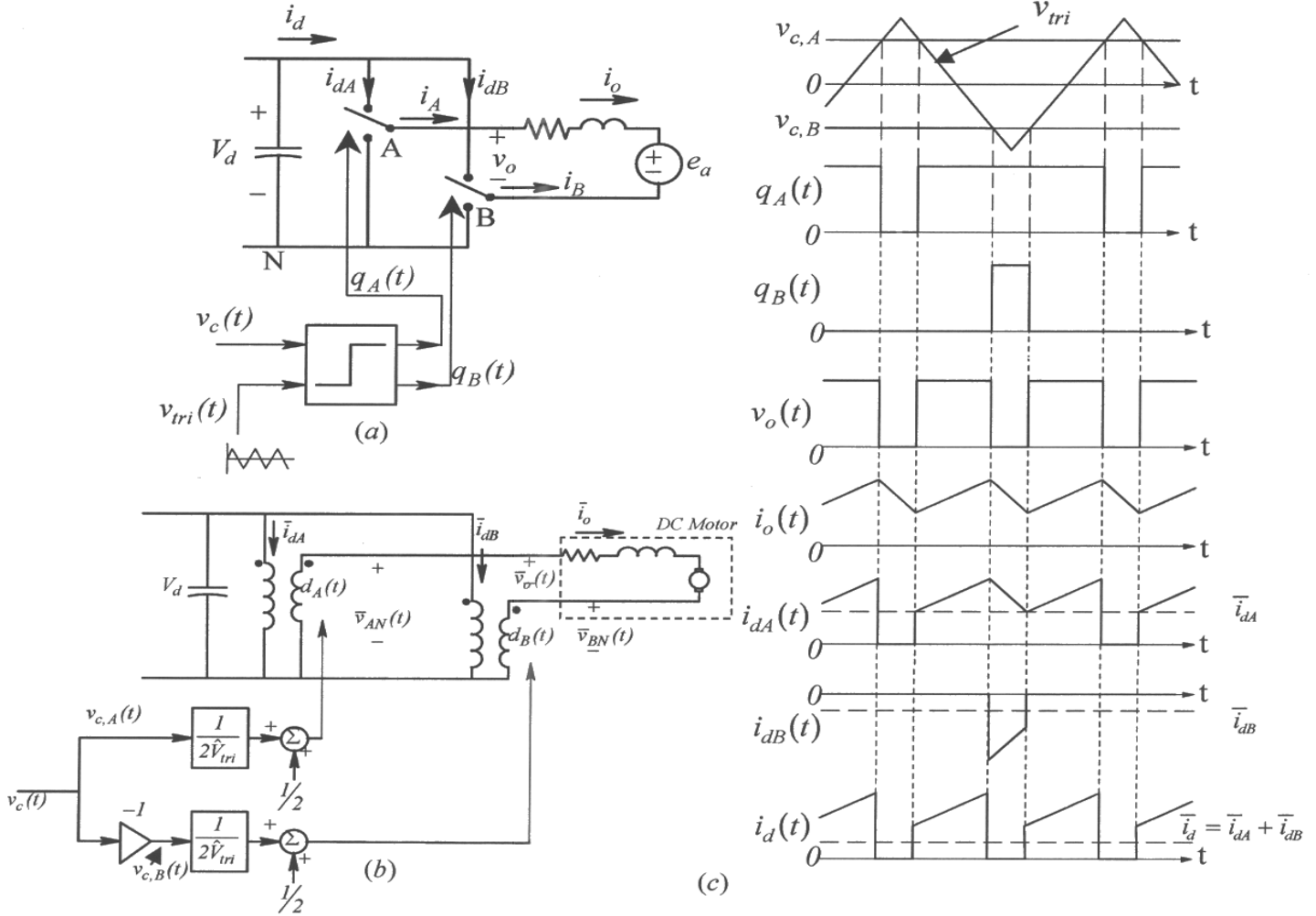


Figure 12-9 Converter for dc-motor drives.

The instantaneous quantities associated with this switch-mode dc-dc converter are pulsating, as shown in Fig. 12-9c. Based on the discussion of harmonic components in the voltage at the current-port and in the current at the voltage-port of each power-pole, we can calculate cancellation of some harmonics in the combination of the two power-poles in a dc-drive converter. A detailed discussion of this can be found in reference [1].

## 12-4 AC-MOTOR DRIVES

Ac-motor drives are the workhorse of industry. These three-phase motors are controlled in speed and position by applying adjustable-magnitude, and adjustable-frequency ac voltages by three bi-directional switching power-poles, as shown in Fig. 12-10a. Their average representation is shown in Fig. 12-10b.

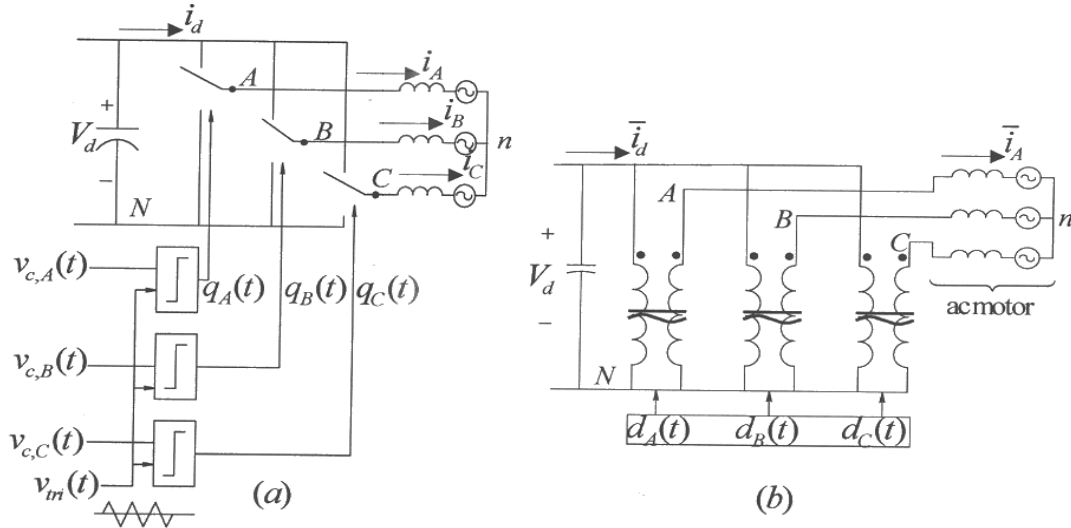


Figure 12-10 Converter for three-phase motor drive and UPS.

In order to synthesize balanced three-phase voltages, the PWM signals for the switches in Fig. 12-10a are obtained by comparing three control signals, which establish the amplitude and the frequency of the output voltages, with a triangular waveform  $v_{tri}$ , as shown in Fig. 12-11

$$\begin{aligned} v_{c,A}(t) &= \hat{V}_c \sin \omega_l t \\ v_{c,B}(t) &= \hat{V}_c \sin(\omega_l t - 120^\circ) \\ v_{c,C}(t) &= \hat{V}_c \sin(\omega_l t - 240^\circ) \end{aligned} \quad (12-10)$$

The resulting voltage waveforms are shown in Fig. 12-11. Using Eq. 12-10 into equations similar to Eq. 12-1 for all three phases produces the following duty-ratios in the average representation shown in Fig. 12-10b, where the control voltages and the duty-ratios are plotted in Fig. 12-12:

$$\begin{aligned} d_A(t) &= 0.5 + \frac{\hat{V}_c}{\hat{V}_{tri}} \sin \omega_l t \\ d_B(t) &= 0.5 + \frac{\hat{V}_c}{\hat{V}_{tri}} \sin(\omega_l t - 120^\circ) \\ d_C(t) &= 0.5 + \frac{\hat{V}_c}{\hat{V}_{tri}} \sin(\omega_l t - 240^\circ) \end{aligned} \quad (12-11)$$

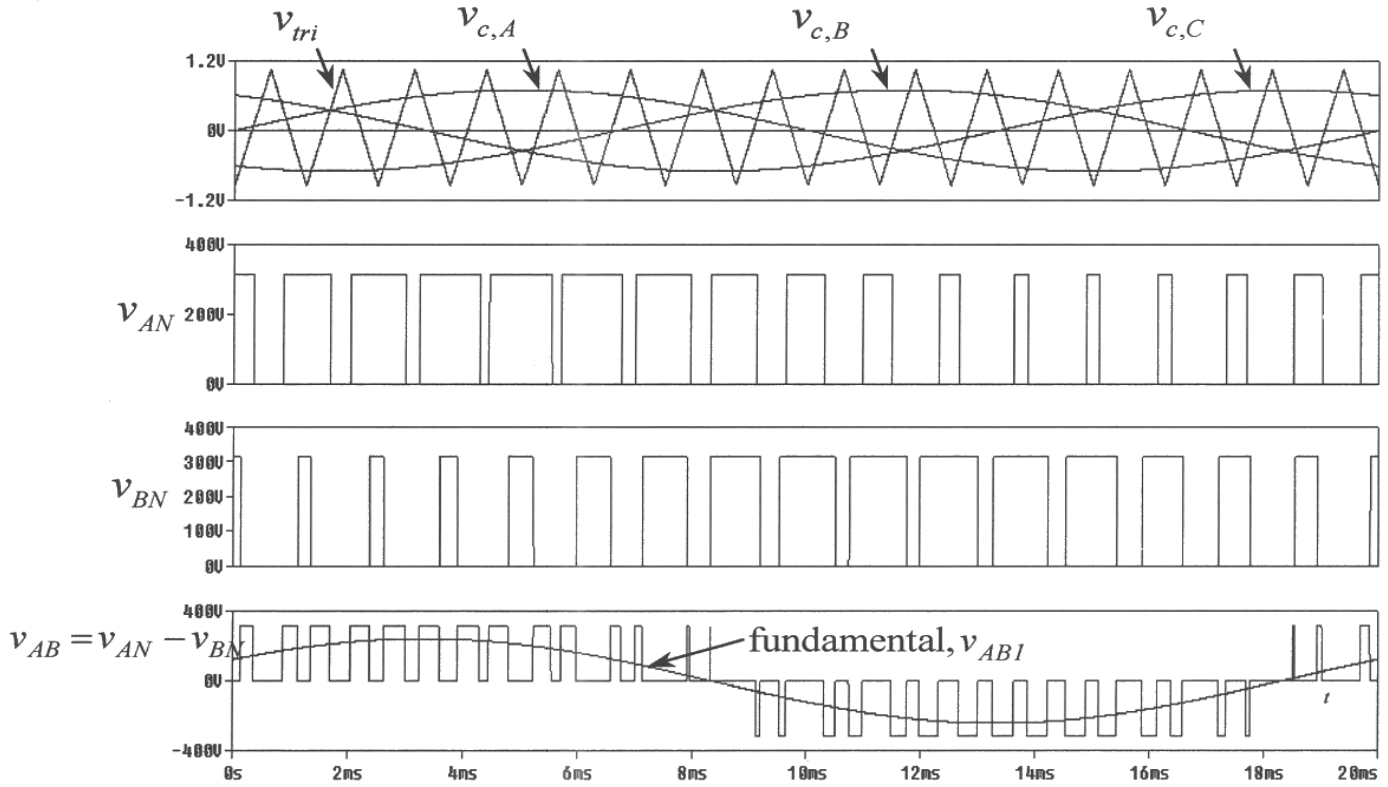


Figure 12-11 Switching waveforms in three-phase converter.

Applying the duty-ratios in Eq. 12-11 in Fig. 12-10b results in the following average output voltages:

$$\begin{aligned}
 \bar{v}_{AN}(t) &= 0.5V_d + 0.5 \underbrace{\frac{V_d}{\hat{V}_{tri}}}_{k_{pole}} \underbrace{\hat{V}_c \sin \omega_l t}_{v_{c,A}} \\
 \bar{v}_{BN}(t) &= 0.5V_d + 0.5 \underbrace{\frac{V_d}{\hat{V}_{tri}}}_{k_{pole}} \underbrace{\hat{V}_c \sin(\omega_l t - 120^\circ)}_{v_{c,B}} \\
 \bar{v}_{CN}(t) &= 0.5V_d + 0.5 \underbrace{\frac{V_d}{\hat{V}_{tri}}}_{k_{pole}} \underbrace{\hat{V}_c \sin(\omega_l t - 240^\circ)}_{v_{c,C}}
 \end{aligned} \tag{12-12}$$

where the pole gain  $k_{pole}$  is the same as in Eq. 12-2, and it amplifies the control voltage for each switching power-pole. These voltages are plotted in Fig. 12-12. The average output voltages of the switching power-poles have the same offset voltage, equal to  $0.5V_d$ . These equal offset voltages in each phase are considered zero-sequence voltages, which cannot cause any current to flow when applied to a balanced three-phase motor load shown in Fig. 12-10a or b.

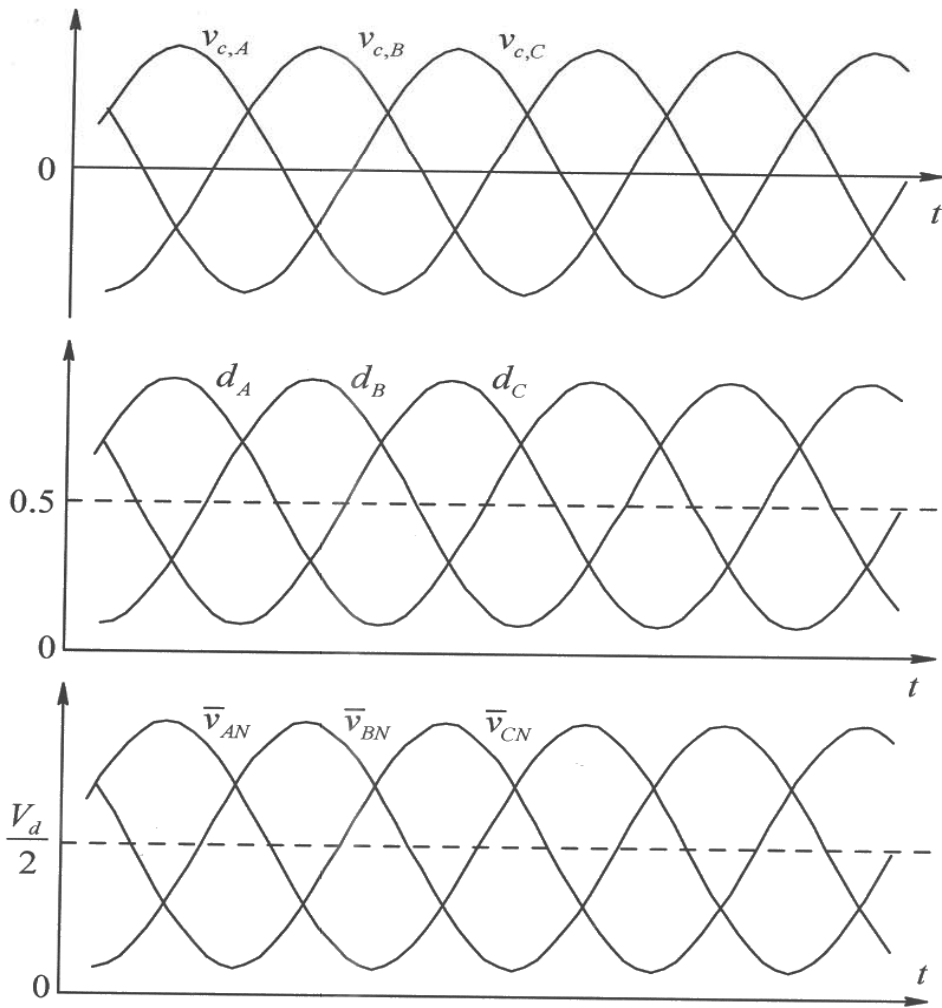


Figure 12-12 Duty-ratios and the average output voltages of the power-pole.

Hence the dc component in each phase voltage (terminal to neutral  $n$ ) of the motor load equals zero. As a consequence in Fig. 12-10b, the average phase-neutral voltages across the motor phases, with respect to the motor neutral  $n$ , are as intended

$$\begin{aligned}
 \bar{v}_{An}(t) &= \left( 0.5 \frac{V_d}{\hat{V}_{tri}} \right) \hat{V}_c \sin \omega_l t \\
 \bar{v}_{Bn}(t) &= \left( 0.5 \frac{V_d}{\hat{V}_{tri}} \right) \hat{V}_c \sin(\omega_l t - 120^\circ) \\
 \bar{v}_{Cn}(t) &= \left( 0.5 \frac{V_d}{\hat{V}_{tri}} \right) \hat{V}_c \sin(\omega_l t - 240^\circ)
 \end{aligned} \tag{12-13}$$

where the amplitude of these phase voltages are

$$\hat{V} = \left( \frac{\hat{V}_c}{\hat{V}_{tri}} \right) \frac{V_d}{2} \tag{12-14}$$

We should note that at high switching frequency  $f_s$  relative to the fundamental frequency  $f_1$  being synthesized, average voltages in Eq. 12-13 equal the fundamental-frequency components ( $v_{A_{n1}}$ ,  $v_{B_{n1}}$ ,  $v_{C_{n1}}$ ) in the voltages applied to the motor phases (at the terminals with respect to the motor-neutral  $n$ ).

To obtain the average currents drawn from the voltage-port of each switching power-pole, we will assume the average currents drawn by the motor load in Fig. 12-10b to be sinusoidal but lagging with respect to the average voltages in each phase by an angle  $\phi_1$ ,

$$\begin{aligned}\bar{i}_A(t) &= \hat{I} \sin(\omega_1 t - \phi_1) \\ \bar{i}_B(t) &= \hat{I} \sin(\omega_1 t - \phi_1 - 120^\circ) \\ \bar{i}_C(t) &= \hat{I} \sin(\omega_1 t - \phi_1 - 240^\circ)\end{aligned}\quad (12-15)$$

Therefore in Fig. 12-10b, the average currents drawn from the voltage-port are

$$\begin{aligned}\bar{i}_{dA}(t) &= d_A(t) \bar{i}_A(t) = 0.5 \bar{i}_A(t) + 0.5 \frac{v_{c,A}(t)}{\hat{V}_{tri}} \bar{i}_A(t) \\ \bar{i}_{dB}(t) &= d_B(t) \bar{i}_B(t) = 0.5 \bar{i}_B(t) + 0.5 \frac{v_{c,B}(t)}{\hat{V}_{tri}} \bar{i}_B(t) \\ \bar{i}_{dC}(t) &= d_C(t) \bar{i}_C(t) = 0.5 \bar{i}_C(t) + 0.5 \frac{v_{c,C}(t)}{\hat{V}_{tri}} \bar{i}_C(t)\end{aligned}\quad (12-16)$$

The total average current drawn by the converter from the dc-side voltage source is the sum of the three currents above:

$$\bar{i}_d(t) = \bar{i}_{dA}(t) + \bar{i}_{dB}(t) + \bar{i}_{dC}(t) \quad (12-17)$$

In Eq. 12-15, applying Kirchoff's law to average currents at the motor-neutral, the sum of three average currents equals zero,

$$\bar{i}_A(t) + \bar{i}_B(t) + \bar{i}_C(t) = 0 \quad (12-18)$$

Therefore, substituting Eqs. 12-16 and making use of Eq. 12-18 in Eq. 12-17

$$\bar{i}_d(t) = \frac{0.5}{\hat{V}_{tri}} [v_{c,A}(t)\bar{i}_A(t) + v_{c,B}(t)\bar{i}_B(t) + v_{c,C}(t)\bar{i}_C(t)] \quad (12-19)$$

Substituting for the control voltages from Eq. 12-10 and for the output currents from Eq. 12-15 into Eq. 12-19

$$\bar{i}_d(t) = 0.5 \frac{\hat{V}_c}{\hat{V}_{tri}} \hat{I} \left[ \begin{aligned} &\sin(\omega_1 t) \sin(\omega_1 t - \phi_1) + \sin(\omega_1 t - 120^\circ) \sin(\omega_1 t - \phi_1 - 120^\circ) \\ &+ \sin(\omega_1 t - 240^\circ) \sin(\omega_1 t - \phi_1 - 240^\circ) \end{aligned} \right] \quad (12-20)$$

that simplifies to a dc current

$$\bar{i}_d(t) = I_d = \frac{3}{4} \frac{\hat{V}_c}{\hat{V}_{tri}} \hat{I} \cos \phi_i \quad (12-21)$$

Substituting Eq. 12-14 into Eq. 12-21

$$V_d \bar{i}_d(t) = \frac{3}{2} \hat{V} \hat{I} \cos \phi_i \quad (12-22)$$

which shows that the average power input at the voltage-port equals the total three-phase power out of the current-port in this converter that is assumed loss-less.

In Fig. 12-10a, the instantaneous quantities associated with this switch-mode converter are pulsating, as shown in Fig. 12-11. Based on the discussion of harmonic components in the voltage at the current-port and the current at the voltage-port of each power-pole, we can calculate cancellation of some harmonics in the combination of the three power-poles in this ac-drive converter. A detailed discussion of this can be found in reference [1].

#### 12-4-1 Space Vector Pulse Width Modulation

The above method of synthesizing the three-phase sinusoidal output is called the sinusoidal-PWM. As discussed in the appendix to this chapter on the accompanying CD, the sinusoidal-PWM is near ideal, except it does not utilize the available dc-link voltage to its fullest. A modified PWM technique called the space vector PWM (SV-PWM) is described in the Appendix on the accompanying CD, which can produce from the same dc-link voltage a three-phase output voltage that is higher by approximately fifteen percent.

#### 12-5 VOLTAGE-LINK STRUCTURE WITH BI-DIRECTIONAL POWER FLOW

In many applications of ac-motor drives, the voltage-link structure in Fig. 12-1 is such that the power flow through it is bi-directional. Normally, power flows from the utility to the motor, and while slowing down, the energy stored in the inertia of machine-load combination is recovered by operating the machine as a generator and feeding power back into the utility grid. This can be accomplished by using three-phase converters discussed in section 12-4 at both ends, as shown in Fig. 12-13a, recognizing that the power flow through these converters is bi-directional. In the normal mode, converter at the utility-end operates as a rectifier and the converter at the machine-end as an inverter. The roles of these two are opposite when the power flows in the reverse direction during energy recovery.

The average representation of these converters by means of ideal transformers is shown in Fig. 12-13b. In this simplified representation, where losses are ignored, the utility source is represented by a source  $v_{sa}$ , etc. in series with the internal system inductance  $L_s$ . The machine is represented by its steady state equivalent circuit, the machine equivalent inductance  $L_{eq}$  in series with the back-emf  $e_A$ , etc. Under balanced three-phase operation at both ends, the role of each converter can be analyzed by means of the per-phase equivalent circuits shown in Fig. 12-13c. In these per-phase equivalent circuits, the fundamental-frequency voltages produced at the ac-side by the two converters are  $v_{a1}$  and  $v_{An1}$ , and the ac-side currents at the two sides can be expressed in the phasor form as

$$\bar{I}_{a1} = \frac{\bar{V}_{sa} - \bar{V}_{a1}}{j\omega_s L_s} \quad (12-23)$$

$$\bar{I}_{A1} = \frac{\bar{V}_{An1} - \bar{E}_A}{j\omega_1 L_{eq}} \quad (12-24)$$

where, the phasors in Eq. 12-23 represent voltages and current at the utility-system frequency  $\omega_s$  typically 60 (or 50 Hz), and the phasors in Eq. 12-24 at the fundamental-frequency  $\omega_1$  synthesized by the machine-side converter.

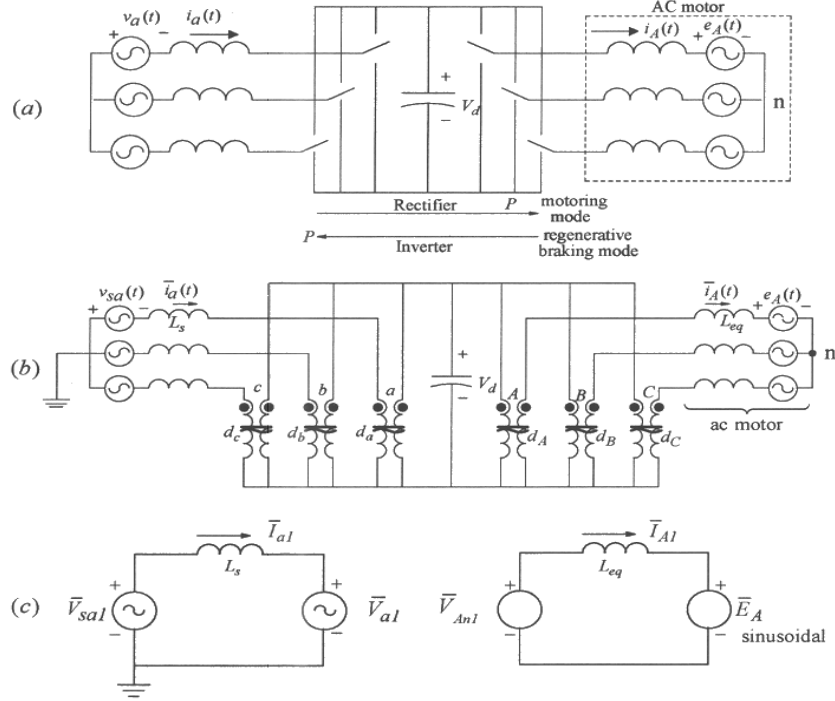


Figure 12-13 Voltage-link structure for bi-directional power flow.

In Fig. 12-13a, for a given utility voltage, it is possible to control the current drawn from the utility by controlling the voltage synthesized by the utility-side converter in magnitude and phase. In these circuits, if the losses are ignored, the average power drawn from the utility source equals the power supplied to the motor. However, the reactive power at the utility-side converter can be controlled, independently of the reactive power at the machine-side converter that depends on the motor load.

## 12-6 UNINTERRUPTIBLE POWER SUPPLIES (UPS)

In considering the synthesis of a low-frequency ac from a dc voltage, the uninterruptible power supplies (UPS) can be considered as a special case of ac-motor drives. UPS are used to provide power to critical loads in industry, business and medical facilities to which power should be available continuously, even during momentary utility power outages. The Computer Business Equipment Manufacturers Association (CBEMA) has specifications that show the voltage tolerance envelope as a function of time. This CBEMA curve shows that the UPS for critical loads are needed, not just for complete power outages but also for “swells” and “sags” in the equipment voltage due to disturbances on the utility grid.

In a UPS, a voltage-link structure shown in Fig. 12-1 is used where the dc-link consists of batteries to shield critical loads from voltage disturbances, as shown in the block diagram of Fig. 12-14. Normally, the power to the load is provided through the two converters, where the utility-side converter also keeps the batteries charged. In the event of power-line outages, energy stored in the batteries allows load power to be supplied continuously. The function of the load-side inverter is to produce, from dc source, ac voltages similar to that in ac-motor drives, except it is a special case where the output voltage has constant specified magnitude and frequency (e.g., 115 V rms, and 60 Hz). The load may be three-phase, where the analysis of section 12-5 applies. In the following section, the case of a single-phase load is considered, since the three-phase case is similar to that in motor drives.

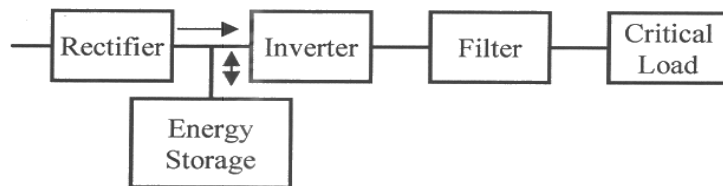


Figure 12-14 Bock diagram of UPS.

### 12-6-1 Single-Phase UPS

The load-side converter of 1-phase UPS is similar in power topology to that in dc-motor drives, as shown in Fig. 12-15a. The average representation is shown in Fig. 12-15b. It

consists of two switching power-poles, where as shown, the inductance of the low-pass filter establishes

the current-ports of the two power-poles. The control voltage is at the desired output frequency to produce the desired output voltage amplitude:

$$v_c(t) = \hat{V}_c \sin \omega_l t \quad (12-25)$$

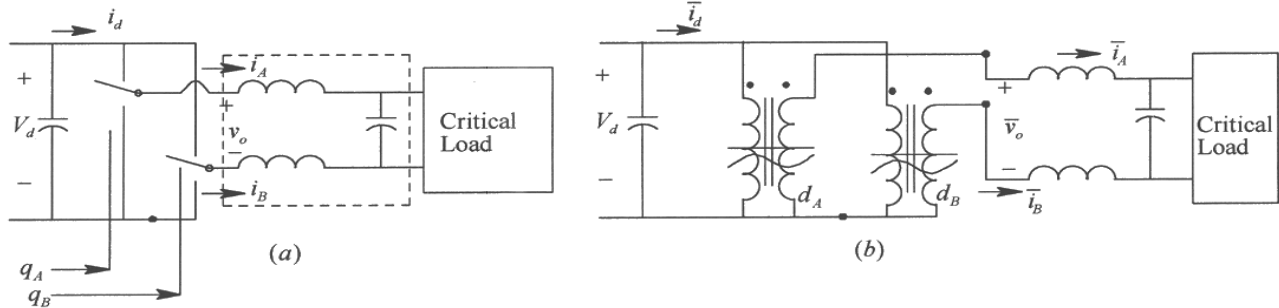


Figure 12-15 Single-phase UPS.

This control signal equals  $v_{c,A}$ . For the switching power-pole  $B$ , a phase shift of  $180^\circ$  is introduced in Eq. 12-25, that is by a factor of  $(-1)$ , to produce its control signal

$$v_{c,B}(t) = \hat{V}_c \sin(\omega_l t - 180^\circ) = -\hat{V}_c \sin \omega_l t \quad (12-26)$$

As shown in Fig. 12-16a, these control signals are compared with a triangular waveform at the switching frequency, typically above 20 kHz to produce the switching functions for the transistors in the switching power-poles. The switching waveforms are shown in Fig. 12-16a.

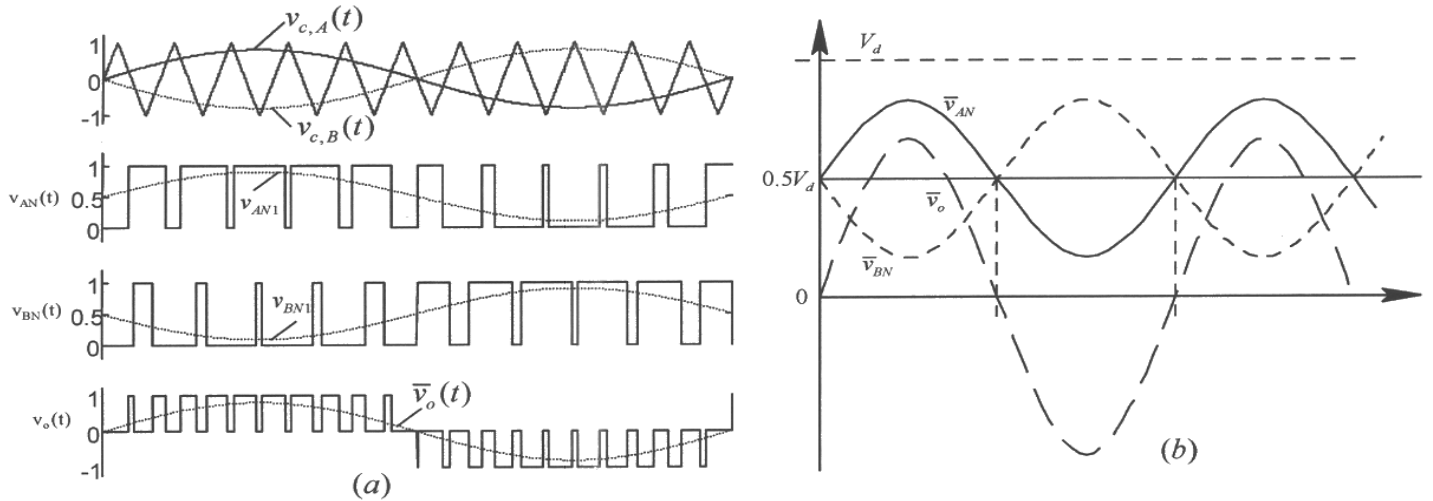


Figure 12-16 UPS waveforms.

Using the expression derived for the duty-ratio in phase  $A$  in Eq. 12-1, and substituting the control voltage for the other pole:

$$\begin{aligned}d_A(t) &= 0.5 + 0.5 \frac{\hat{V}_c}{\hat{V}_{tri}} \sin \omega_l t \\d_B(t) &= 0.5 - 0.5 \frac{\hat{V}_c}{\hat{V}_{tri}} \sin \omega_l t\end{aligned}\quad (12-27)$$

With these duty-ratios, the average outputs of the two power-poles and the average output voltage  $\bar{v}_o(t)$  are as follows, plotted in Fig. 12-16b

$$\begin{aligned}\bar{v}_{AN}(t) &= 0.5V_d + 0.5 \frac{\hat{V}_c}{\hat{V}_{tri}} V_d \sin \omega_l t \\\bar{v}_{BN}(t) &= 0.5V_d - 0.5 \frac{\hat{V}_c}{\hat{V}_{tri}} V_d \sin \omega_l t \\\bar{v}_o(t) &= \bar{v}_{AN}(t) - \bar{v}_{BN}(t) = \frac{\hat{V}_c}{\hat{V}_{tri}} V_d \sin \omega_l t\end{aligned}\quad (12-28)$$

where,

$$\hat{V}_o = \frac{\hat{V}_c}{\hat{V}_{tri}} V_d \quad (12-29)$$

In order to calculate the average current drawn from the dc source, we will assume that the average ac-side current is sinusoidal and lagging behind the output ac voltage by an angle  $\phi_l$ , as shown in Fig. 12-17:

$$\bar{i}_o(t) = \hat{I}_o \sin(\omega_l t - \phi_l) \quad (12-30)$$

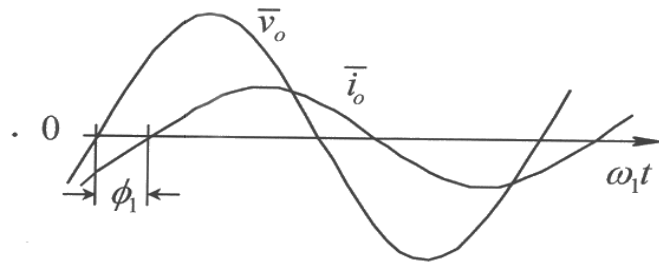


Figure 12-17 Output voltage and current.

Therefore, equating average input power to the output power, the average input current is

$$\begin{aligned}\bar{i}_d &= \frac{\bar{v}_o \bar{i}_o}{V_d} = \frac{\hat{V}_c}{\hat{V}_{tri}} \hat{I}_o \sin \omega_l t \times \sin(\omega_l t - \phi_l) \\&= \underbrace{0.5 \frac{\hat{V}_c}{\hat{V}_{tri}} \hat{I}_o}_{I_d} - \underbrace{0.5 \frac{\hat{V}_c}{\hat{V}_{tri}} \hat{I}_o \sin(2\omega_l t - \phi_l)}_{i_{d2}(t)}\end{aligned}\quad (12-31)$$

which shows that the average current drawn from the dc source has a dc component  $I_d$  that is responsible for the average power transfer to the ac side of the converter, and a second harmonic component  $i_{d2}$  (at twice the frequency of the ac output), which is undesirable. The dc-link storage in a 1-phase inverter must be sized to accommodate the flow of this large ac current at twice the output frequency, similar to that in *PFCs* discussed in Chapter 6. Of course, we should not forget that the above discussion is in terms of average representation of the switching power-poles. Therefore, the dc-link storage must also accommodate the flow of switching-frequency ripple in  $i_d$  discussed below.

The switching waveforms in the single-phase UPS are shown in Fig. 12-16a, which confirm that the voltage  $v_o(t)$  and  $i_d(t)$  are pulsating at the switching frequency. A low-pass filter is necessary to remove the output voltage harmonic frequencies, which were discussed earlier in a generic manner for each switching power-pole. The pulsating current ripple in  $i_d(t)$  can be by-passed from being supplied by the batteries by placing a small high quality capacitor with a very low equivalent series inductance.

## REFERENCES

1. N. Mohan, T. M. Undeland, and W.P. Robbins, *Power Electronics: Converters, Applications and Design*, 3<sup>rd</sup> Edition, Wiley & Sons, New York, 2003.

## PROBLEMS

### Switching Power-Pole

- 12-1 In a switch-mode converter pole-*A*,  $V_d = 150V$ ,  $\hat{V}_{tri} = 5V$ , and  $f_s = 20\text{kHz}$ . Calculate the values of the control signal  $v_{c,A}$  and the pole duty-ratio  $d_A$  during which the switch is in its top position, for the following values of the average output voltage:  $\bar{v}_{AN} = 125V$  and  $\bar{v}_{AN} = 50V$ .
- 12-2 In a converter pole, the  $i_A(t)$  waveform is as shown in Fig. 12-5b. Including the ripple, show that the current relationship of an ideal transformer is valid.

### DC-Motor Drives

- 12-3 A switch-mode dc-dc converter uses a PWM-controller IC which has a triangular waveform signal at 25 kHz with  $\hat{V}_{tri} = 3 V$ . If the input dc source voltage  $V_d = 150V$ , calculate the gain  $k_{PWM}$  in Eq. 12-6 of this switch-mode amplifier.

- 12-4 In a switch-mode dc-dc converter,  $v_c / \hat{V}_{tri} = 0.8$  with a switching frequency  $f_s = 20 \text{ kHz}$  and  $V_d = 150V$ . Calculate and plot the ripple in the output voltage  $v_o(t)$ .
- 12-5 A switch-mode dc-dc converter is operating at a switching frequency of  $20 \text{ kHz}$ , and  $V_d = 150 \text{ V}$ . The average current being drawn by the dc motor is  $8.0 \text{ A}$ . In the equivalent circuit of the dc motor,  $E_a = 100V$ ,  $R_a = 0.25\Omega$ , and  $L_a = 4 \text{ mH}$ . (a) Plot the output current and calculate the peak-to-peak ripple, and (b) plot the dc-side current.
- 12-6 In Problem 12-5, the motor goes into regenerative braking mode. The average current being supplied by the motor to the converter during braking is  $8.0 \text{ A}$ . Plot the voltage and current waveforms on both sides of this converter at that this instant. Calculate the average power flow into the converter.
- 12-7 In Problem 12-5, calculate  $\bar{i}_{dA}$ ,  $\bar{i}_{dB}$ , and  $\bar{i}_d (= I_d)$ .
- 12-8 Repeat Problem 12-5 if the motor is rotating in the reverse direction, with the same current draw and the same induced emf  $E_a$  value of the opposite polarity.
- 12-9 Repeat Problem 12-8 if the motor is braking while it has been rotating in the reverse direction. It supplies the same current and produces the same induced emf  $E_a$  value of the opposite polarity.
- 12-10 Repeat problem 12-5 if a bi-polar voltage switching is used in the dc-dc converter. In such a switching scheme, the two bi-positional switches are operated in such a manner that when switch-*A* is in the top position, switch-*B* is in its bottom position, and vice versa. The switching signal for pole-*A* is derived by comparing the control voltage (as in Problem 12-5) with the triangular waveform.

### Three-Phase AC-Motor Drives

- 12-11 Plot  $d_A(t)$  if the output voltage of the converter pole-*A* is  $\bar{v}_{AN}(t) = \frac{V_d}{2} + 0.85 \frac{V_d}{2} \sin(\omega_l t)$ , where  $\omega_l = 2\pi \times 60 \text{ rad/s}$ .
- 12-12 In a three-phase dc-ac inverter,  $V_d = 300V$ ,  $\hat{V}_{tri} = 1V$ ,  $\hat{V}_c = 0.75V$ , and  $f_1 = 45 \text{ Hz}$ . Calculate and plot  $d_A(t)$ ,  $d_B(t)$ ,  $d_C(t)$ ,  $\bar{v}_{AN}(t)$ ,  $\bar{v}_{BN}(t)$ ,  $v_{CN}(t)$ , and  $\bar{v}_{An}(t)$ ,  $\bar{v}_{Bn}(t)$ , and  $\bar{v}_{Cn}(t)$ .
- 12-13 In a balanced three-phase dc-ac inverter, the phase-*A* average output voltage is  $\bar{v}_{An}(t) = \frac{V_d}{2} 0.75 \sin(\omega_l t)$ , where  $V_d = 300V$  and  $\omega_l = 2\pi \times 45 \text{ rad/s}$ . The inductance  $L$  in each phase is  $5 \text{ mH}$ . The ac-motor internal voltage in phase *A*

can be represented as  $e_A(t) = 106.14 \sin(\omega_l t - 6.6^\circ) V$ . (a) Calculate and plot  $d_A(t)$ ,  $d_B(t)$ , and  $d_C(t)$ , and (b) sketch  $\bar{i}_A(t)$  and  $\bar{i}_{dA}(t)$ .

- 12-14 In Problem 12-13, calculate and plot  $\bar{i}_d(t)$ , which is the average dc current drawn from the dc-side.

### Single-Phase UPS

- 12-15 In a 1-phase UPS,  $V_d = 300 V$ ,  $\bar{v}_o(t) = 170 \sin(2\pi \times 60t) V$ , and  $\bar{i}_o(t) = 10 \sin(2\pi \times 60t - 30^\circ) A$ . Calculate and plot  $d_A(t)$ ,  $d_B(t)$ ,  $\bar{v}_{AN}(t)$ ,  $\bar{v}_{BN}(t)$ ,  $I_d$ ,  $i_{d2}(t)$ , and  $\bar{i}_d(t)$ .

- 12-16 In Problem 12-15, calculate  $q_A(t)$  and  $q_B(t)$  at  $\omega t = 90^\circ$ .

# Chapter 13

## DESIGNING FEEDBACK CONTROLLERS FOR MOTOR DRIVES

### 13-1 INTRODUCTION

Many applications, such as robotics and factory automation, require precise control of speed and position. In such applications, a feedback control, as illustrated by Fig. 13-1, is used. This feedback control system consists of a power-processing unit (PPU), a motor, and a mechanical load. The output variables such as torque and speed are sensed and are fed back, to be compared with the desired (reference) values. The error between the reference and the actual values are amplified to control the power-processing unit to minimize or eliminate this error. A properly designed feedback controller makes the system insensitive to disturbances and changes in the system parameters.

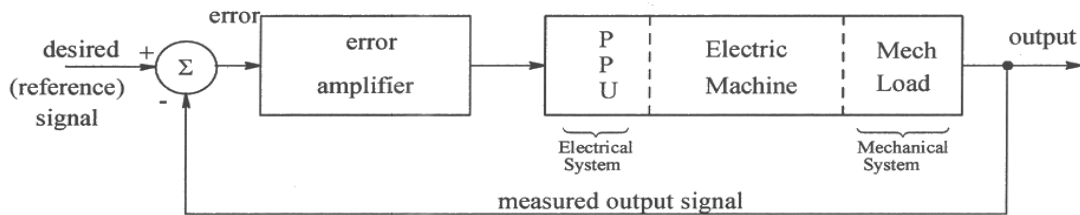


Fig 13-1 Feedback controlled drive.

The objective of this chapter is to discuss the design of motor-drive controllers. A dc-motor drive is used as an example, although the same design concepts can be applied in controlling brushless-dc motor drives and vector-controlled induction-motor drives. In the following discussion, it is assumed that the power-processing unit is of a switch-mode type and has a very fast response time. A permanent-magnet dc machine with a constant field flux  $\phi_f$  is assumed.

### 13-2 CONTROL OBJECTIVES

The control system in Fig. 13-1 is shown simplified in Fig. 13-2, where  $G_p(s)$  is the Laplace-domain transfer function of the plant consisting of the power-processing unit, the motor, and the mechanical load.  $G_c(s)$  is the controller transfer function. In response to a desired (reference) input  $X^*(s)$ , the output of the system is  $X(s)$ , which (ideally) equals the reference input. The controller  $G_c(s)$  is designed with the following objectives in mind:

- a zero steady state error.
- a good dynamic response (which implies both a fast transient response, for example to a step-change in the input, and a small settling time with very little overshoot).

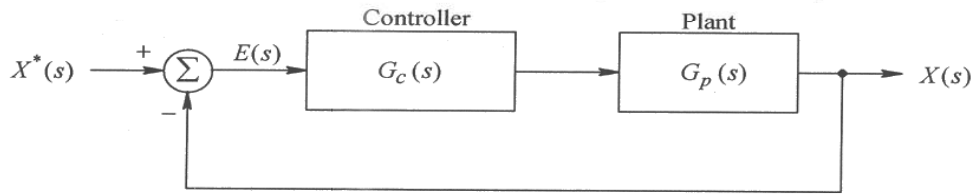


Fig 13-2 Simplified control system representation.

To keep the discussion simple, a unity feedback will be assumed. The open-loop transfer function (including the forward path and the unity feedback path)  $G_{OL}(s)$  is

$$G_{OL}(s) = G_c(s)G_p(s) \quad (13-1)$$

The closed-loop transfer function  $\frac{X(s)}{X^*(s)}$  in a unity feedback system is

$$G_{CL}(s) = \frac{G_{OL}(s)}{1 + G_{OL}(s)} \quad (13-2)$$

In order to define a few necessary control terms, we will consider a generic Bode plot of the open-loop transfer function  $G_{OL}(s)$  in terms of its magnitude and phase angle, shown in Fig. 13-3a as a function of frequency. The frequency at which the gain equals unity (that is  $|G_{OL}(s)| = 0 \text{ db}$ ) is defined as the crossover frequency  $f_c$  (angular frequency  $\omega_c$ ). At the crossover frequency, the phase delay introduced by the open-loop transfer function must be less than  $180^\circ$  in order for the closed-loop feedback system to be stable. Therefore, at  $f_c$ , the phase angle  $\phi_{OL}|_{f_c}$  of the open-loop transfer function, measured with respect to  $-180^\circ$ , is defined as the Phase Margin (PM):

$$\text{Phase Margin (PM)} = \phi_{OL}|_{f_c} - (-180^\circ) = \phi_{OL}|_{f_c} + 180^\circ \quad (13-3)$$

Note that  $\phi_{OL}|_{f_c}$  has a negative value. For a satisfactory dynamic response without oscillations, the phase margin should be greater than  $45^\circ$ , preferably close to  $60^\circ$ .

The magnitude of the closed-loop transfer function is plotted in Fig. 13-3b (idealized by the asymptotes), in which the bandwidth is defined as the frequency at which the gain drops to  $(-3 \text{ dB})$ . As a first-order approximation in many practical systems,

$$\text{Closed-loop bandwidth} \approx f_c \quad (13-4)$$

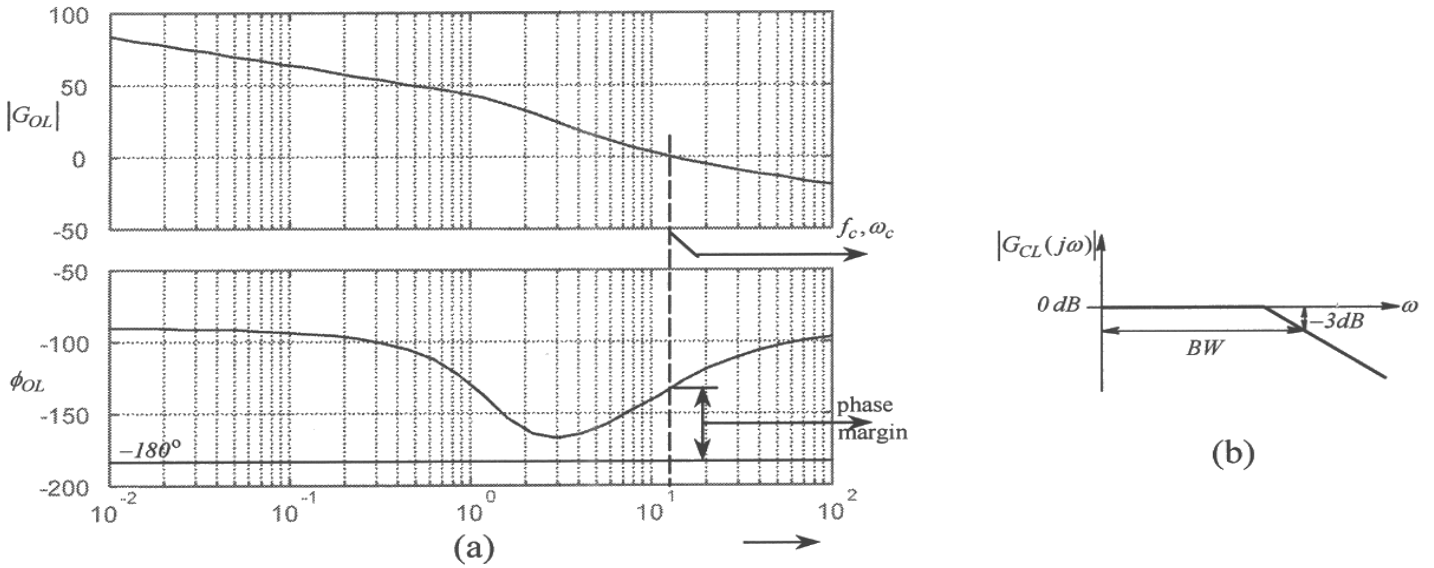


Figure 13-3 (a) Phase Margin; (b) bandwidth.

For a fast transient response by the control system, for example a response to a step-change in the input, the bandwidth of the closed-loop should be high. From Eq. 13-4, this requirement implies that the crossover frequency  $f_c$  (of the open-loop transfer function shown in Fig. 13-3a) should be designed to be high.

### 13-3 CASCADE CONTROL STRUCTURE

In the following discussion, a cascade control structure such as that shown in Fig. 13-4 is used. The cascade control structure is commonly used for motor drives because of its flexibility. It consists of distinct control loops; the innermost current (torque) loop is followed by the speed loop. If position needs to be controlled accurately, the outermost position loop is superimposed on the speed loop. Cascade control requires that the bandwidth (speed of response) increase towards the inner loop, with the torque loop being the fastest and the position loop being the slowest. The cascade control structure is widely used in industry.

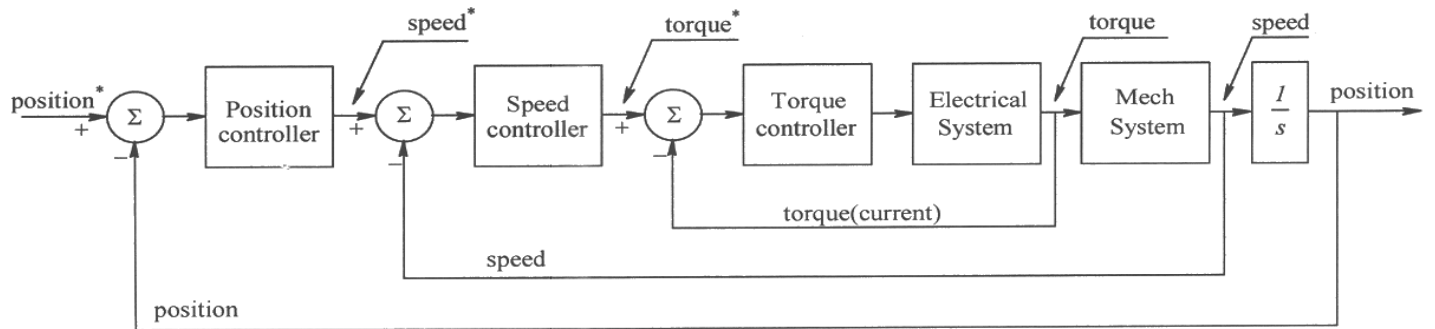


Figure 13-4 Cascade control of a motor drive.

## 13-4 STEPS IN DESIGNING THE FEEDBACK CONTROLLER

Motion control systems often must respond to large changes in the desired (reference) values of the torque, speed, and position. They must reject large, unexpected load disturbances. For large changes, the overall system is often nonlinear. This nonlinearity comes about because the mechanical load is often highly nonlinear. Additional nonlinearity is introduced by voltage and current limits imposed by the power-processing unit and the motor. In view of the above, the following steps for designing the controller are suggested:

1. The first step is to assume that, around the steady-state operating point, the input reference changes and the load disturbances are all small. In such a small-signal analysis, the overall system can be assumed to be linear around the steady-state operating point, thus allowing the basic concepts of linear control theory to be applied.
2. Based on the linear control theory, once the controller has been designed, the entire system can be simulated on a computer under large-signal conditions to evaluate the adequacy of the controller. The controller must be "adjusted" as appropriate.

## 13-5 SYSTEM REPRESENTATION FOR SMALL-SIGNAL ANALYSIS

For ease of the analysis described below, the system in Fig. 13-4 is assumed linear and the steady-state operating point is assumed to be zero for all of the system variables. This linear analysis can be then extended to nonlinear systems and to steady-state operating conditions other than zero. The control system in Fig. 13-4 is designed with the highest bandwidth (associated with the torque loop), which is one or two orders of magnitude smaller than the switching frequency  $f_s$ . As a result, in designing the controller, the switching-frequency components in various quantities are of no consequence. Therefore, we will use the average variables discussed in Chapter 3, where the switching-frequency components were eliminated.

### 13-5-1 The Average Representation of the Power-Processing Unit (PPU)

For the purposes of designing the feedback controller, we will assume that the dc-bus voltage  $V_{dc}$  within the PPU shown in Fig. 13-5a is constant. Following the averaging analysis in Chapter 3, the average representation of the switch-mode converter is shown in Fig. 13-5b. In terms of the dc-bus voltage  $V_{dc}$  and the triangular-frequency waveform peak  $\hat{V}_{tri}$ , the average output voltage  $\bar{v}_a(t)$  of the converter is linearly proportional to the control voltage:

$$\bar{v}_a(t) = k_{PWM} v_c(t) \quad (k_{PWM} = \frac{V_{dc}}{\hat{V}_{tri}}) \quad (13-5)$$

where  $k_{PWM}$  is the gain constant of the PWM converter. Therefore, in Laplace domain, the PWM controller and the dc-dc switch-mode converter can be represented simply by a gain-constant  $k_{PWM}$ , as shown in Fig. 13-5c:

$$V_a(s) = k_{PWM} V_c(s) \quad (13-6)$$

where  $V_a(s)$  is the Laplace transform of  $\bar{v}_a(t)$ , and  $V_c(s)$  is the Laplace transform of  $v_c(t)$ . The above representation is valid in the linear range, where  $-\hat{V}_{tri} \leq v_c \leq \hat{V}_{tri}$ .

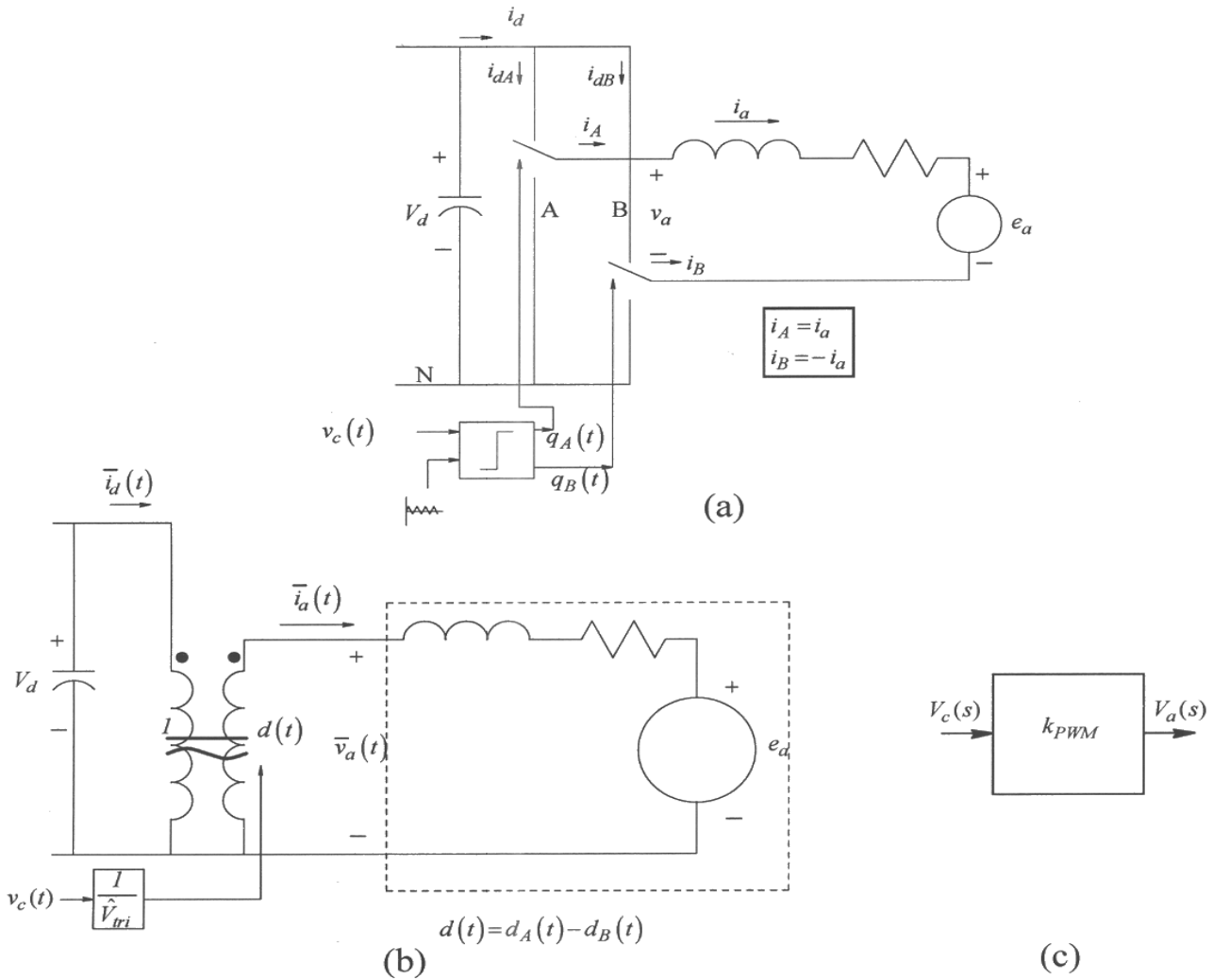


Figure 13-5 (a) Switch-mode converter for dc motor drives; (b) average model of the switch-mode converter; (c) linearized representation.

### 13-5-2 Modeling of the DC Machine and the Mechanical Load

The dc motor and the mechanical load are modeled as shown by the equivalent circuit in Fig. 13-6a, in which the speed  $\omega_m(t)$  and the back-emf  $e_a(t)$  are assumed not to contain switching-frequency components. The electrical and the mechanical equations corresponding to Fig. 13-6a are

$$\bar{v}_a(t) = e_a(t) + R_a \bar{i}_a(t) + L_a \frac{d}{dt} \bar{i}_a(t), \quad e_a(t) = k_E \omega_m(t) \quad (13-7)$$

and

$$\frac{d}{dt} \omega_m(t) = \frac{\bar{T}_{em}(t) - T_L}{J_{eq}}, \quad \bar{T}_{em}(t) = k_T \bar{i}_a(t) \quad (13-8)$$

where the equivalent load inertia  $J_{eq}$  ( $= J_M + J_L$ ) is the sum of the motor inertia and the load inertia, and the damping is neglected (it could be combined with the load torque  $T_L$ ). In the simplified procedure presented here, the controller is designed to follow the changes in the torque, speed, and position reference values (and hence the load torque in Eq. 13-8 is assumed to be absent). Eqs. 13-7 and 13-8 can be expressed in the Laplace domain as

$$V_a(s) = E_a(s) + (R_a + sL_a)I_a(s) \quad (13-9)$$

or

$$I_a(s) = \frac{V_a(s) - E_a(s)}{R_a + sL_a}, \quad E_a(s) = k_E \omega_m(s) \quad (13-10)$$

We can define the Electrical Time Constant  $\tau_e$  as

$$\tau_e = \frac{L_a}{R_a} \quad (13-11)$$

Therefore, Eq. 13-10 can be written in terms of  $\tau_e$  as

$$I_a(s) = \frac{1/R_a}{1 + \frac{s}{1/\tau_e}} \{V_a(s) - E_a(s)\}, \quad E_a(s) = k_E \omega_m(s) \quad (13-12)$$

From Eq. 13-8, assuming the load torque to be absent in the design procedure,

$$\omega_m(s) = \frac{T_{em}(s)}{sJ_{eq}}, \quad T_{em}(s) = k_T I_a(s) \quad (13-13)$$

Eqs. 13-10 and 13-13 can be combined and represented in block-diagram form, as shown in Fig. 13-6b.

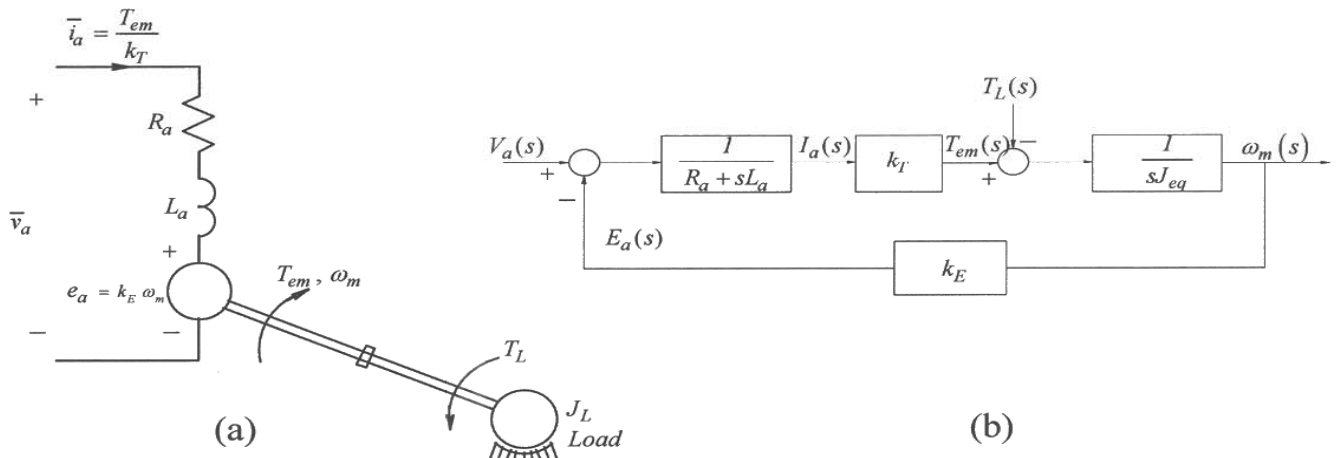


Fig 13-6 DC motor and mechanical load (a) equivalent circuit; (b) block diagram.

## 13-6 CONTROLLER DESIGN

The controller in the cascade control structure shown in Fig. 13-4 is designed with the objectives discussed in section 13-2 in mind. In the following section, a simplified design procedure is described.

### 13-6-1 PI Controllers

Motion control systems often utilize a proportional-integral (PI) controller, as shown in Fig. 13-7. The input to the controller is the error  $E(s) = X^*(s) - X(s)$ , which is the difference between the reference input and the measured output.

In Fig. 13-7, the proportional controller produces an output proportional to the error input:

$$V_{c,p}(s) = k_p E(s) \quad (13-14)$$

where  $k_p$  is the proportional-controller gain. In torque and speed loops, proportional controllers, if used alone, result in a steady-state error in response to step-change in the input reference. Therefore, they are used in combination with the integral controller described below.

In the integral controller shown in Fig. 13-7, the output is proportional to the integral of the error  $E(s)$ , expressed in the Laplace domain as

$$V_{c,i}(s) = \frac{k_i}{s} E(s) \quad (13-15)$$

where  $k_i$  is the integral-controller gain. Such a controller responds slowly because its action is proportional to the time integral of the error. The steady-state error goes to zero

for a step-change in input because the integrator action continues for as long as the error is not zero.

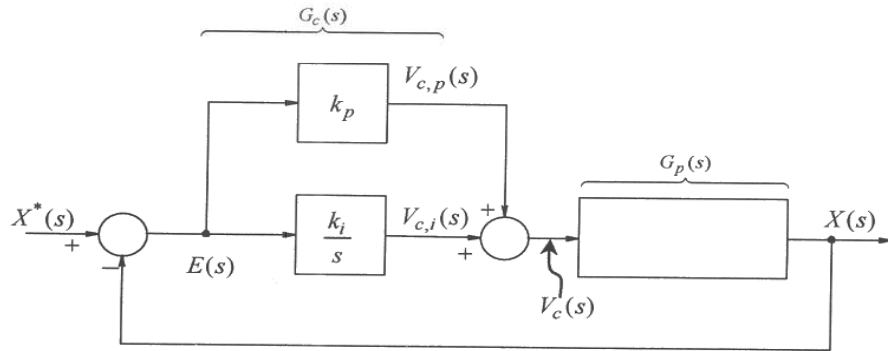


Figure 13-7 PI controller.

In motion-control systems, the P controllers in the position loop and the PI controllers in the speed and torque loop are often adequate. Therefore, we will not consider differential (D) controllers. As shown in Fig. 13-7,  $V_c(s) = V_{c,p}(s) + V_{c,i}(s)$ . Therefore, using Eqs. 13-14 and 13-15, the transfer function of a PI controller is

$$\frac{V_c(s)}{E(s)} = (k_p + \frac{k_i}{s}) = \frac{k_i}{s} [1 + \frac{s}{k_i/k_p}] \quad (13-16)$$

### 13-7 EXAMPLE OF A CONTROLLER DESIGN

In the following discussion, we will consider the example of a permanent-magnet dc-motor supplied by a switch-mode PWM dc-dc converter. The system parameters are given as follows in Table 13-1:

Table 13-1 DC-Motor Drive System

System Parameter	Value
$R_a$	$2.0\Omega$
$L_a$	$5.2\text{ mH}$
$J_{eq}$	$152 \times 10^{-6} \text{ kg} \cdot \text{m}^2$
$B$	0
$K_E$	$0.1V / (\text{rad} / \text{s})$
$k_T$	$0.1Nm / A$
$V_d$	$60V$
$\hat{V}_{tri}$	$5V$
$f_s$	$33\text{ kHz}$

We will design the torque, speed, and position feedback controllers (assuming a unity feedback) based on the small-signal analysis, in which the load nonlinearity and the effects of the limiters can be ignored.

### 13-7-1 The Design of the Torque (Current) Control Loop

As mentioned earlier, we will begin with the innermost loop in Fig. 13-8a (utilizing the transfer function block diagram of Fig. 13-6b to represent the motor-load combination, Fig. 13-5c to represent the PPU, and Fig. 13-7 to represent the PI controller).

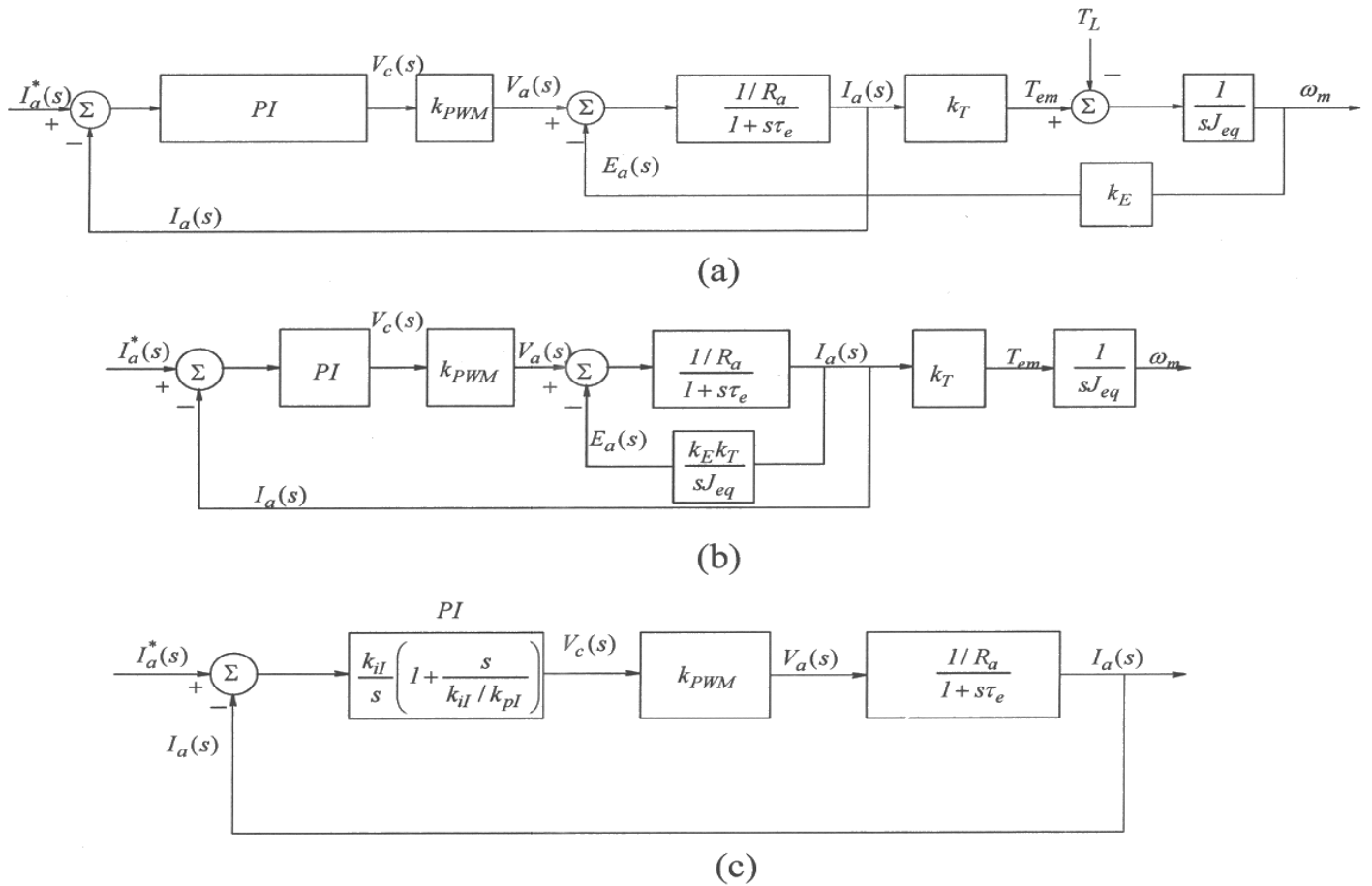


Fig. 13-8 Design of the torque control loop.

In permanent-magnet dc motors in which  $\phi_f$  is constant, the current and the torque are proportional to each other, related by the torque constant  $k_T$ . Therefore, we will consider the current to be the control variable because it is more convenient to use. Notice that there is a feedback in the current loop from the output speed. This feedback dictates the induced back-emf. Neglecting  $T_L$ , and considering the current to be the output,  $E_a(s)$  can be calculated in terms of  $I_a(s)$  in Fig. 13-8a as  $E_a(s) = \frac{k_T k_E}{s J_{eq}} I_a(s)$ . Therefore, Fig. 13-8a can be redrawn as shown in Fig. 13-8b. Notice that the feedback term depends

inversely on the inertia  $J_{eq}$ . Assuming that the inertia is sufficiently large to justify neglecting the feedback effect, we can simplify the block diagram, as shown in Fig. 13-8c.

The current-controller in Fig. 13-8c is a proportional-integral (PI) error amplifier with the proportional gain  $k_{pl}$  and the integral gain  $k_{il}$ . Its transfer function is given by Eq. 13-16. The subscript “I” refers to the current loop. The open-loop transfer function  $G_{I,OL}(s)$  of the simplified current loop in Fig. 13-8c is

$$G_{I,OL}(s) = \underbrace{\frac{k_{il}}{s} \left[ 1 + \frac{s}{k_{il}/k_{pl}} \right]}_{PI\text{-controller}} \underbrace{\frac{k_{PWM}}{PPU}}_{PPU} \underbrace{\frac{1/R_a}{1 + \frac{s}{1/\tau_e}}}_{motor} \quad (13-17)$$

To select the gain constants of the PI controller in the current loop, a simple design procedure, which results in a phase margin of 90 degrees, is suggested as follows:

- Select the zero  $(k_{il}/k_{pl})$  of the PI controller to cancel the motor pole at  $(1/\tau_e)$  due to the electrical time-constant  $\tau_e$  of the motor. Under these conditions,

$$\frac{k_{il}}{k_{pl}} = \frac{1}{\tau_e} \quad \text{or} \quad k_{pl} = \tau_e k_{il} \quad (13-18)$$

Cancellation of the pole in the motor transfer function renders the open-loop transfer function to be

$$G_{I,OL}(s) = \frac{k_{I,OL}}{s} \quad (13-19a)$$

where

$$k_{I,OL} = \frac{k_{il} k_{PWM}}{R_a} \quad (13-19b)$$

- In the open-loop transfer function of Eq. 13-19a, the crossover frequency  $\omega_{cl} = k_{I,OL}$ . We will select the crossover frequency  $f_{cl} (= \omega_{cl}/2\pi)$  of the current open-loop to be approximately one to two orders of magnitude smaller than the switching frequency of the power-processing unit in order to avoid interference in the control loop from the switching-frequency noise. Therefore, at the selected crossover frequency, from Eq. 13-19b,

$$k_{il} = \frac{\omega_{cl} R_a}{k_{PWM}} \quad (13-20)$$

This completes the design of the torque (current) loop, as illustrated by the example below, where the gain constants  $k_{pI}$  and  $k_{iI}$  can be calculated from Eqs. 13-18 and 13-20.

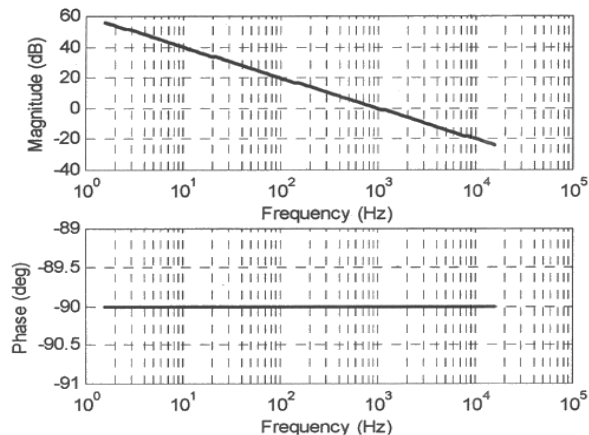
▲ **Example 13-1** Design the current loop for the example system of Table 13-1, assuming that the crossover frequency is selected to be 1 kHz.

*Solution* From Eq. 13-20, for  $\omega_{cI} = 2\pi \times 10^3 \text{ rad/s}$ ,

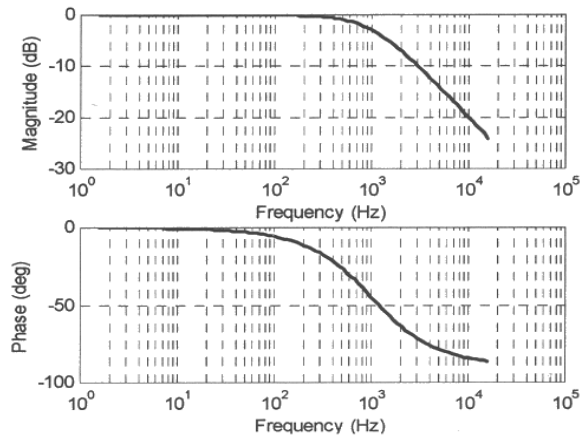
$$k_{iI} = \frac{\omega_{cI} R_a}{k_{PWM}} = 1050.0$$

and, from Eq. 13-18,

$$k_{pI} = k_{iI} \tau_e = k_{iI} \frac{L_a}{R_a} = 2.73 .$$



(a)



(b)

Figure 13-9 Frequency response of the current loop (a) open loop; (b) closed loop.

The open-loop transfer function is plotted in Fig. 13-9a, which shows that the crossover frequency is 1 kHz, as assumed previously. The closed-loop transfer function is plotted in Fig. 13-9b. ▲

### 13-7-2 The Design of the Speed Loop

We will select the bandwidth of the speed loop to be one order of magnitude smaller than that of the current (torque) loop. Therefore, the closed-current loop can be assumed ideal for design purposes and represented by unity, as shown in Fig. 13-10. The speed controller is of the proportional-integral (PI) type. The resulting open-loop transfer function  $G_{\Omega,OL}(s)$  of the speed loop in the block diagram of Fig. 13-10 is as follows, where the subscript “ $\Omega$ ” refers to the speed loop:

$$G_{\Omega,OL}(s) = \underbrace{\frac{k_{i\Omega}}{s} \left[ 1 + s / (k_{i\Omega} / k_{p\Omega}) \right]}_{PI \text{ controller}} \underbrace{\frac{1}{sJ_{eq}}}_{\text{current loop}} \underbrace{\frac{k_T}{sJ_{eq}}}_{\text{torque+inertia}} \quad (13-21)$$

Eq. 13-21 can be rearranged as

$$G_{\Omega,OL}(s) = \left( \frac{k_{i\Omega} k_T}{J_{eq}} \right) \frac{1 + s / (k_{i\Omega} / k_{p\Omega})}{s^2} \quad (13-22)$$

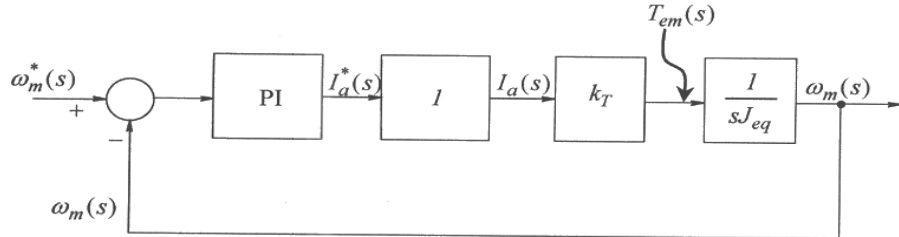


Fig 13-10 Block diagram of the speed loop.

This shows that the open-loop transfer function consists of a double pole at the origin. At low frequencies in the Bode plot, this double pole at the origin causes the magnitude to decline at the rate of  $-40$  db per decade while the phase angle is at  $-180^\circ$ . We can select the crossover frequency  $\omega_{c\Omega}$  to be one order of magnitude smaller than that of the current loop. Similarly, we can choose a reasonable value of the phase margin  $\phi_{pm,\Omega}$ . Therefore, Eq. 13-22 yields two equations at the crossover frequency:

$$\left| \left( \frac{k_{i\Omega} k_T}{J_{eq}} \right) \frac{1 + s / (k_{i\Omega} / k_{p\Omega})}{s^2} \right|_{s=j\omega_{c\Omega}} = 1 \quad (13-23)$$

and

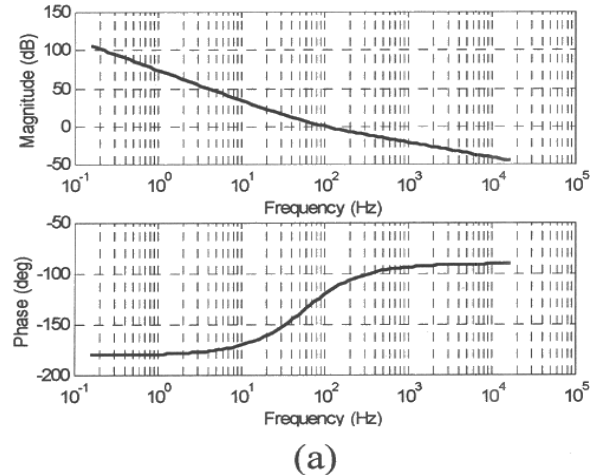
$$\angle \left( \left( \frac{k_{i\Omega} k_T}{J_{eq}} \right) \frac{1 + s / (k_{i\Omega} / k_{p\Omega})}{s^2} \right)_{s=j\omega_{c\Omega}} = -180^\circ + \phi_{pm,\Omega} \quad (13-24)$$

The two gain constants of the PI controller can be calculated by solving these two equations, as illustrated by the following example.

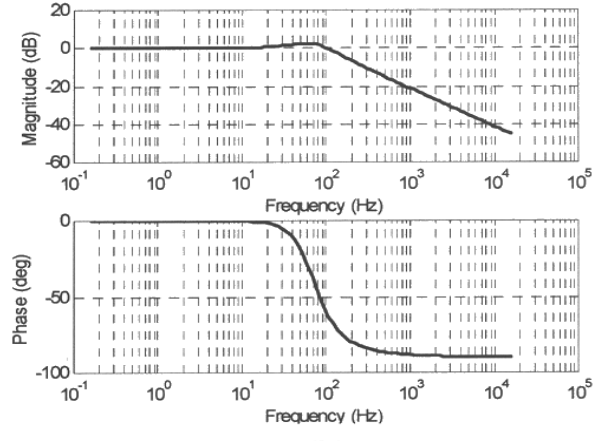
▲ **Example 13-2** Design the speed loop controller, assuming the speed loop crossover frequency to be one order of magnitude smaller than that of the current loop in Example 13-2; that is,  $f_{c\Omega} = 100 \text{ Hz}$ , and thus  $\omega_{c\Omega} = 628 \text{ rad/s}$ . The phase margin is selected to be  $60^\circ$ .

*Solution* In Eqs. 13-23 and 13-24, substituting  $k_T = 0.1 \text{ Nm/A}$ ,  $J_{eq} = 152 \times 10^{-6} \text{ kg} \cdot \text{m}^2$ , and  $\phi_{PM,\Omega} = 60^\circ$  at the crossover frequency, where  $s = j\omega_{c\Omega} = j628$ , we can calculate that

$$k_{p\Omega} = 0.827 \text{ and } k_{i\Omega} = 299.7.$$



(a)



(b)

Figure 13-11 Speed loop response (a) open loop; (b) closed loop.

The open- and the closed-loop transfer functions are plotted in Figs. 13-11a and 13-11b. ▲

### 13-7-3 The Design of the Position Control Loop

We will select the bandwidth of the position loop to be one order of magnitude smaller than that of the speed loop. Therefore, the speed loop can be idealized and represented by unity, as shown in Fig. 13-12. For the position controller, it is adequate to have only a proportional gain  $k_{p\theta}$  because of the presence of a true integrator ( $1/s$ ) in Fig. 13-12 in the open-loop transfer function. This integrator will reduce the steady state error to zero for a step-change in the reference position. With this choice of the controller, and with the closed-loop response of the speed loop assumed to be ideal, the open-loop transfer function  $G_{\theta,OL}(s)$  is

$$G_{\theta,OL}(s) = \frac{k_{\theta}}{s} \quad (13-25)$$

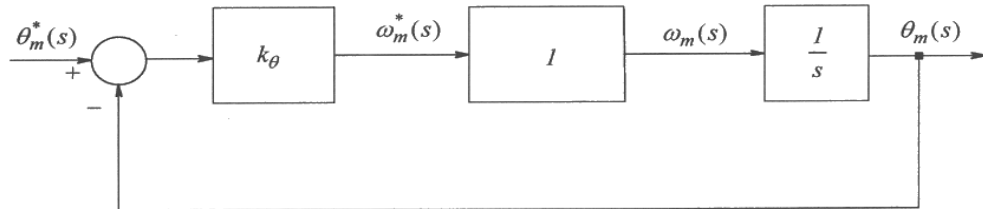


Fig 13-12 Block diagram of position loop.

Therefore, selecting the crossover frequency  $\omega_{c\theta}$  of the open-loop allows  $k_{\theta}$  to be calculated as

$$k_{\theta} = \omega_{c\theta} \quad (13-26)$$

▲ **Example 13-3** For the example system of Table 13-1, design the position-loop controller, assuming the position-loop crossover frequency to be one order of magnitude smaller than that of the speed loop in Example 13-3 (that is,  $f_{c\theta} = 10 \text{ Hz}$  and  $\omega_{c\theta} = 62.8 \text{ rad/s}$ ).

*Solution* From Eq. 13-26,  $k_\theta = \omega_{c\theta} = 62.8 \text{ rad/s}$ .

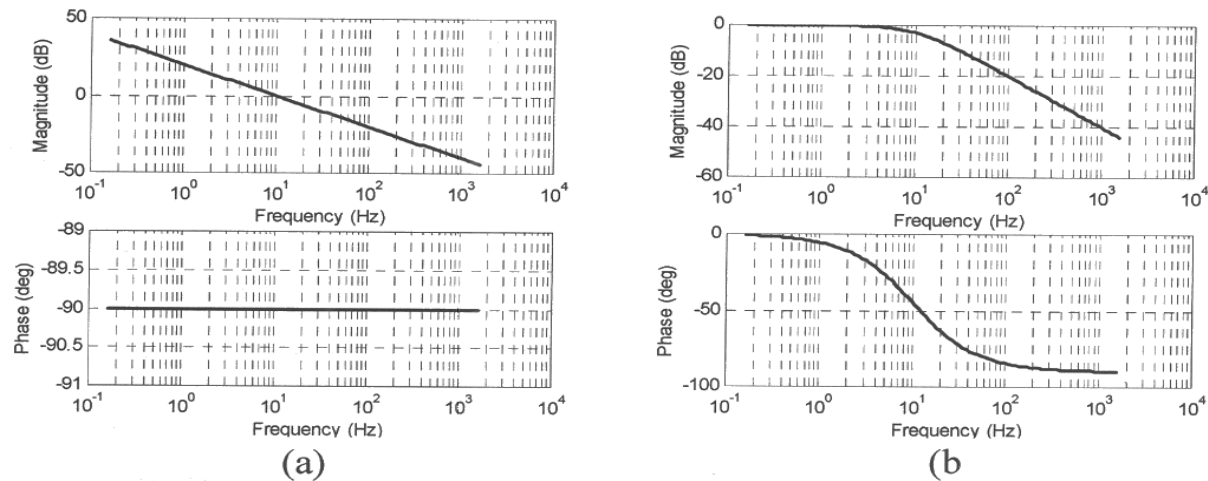


Figure 13-13 Position loop response (a) open loop; (b) closed loop.

The open- and the closed-loop transfer functions are plotted in Figs. 13-13a and 13-13b. ▲

## REFERENCE

1. M. Kazmierkowski and H. Tunia, "Automatic Control of Converter-Fed Drives," Elsevier, 1994, 559 pages.

## PROBLEMS

- 13-1 In a unity feedback system, the open-loop transfer function is of the form

$$G_{OL}(s) = \frac{k}{1 + s/\omega_p}. \text{ Calculate the bandwidth of the closed-loop transfer function.}$$

How does the bandwidth depend on  $k$  and  $\omega_p$ ?

- 13-2 In a feedback system, the forward path has a transfer function of the form

$$G(s) = \frac{k}{1 + s/\omega_p}, \text{ and the feedback path has a gain of } k_{fb} \text{ which is less than unity. Calculate the bandwidth of the closed-loop transfer function. How does the bandwidth depend on } k_{fb}?$$

- 13-3 In designing the torque loop of Example 13-1, include the effect of the back-emf, shown in Fig. 13-8a. Design a PI controller for the same open-loop crossover frequency and for a phase margin of 60 degrees. Compare your results with those in Example 13-1.

- 13-4 In designing the speed loop of Example 13-2, include the torque loop by a first-order transfer function based on the design in Example 13-1. Design a PI controller for the same open-loop crossover frequency and the same phase margin as in Example 13-2 and compare results.
- 13-5 In designing the position loop of Example 13-3, include the speed loop by a first-order transfer function based on the design in Example 13-2. Design a P-type controller for the same open-loop crossover frequency as in Example 13-3 and for a phase margin of 60 degrees. Compare your results with those in Example 13-3.
- 13-6 In an actual system in which there are limits on the voltage and current that can be supplied, why and how does the initial steady-state operating point make a difference for large-signal disturbances?
- 13-7 Obtain the time response of the system designed in Example 13-2, in terms of the change in speed, for a step-change of the load-torque disturbance.
- 13-8 Obtain the time response of the system designed in Example 13-3, in terms of the change in position, for a step-change of the load-torque disturbance.
- 13-9 In the example system of Table 13-1, the maximum output voltage of the dc-dc converter is limited to  $60\text{ V}$ . Assume that the current is limited to  $8\text{ A}$  in magnitude. How do these two limits impact the response of the system to a large step-change in the reference value?
- 13-10 In Example 13-2, design the speed-loop controller, without the inner current loop, for the same crossover frequency and phase margin as in Example 13-2. Compare results with the system of Example 13-2.

# Chapter 14

## THYRISTOR CONVERTERS

### 14-1 INTRODUCTION

Historically, thyristor converters were used to perform tasks that are now performed by switch-mode converters discussed in previous chapters. Thyristor converters are now typically used in utility applications at very high power levels. In this chapter, we will examine the operating principles of thyristor-based converters.

### 14-2 Thyristors (SCRs)

Thyristors are a device that can be considered as a controlled diode. Like diodes, they are available in very large voltage and current ratings, making them attractive for use in applications at very high power levels.

Thyristors, shown by their symbol in Fig. 14-1a are sometimes referred to by their trade name of Silicon Controlled Rectifiers (SCRs). These are 4-layer (p-n-p-n) devices as shown in Fig. 14-1b. When a reverse ( $v_{AK} < 0$ ) voltage is applied, the flow of current is blocked by the junctions pn1 and pn3. When a forward ( $v_{AK} > 0$ ) polarity voltage is applied and the gate terminal is open, the flow of current is blocked by the junction pn2, and the thyristor is considered to be in a forward-blocking state. In this forward-blocking state, applying a small positive voltage to the gate with respect to the cathode for a short interval supplies a pulse of gate current  $i_G$  that latches the thyristor in its on state, and subsequently the gate-current pulse can be removed.

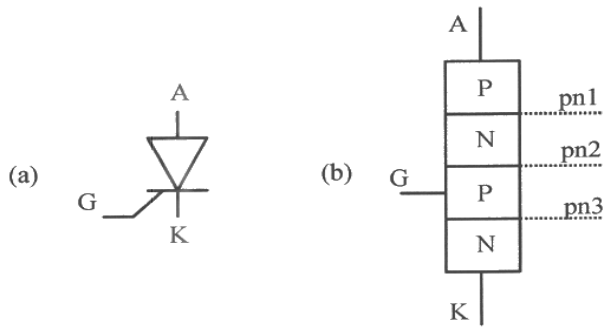


Figure 14-1 Thyristors.

The operation of thyristors is illustrated by means of a simple  $R-L$  circuit in Fig. 14-2a. At  $\omega t = 0$ , the positive-half-cycle of the input voltage begins, beyond which a forward

voltage appears across the thyristor (anode  $A$  is positive with respect to cathode  $K$ ), and if the thyristor were a diode, a current would begin to flow in this circuit. This instant  $\omega t = 0$  in this circuit we will refer as the instant of natural conduction. With the thyristor forward blocking, the start of conduction can be controlled (delayed) with respect to  $\omega t = 0$  by a delay angle  $\alpha$  at which instant the gate-current pulse is applied. Once in the conducting state, the thyristor behaves like a diode with a very small voltage drop of the order of 1 to 2 volts across it (we will idealize it as zero), and the  $R-L$  load voltage  $v_d$  equals  $v_s$ , as shown in Fig. 14-2b.

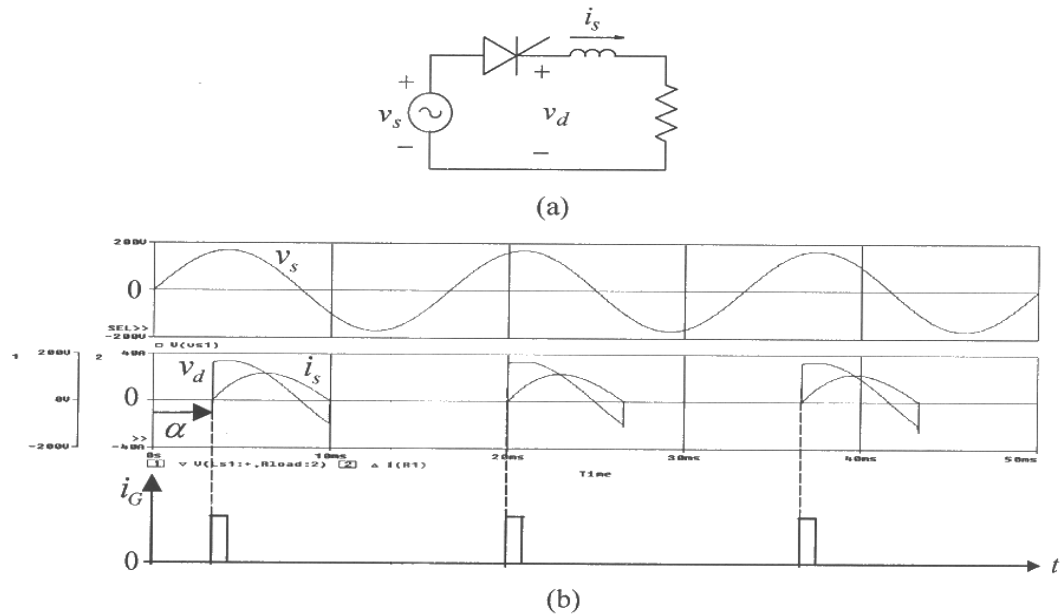


Figure 14-2 A simple thyristor circuit.

The current waveform in Fig. 14-2b show that due to the inductor, the current comes to zero sometime in the negative half-cycle of the input voltage. The current through the thyristor cannot reverse and remains zero for the remainder of the input voltage cycle. In the next voltage cycle, the current conduction again depends on the instant during the positive half-cycle at which the gate pulse is applied. By controlling the delay angle (or the phase control as it is often referred), we can control the average voltage  $v_d$  across the  $R-L$  load. This principle can be extended to the practical circuits discussed below.

### 14-3 Single-Phase, Phase-Controlled Thyristor Converters

Fig. 14-3a shows a commonly used Full-Bridge phase-controlled converter for controlled rectification of the single-phase utility voltage. To understand the operating principle, it is redrawn as in Fig. 14-3b, where the ac-side inductance  $L_s$  is ignored and the dc-side load is represented as drawing a constant current  $I_d$ . The waveforms are shown in Fig. 14-4.

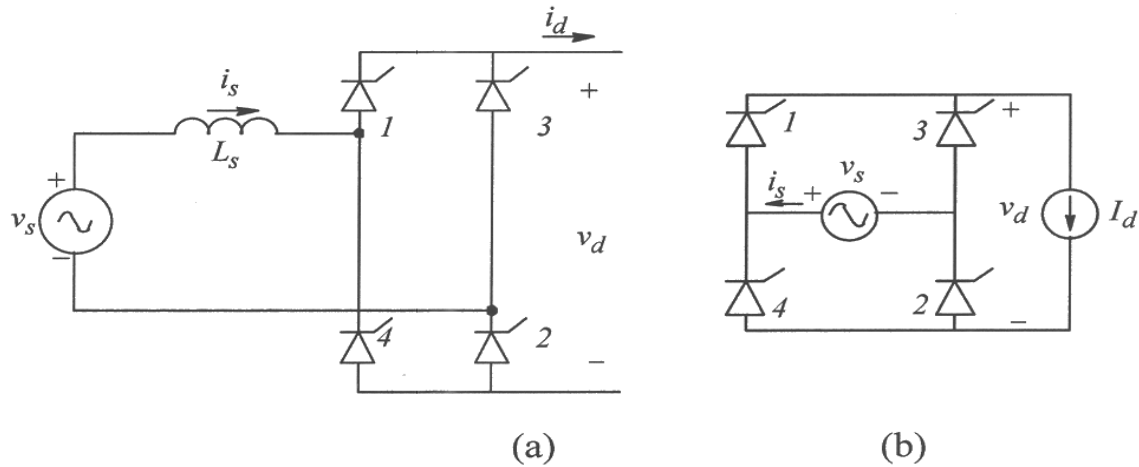


Figure 14-3 Full-Bridge, single-phase thyristor converter.

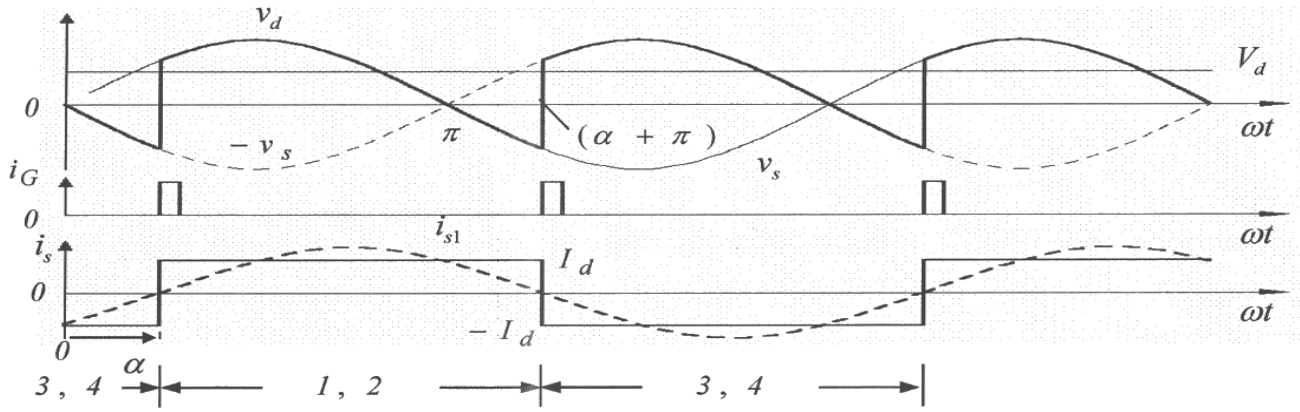


Figure 14-4 Single-phase thyristor converter waveforms.

Thyristors 1 and 2, and thyristors 3 and 4 are treated as two pairs, where each thyristor pair is supplied gate pulses delayed by an angle  $\alpha$  with respect to its instant of natural conduction;  $\omega t = 0^\circ$  for thyristors 1 and 2, and  $\omega t = 180^\circ$  for thyristors 3 and 4, as shown in Fig. 14-4. In the positive half-cycle of the input voltage, thyristors 1 and 2 are forward-blocking until they are gated at  $\omega t = \alpha$  when they immediately begin to conduct, and thyristors 3 and 4 become reverse-blocking. In this state,

$$v_d(t) = v_s(t) \quad \text{and} \quad i_s(t) = I_d \quad \alpha < \omega t \leq \alpha + \pi \quad (14-1)$$

These relationships hold true until  $\alpha + \pi$  in the negative half-cycle of the input voltage, when thyristors 3 and 4 are gated and begin conducting. In this state,

$$v_d(t) = -v_s(t) \quad \text{and} \quad i_s(t) = -I_d \quad \alpha + \pi < \omega t \leq \alpha + 2\pi \quad (14-2)$$

which holds true for one half-cycle, until the next half-cycle begins with the gating of thyristors 1 and 2.

Assuming the input ac voltage to be sinusoidal, the average value  $V_d$  of the voltage across the dc-side of the converter can be obtained by averaging the  $v_d(t)$  waveform in Fig. 14-4 over one half-cycle during  $\alpha < \omega t \leq \alpha + \pi$ :

$$V_d = \frac{1}{\pi} \int_{\alpha}^{\alpha+\pi} \hat{V}_s \sin \omega t \cdot d(\omega t) = \frac{2}{\pi} \hat{V}_s \cos \alpha \quad (14-3)$$

On the ac-side, the input current  $i_s$  waveform is shifted by an angle  $\alpha$  with respect to the input voltage as shown in Fig. 14-4, and the fundamental-frequency component  $i_{s1}(t)$  has a peak value of

$$\hat{I}_{s1} = \frac{4}{\pi} I_d \quad (14-4)$$

In terms of voltage and current peak values, the power drawn from the ac-side is

$$P = \frac{1}{2} \hat{V}_s \hat{I}_{s1} \cos \alpha \quad (14-5)$$

Assuming no power loss in the thyristor converter, the input power equals the power to the dc-side of the converter. Using Eqs. 14-3 and 14-4, we can reconfirm the following relationship:

$$P = \frac{1}{2} \hat{V}_s \hat{I}_{s1} \cos \alpha = V_d I_d \quad (14-6)$$

Power flow can be controlled by the delay angle  $\alpha$ ; increasing it toward  $90^\circ$  reduces the average dc-side voltage  $V_d$  while simultaneously shifting the input current  $i_s(t)$  waveform farther away with respect to the input voltage waveform. The dc voltage as a function of  $\alpha$  is plotted in Fig. 14-5a and the corresponding power direction is shown in Fig. 14-5b. The waveforms in Fig. 14-4 show that for the delay angle  $\alpha$  in a range of  $0^\circ$  to  $90^\circ$ ,  $V_d$  has a positive value as plotted in Figs. 14-5a and b, and the converter operates as a rectifier, with power flowing from the ac-side to the dc-side.

Delaying the gating pulse such that  $\alpha$  is greater than  $90^\circ$  in Fig. 14-4 makes  $V_d$  in Eq. 14-3 negative, and the converter operates as an inverter as shown in Fig. 14-5b, with power flowing from the dc-side to the ac-side. In practice, the upper limit on  $\alpha$  in the inverter is below  $180^\circ$ , for example  $160^\circ$  to avoid a phenomenon known as the commutation failure, where the current fails to commutate fully from the conducting thyristor pair to the next pair, prior to the instant beyond which the conducting pair keeps

on conducting for another half-cycle. This commutation-failure phenomena is fully described in [1].

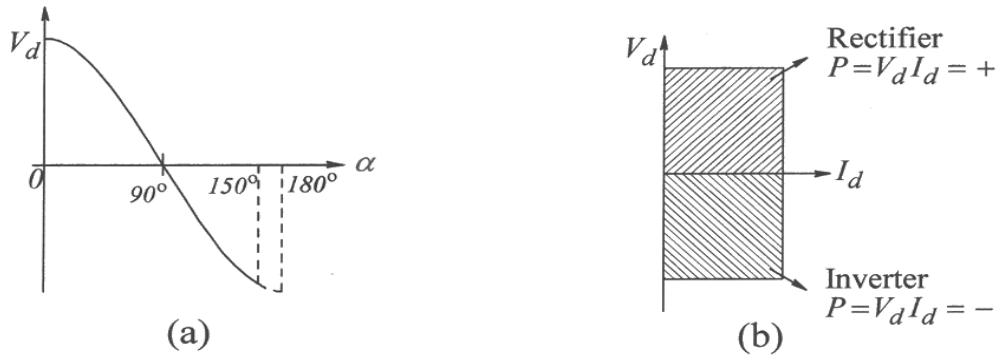


Fig. 14-5 Effect of the delay angle  $\alpha$ .

### 14-3-1 The Effect of $L_s$ on Current Commutation

Previously, our assumption was that the ac-side inductance  $L_s$  equals zero. In the presence of this inductance, the input current takes a finite amount of time to reverse its direction, as the current “commutes” from one thyristor pair to the next.

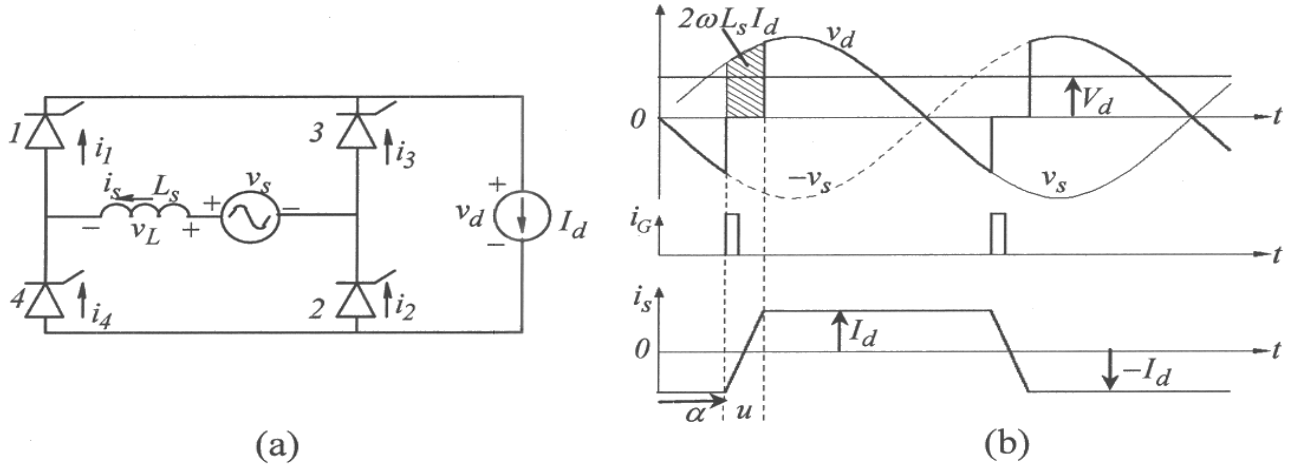


Figure 14-6 Effect of  $L_s$  on Current Commutation.

From basic principles, we know that changing the current through the inductor  $L_s$  in the circuit of Fig. 14-6a requires a finite amount of volt-seconds. The dc-side is still represented by a dc current  $I_d$ . The waveforms are shown in Fig. 14-6b, where thyristors 3 and 4 are conducting prior to  $\omega t = \alpha$ , and  $i_s = -I_d$ .

At  $\omega t = \alpha$ , thyristors 1 and 2, which have been forward blocking, are gated and hence they immediately begin to conduct. However, the current through them doesn't jump instantaneously as in the case of  $L_s = 0$  where  $i_s$  instantaneously changed from  $(-I_d)$  to

$(+I_d)$ . With a finite  $L_s$ , during a short interval called the commutation interval  $u$ , all thyristors conduct, applying  $v_s$  across  $L_s$  in Fig. 14-6a. The volt-radians needed to change the inductor current from  $(-I_d)$  to  $(+I_d)$  can be calculated by integrating the inductor voltage  $v_L (= L_s \cdot di_s / dt)$  from  $\alpha$  to  $(\alpha + u)$ , as follows:

$$\int_{\alpha}^{\alpha+u} v_L d(\omega t) = L_s \int_{\alpha}^{\alpha+u} \frac{di_s}{dt} d(\omega t) = \omega L_s \int_{-I_d}^{I_d} di_s = \omega L_s (2I_d) \quad (14-7)$$

The above volt-radians are “lost” from the integral of the dc-side voltage waveform in Fig. 14-6b every half-cycle, as shown by the shaded area in Fig. 14-6b. Therefore, dividing the volt-radians in Eq. 14-7 by the  $\pi$  radians each half-cycle, the voltage drop in the dc-side voltage is

$$\Delta V_d = \frac{2}{\pi} \omega L_s I_d \quad (14-8)$$

This voltage is lost from the dc-side average voltage in the presence of  $L_s$ . Therefore, the average voltage is smaller than that in Eq. 14-3:

$$V_d = \frac{2}{\pi} V_s \cos \alpha - \frac{2}{\pi} \omega L_s I_d \quad (14-9)$$

We should note that the voltage drop in the presence of  $L_s$  doesn't mean a power loss in  $L_s$ ; it simply means a reduction in the voltage available on the dc-side.

#### 14-4 THREE-PHASE, FULL-BRIDGE THYRISTOR CONVERTERS

Three-phase Full-Bridge converters use six thyristors, as shown in Fig. 14-7a. A simplified converter for initial analysis is shown in Fig. 14-7b, where the ac-side inductance  $L_s$  is assumed zero, thyristors are divided into a top group and a bottom group, similar to the three-phase diode rectifiers, and the dc-side is represented by a current source  $I_d$ .

The converter waveforms, where the delay angle  $\alpha$  (measured with respect the instant at which phase voltage waveforms cross each other) is zero are similar to that in diode rectifiers discussed in Chapter 5 (see Figs. 5-11 and 5-12). The average dc voltage is as calculated in Eq. 5-23, where  $\hat{V}_{LL}$  is the peak value of the ac input voltage:

$$V_{do} = \frac{1}{\pi/3} \int_{-\pi/6}^{\pi/6} \hat{V}_{LL} \cos \omega t \cdot d(\omega t) = \frac{3}{\pi} \hat{V}_{LL} \quad (14-10)$$

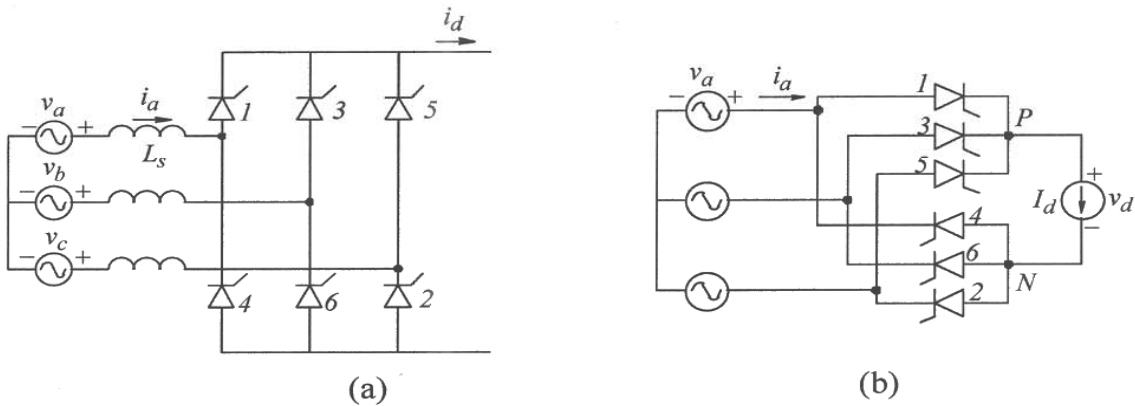


Figure 14-7 Three-phase Full-Bridge thyristor converter.

Delaying the gate pulses to the thyristors by an angle  $\alpha$  measured with respect to their instants of natural conduction, the waveforms are shown in Fig. 14-8, where  $L_s = 0$ .

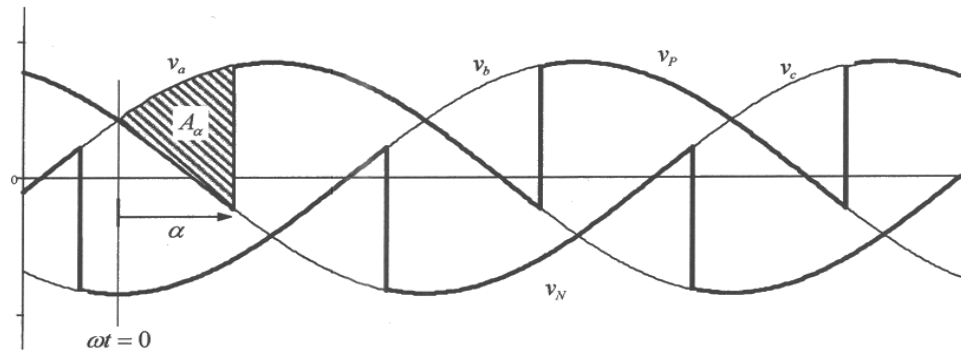


Figure 14-8 Waveforms with  $L_s = 0$ .

In the dc-side output voltage waveforms, the area  $A_\alpha$  corresponds to “volt-radians loss” due to delaying the gate pulses by  $\alpha$  every  $\pi/3$  radian. Assuming the time-origin as shown in Fig. 14-8 at the instant at which the phase voltage waveforms cross, the line-line voltage  $v_{ac}$  waveform can be expressed as  $\hat{V}_{LL} \sin \omega t$ . Therefore from Fig. 14-8, the drop  $\Delta V_\alpha$  in the average dc-side voltage can be calculated as

$$\Delta V_\alpha = \frac{1}{\pi/3} \underbrace{\int_0^\alpha \hat{V}_{LL} \sin \omega t \cdot d(\omega t)}_{A_\alpha} = \frac{3}{\pi} \hat{V}_{LL} (1 - \cos \alpha) \quad (14-11)$$

#### 14-4-1 Effect of $L_s$

As shown in the waveforms of Fig. 14-9, the average dc output voltage due to the presence of  $L_s$  is reduced by the area  $A_u$  every  $\pi/3$  radian. During the commutation interval  $u$ , from  $\alpha$  to  $\alpha + u$ , the instantaneous dc voltage is reduced due to the voltage drop across the inductance in series with the thyristor to which the current is

commutating from 0 to  $(+I_d)$ . Using the procedure in Eq. 14-7 for single-phase converters,

$$A_u = \int_{\alpha}^{\alpha+u} v_L d(\omega t) = \omega L_s \int_0^{I_d} di_s = \omega L_s I_d \quad (14-12)$$

and therefore the voltage drop due to the presence of  $L_s$  is

$$\Delta V_u = \frac{A_u}{\pi/3} = \frac{3}{\pi} \omega L_s I_d \quad (14-13)$$

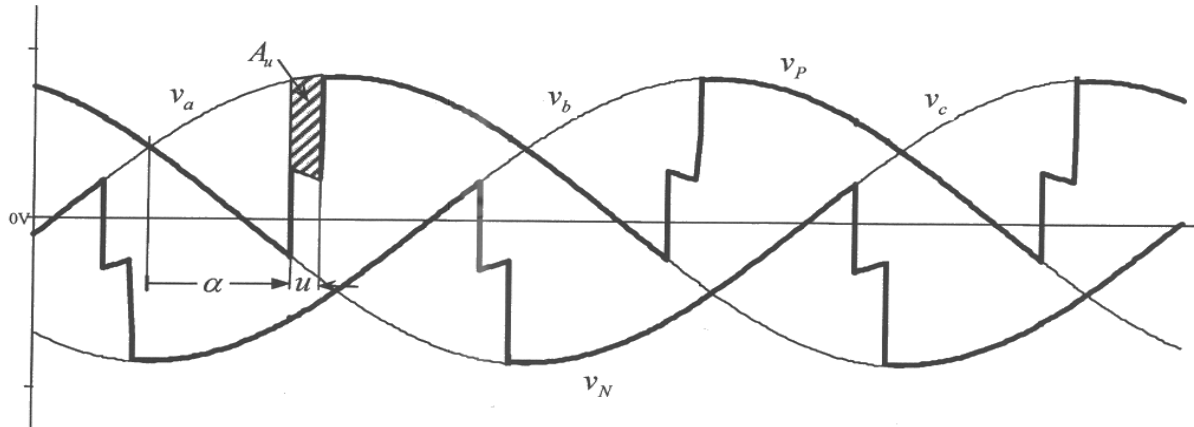


Figure 14-9 Waveforms with  $L_s$ .

Therefore, the dc-side output voltage can be written as

$$V_d = V_{do} - \Delta V_\alpha - \Delta V_u \quad (14-14)$$

Substituting results from Eqs. 14-10, 14-11, and 14-13 into Eq. 14-14

$$V_d = \frac{3}{\pi} \hat{V}_{LL} \cos \alpha - \frac{3}{\pi} \omega L_s I_d \quad (14-15)$$

Similar to single-phase converters, three-phase thyristor converters go into inverter mode with the delay angle  $\alpha$  exceeding  $90^\circ$ . In the inverter mode, the upper limit on  $\alpha$  is less than  $180^\circ$  to avoid commutation failure, just like in single-phase converters. Further details on thyristor converters can be found in Reference [1].

## 14-5 Current-Link Systems

Thyristors are available in very large current and voltage ratings of several kAs and several kVs that can be connected in series. In addition, thyristor converters can block voltages of both polarities but conduct current only in the forward direction. This capability has led to the interface realized by thyristor-converters with a dc-current link in the middle, as shown in Fig. 14-10. Unlike in voltage-link systems, the transfer of power in current-link systems can be reversed in direction by reversing the voltage polarity of the dc-link. This structure is used at very high power levels, at tens of hundreds of MWs, for example in High Voltage DC Transmission (HVDC).

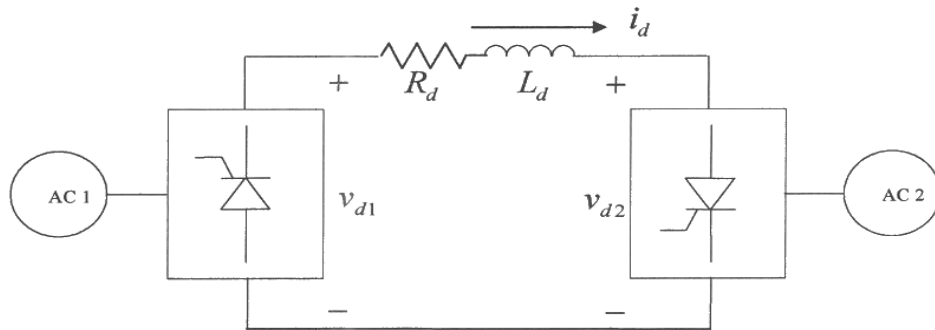


Figure 14-10 Block diagram of current-link systems.

Thyristors in these two converters shown in Fig. 14-10 are connected to allow the flow of current in the dc-link by thyristors in converter 1 pointing up, and the thyristors in converter 2 connected to point downward. In Fig. 14-10, subscripts 1 and 2 refer to systems 1 and 2 and  $R_d$  is the resistance of the dc-link inductance. Assuming each converter a six-pulse thyristor converter as discussed previously,

$$V_{d1} = \frac{3}{\pi} \hat{V}_{LL1} \cos \alpha_1 - \frac{3}{\pi} \omega L_{s1} I_d \quad (14-16)$$

$$V_{d2} = \frac{3}{\pi} \hat{V}_{LL2} \cos \alpha_2 - \frac{3}{\pi} \omega L_{s2} I_d \quad (14-17)$$

By controlling the delay angles  $\alpha_1$  and  $\alpha_2$  in a range of  $0^\circ$  to  $180^\circ$  (practically, this value is limited to approximately  $150^\circ$ ), the average voltage and the average current in the system of Fig. 14-10 can be controlled, where current flow through the dc-link can be expressed as

$$I_d = \frac{V_{d1} + V_{d2}}{R_d} \quad (14-18)$$

where the dc-link resistance  $R_d$  is generally very small. In such a system, for the power flow from system 1 to system 2,  $V_{d2}$  is made negative by controlling  $\alpha_2$  such that it operates as an inverter and establishes the voltage of the dc-link. The converter 1 is operated as a rectifier at a delay angle  $\alpha_1$  such that it controls the current in the dc-link. The converse is true for these two converters if the power is to flow from system 2 to system 1.

The above discussion of current-link systems shows the operating principle behind HVDC transmission systems discussed in the next chapter, where using transformers, six-pulse thyristor converters are connected in series on the dc-side and in parallel on the ac-side to yield higher effective pulse number.

## REFERENCE

1. N. Mohan, T. M. Undeland, and W.P. Robbins, *Power Electronics: Converters, Applications and Design*, 3<sup>rd</sup> Edition, Wiley & Sons, New York, 2003.

## PROBLEMS

### Single-Phase Thyristor Converters

In a single-phase thyristor converter,  $V_s = 120V(rms)$  at  $60\text{Hz}$ , and  $L_s = 3\text{mH}$ . The delay angle  $\alpha = 30^\circ$ . This converter is supplying  $1\text{kW}$  of power. The dc-side current  $i_d$  can be assumed purely dc.

- 14-1 Calculate the commutation angle  $u$ .
- 14-2 Draw the waveforms for the converter variables.
- 14-3 Calculate the DPF, %THD in the input current, and the PF of operation of this converter.

### Three-Phase Thyristor Converters

In a three-phase thyristor converter,  $V_{LL} = 460V(rms)$  at  $60\text{Hz}$ , and  $L_s = 5\text{mH}$ . The delay angle  $\alpha = 30^\circ$ . This converter is supplying  $5\text{kW}$  of power. The dc-side current  $i_d$  can be assumed purely dc.

- 14-4 Calculate the commutation angle  $u$ .
- 14-5 Draw the waveforms for the converter variables.
- 14-6 Calculate the DPF, %THD in the input current, and the PF of operation of this converter.

# Chapter 15

## UTILITY APPLICATIONS OF POWER ELECTRONICS

### 15-1 INTRODUCTION

Power electronics applications in utility systems are growing very rapidly, which promise to change the landscape of future power systems in terms of generation, operation and control. The goal of this chapter is to briefly present an overview of these applications to prepare students for new challenges in the deregulated utility environment and to motivate them to take further courses in this field, where a separate advanced-level graduate course is designed, for example at the University of Minnesota, to discuss these topics in detail.

In discussing these applications, we will observe that the power electronic converters are the same or modifications of those that we have already discussed in earlier chapters. Therefore, within the scope of this book, it will suffice to discuss these applications in terms of the block diagrams of various converters. These utility applications of power electronics can be categorized as follows:

- Distributed Generation (DG)
  - Renewable Resources (Wind, Photovoltaic, etc.)
  - Fuel Cells and Micro-Turbines
  - Storage - Batteries, Super-conducting Magnetic Storage, Flywheels
- Power Electronic Loads - Adjustable Speed Drives
- Power Quality Solutions
  - Dual Feeders
  - Uninterruptible Power Supplies
  - Dynamic Voltage Restorers
- Transmission and Distribution (T&D)
  - High Voltage DC (HVDC) and HVDC-Light
  - Flexible AC Transmission (FACTS)
    - Shunt Compensation
    - Series Compensation
    - Static Phase Angle Control and Unified Power Flow Controllers

## 15-2 POWER SEMICONDUCTOR DEVICES AND THEIR CAPABILITIES [1]

Fig. 15-1a shows the commonly used symbols of power devices. The power handling capabilities and switching speeds of these devices are indicated in Fig. 15-1b. All these devices allow current flow only in their forward direction (the intrinsic anti-parallel diode of MOSFETs can be explained separately). Transistors (intrinsically or by design) can block only the forward polarity voltage, whereas thyristors can block both forward and reverse polarity voltages. Diodes are uncontrolled devices, which conduct current in the forward direction and block a reverse voltage. At very high power levels, integrated-gate controlled thyristors (IGCTs), which have evolved from the gate-turn-off thyristors, are used. Thyristors are semi-controlled devices that can switch-on at the desired instant in their forward-blocking state, but cannot be switched off from their gate and hence rely on the circuit in which they are connected to switch them off. However, thyristors are available in very large voltage and current ratings.

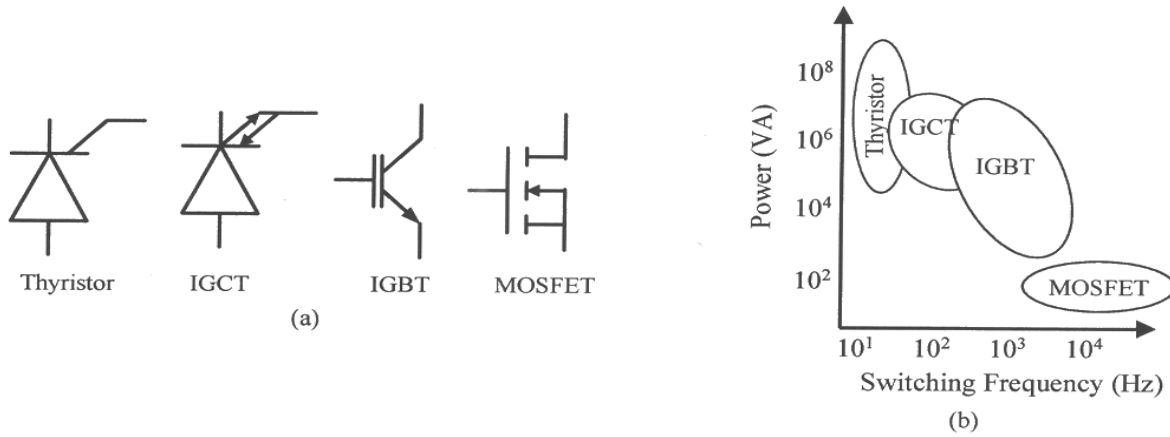


Figure 15-1 Power semiconductor devices.

## 15-3 CATEGORIZING POWER ELECTRONIC SYSTEMS

In a very broad sense, the role of power electronics in these power system applications can be categorized as follows:

### 15-3-1 Solid-State Switches

By connecting two thyristors in anti-parallel (back-to-back) as shown in Fig. 15-2, it is possible to realize a solid-state switch which can conduct current in both directions, and turn-on or turn-off in an ac circuit with a delay of no more than one-half the line-frequency cycle. Such switches are needed for applications such as dual feeders, shunt-compensation for injecting reactive power at a bus for voltage control, and series-compensation of transmission lines.

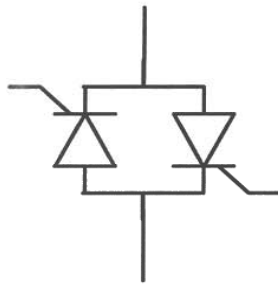


Figure 15-2 Back-to-back thyristors to act as a solid-state switch.

### 15-3-2 Converters as an Interface

Power electronic converters provide the needed interface between the electrical source, often the utility, and the load, as shown in Fig. 15-3. The electrical source and the electrical load can, and often do, differ in frequency, voltage amplitudes and the number of phases. The power electronics interface allows the transfer of power from the source to the load in the most energy efficient manner, in which it is possible for the source and load to reverse roles. These interfaces can be classified as below.

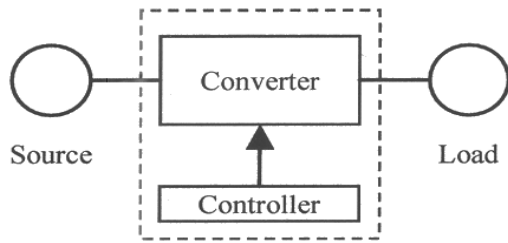


Figure 15-3 Power electronics interface.

#### 15-3-2-1 Voltage-Link Systems

The semiconductor devices such as transistors of various types and diodes can only block forward-polarity voltages. These devices with only unipolar voltage-blocking capability have led to the structure with two converters, where the dc ports of these two converters are connected to each other with a parallel capacitor forming a dc-link in Fig. 15-4, across which the voltage polarity does not reverse, thus allowing unipolar voltage-handling transistors to be used within these converters. The transfer of power can be reversed in direction by reversing the direction of currents associated with the dc-link system.

Voltage-link converters consist of switching power-poles as the building blocks, which can synthesize the desired output by means of Pulse Width Modulation (PWM) and have the bi-directional power flow capability. Such switching power-poles can be modeled by means of an ideal transformer with a controllable turns-ratio, as discussed in Chapter 12.

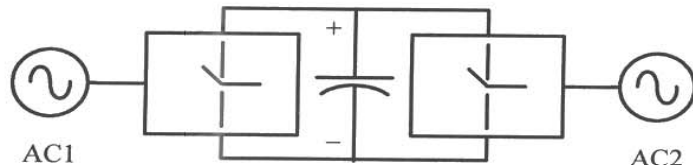


Fig. 15-4 Block diagram of the voltage-link systems.

### 15-3-2-2 Current-Link Systems

Thyristors can block voltages of both polarities but conduct current only in the forward direction. This capability has led to the interface realized by thyristor-converters with a dc-current link in the middle, as shown in Fig. 15-5. The transfer of power can be reversed in direction by reversing the voltage polarity of the dc-link, but the currents in the link remain in the same direction. This structure is used at very high power levels, at tens of hundreds of MWs, for example in High Voltage DC Transmission (HVDC).

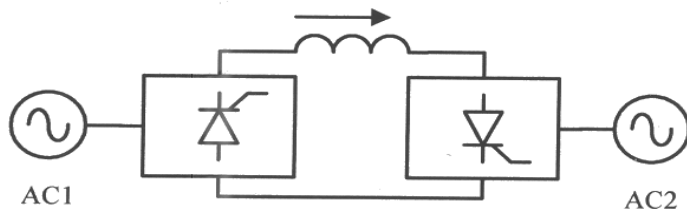


Figure 15-5 Block diagram of the current-link systems.

In the following sections, various utility applications and the role of power electronics in them are examined further.

## 15-4 DISTRIBUTED GENERATION (DG) APPLICATIONS

Distributed generation, shown in Fig. 15-6 from the control perspective, promises to change the landscape of how power systems of the future will be operated and controlled. These generators may have decentralized (local) control, in addition to a central supervisory control.

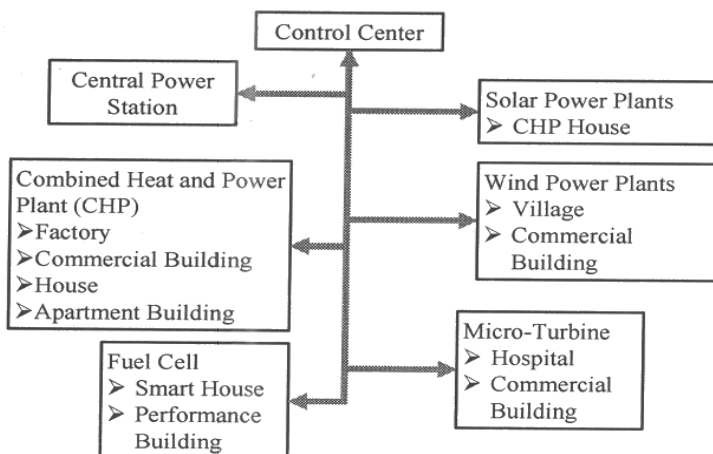


Figure 15-6 Distributed Generation (DG) systems.

There is a move away from large central power plants towards distributed generation due to environmental and economic reasons. Renewable resources such as wind and photovoltaic systems are growing in their popularity. There are proposals to place highly efficient small-scale power plants, based on fuel cells and micro-turbines, near load centers to simultaneously avoid transmission congestion and line losses. Many of distributed generation systems are discussed below.

### 15-4-1 Wind-Electric Systems

Wind energy is the fastest growing energy resource in the world. In 2002, the amount of installed wind energy in the world reached nearly 30,000 MW, and the installed wind energy in the U.S. alone increased by 66% in 2001. This remarkable growth is spurred by a combination of environmental concerns, decreasing costs of wind electric systems, and financial incentives for wind park developers.

There are many schemes for harnessing wind energy, out of which those using doubly-fed induction generators are enjoying increased popularity. As shown in Fig. 15-7, in this system, the stator which produces most of the power is connected directly to the grid. The rotor windings are accessible through slip-rings and brushes to a power electronic converter system, which supplies the rotor current. By injecting currents into the rotor, the machine can be made to act like a generator at both sub-synchronous and super-synchronous speeds. The converter rating is about 15% of the rated power, for example, in the 750 kW doubly-fed induction machines used in the southwestern Minnesota for wind-electric systems, only 150 kW flows through the rotor, and the rest through the stator. Injecting current into the rotor provides control over the real and the reactive power (leading or lagging).

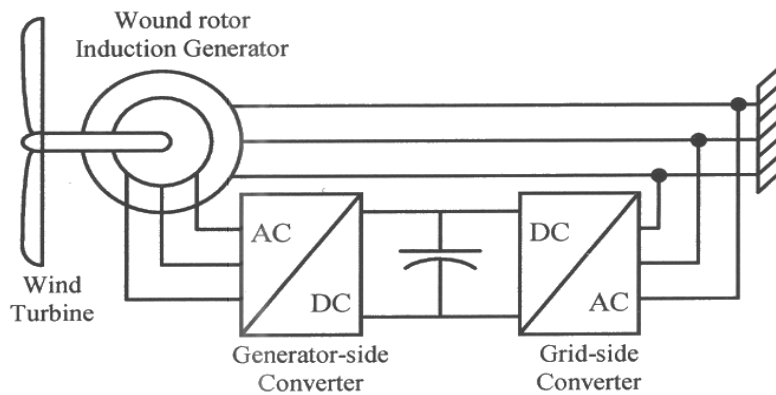


Figure 15-7 Doubly-fed induction generators for wind-electric systems.

### 15-4-2 Photovoltaic (PV) Systems

Photovoltaic systems are the ultimate in distributed generation and have even a greater potential than the wind-electric systems. In 1997, PV systems surpassed the 500 MW

threshold in worldwide installation, and annual global sales of \$1 billion. A few years back, the Clinton administration announced the ‘million solar roof initiative’, emphasizing the growing importance of PV systems.

In PV systems, the PV arrays (typically four of them connected in series) provide a voltage of 52-V to 90-V DC, which the power electronic system, as shown in Fig. 15-8, converts to 120V/60Hz sinusoidal voltage suitable for interfacing with the single-phase utility. PV modules are still very expensive, as much as \$1,500 for only a 300 W peak output. Such PV modules can be connected in parallel for higher output capacity. Presently there is not much economy of scale in the PV modules, making it prudent to invest in steps.

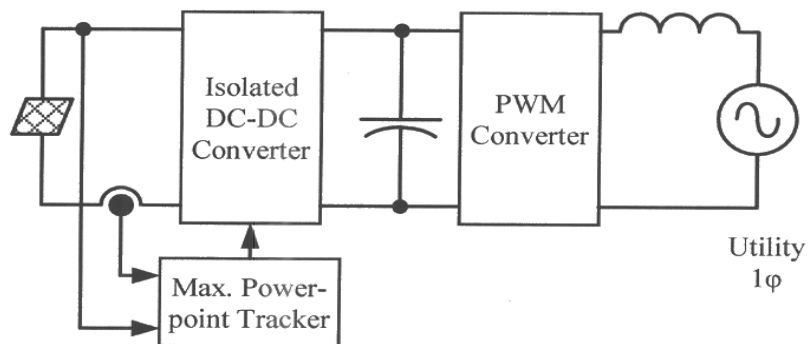


Figure 15-8 Photovoltaic systems.

### 15-4-3 Fuel Cell Systems

Lately, there has been a great deal of interest in, and effort being devoted to fuel cell systems. The reason has to do with their efficiency, which can be as high as 60 percent. The input to the fuel cell can be natural gas or gasoline and the output is a dc voltage. The need for power electronics converters to interface with the utility is the same in the fuel-cell systems as that for the photovoltaic systems.

### 15-4-4 Micro-Turbines

These use highly efficient aircraft engines, for example to produce peak power when it is needed, with the natural gas as the input fuel. To improve efficiency, the turbine speed should be allowed to vary based on loading. This will cause the frequency of the generated output to vary, requiring a power-electronic interface as that in adjustable-speed drives.

### 15-4-5 Energy Storage Systems

Although not a primary source of energy, storage plants offer the benefit of load-leveling and peak-shaving in power systems, because of the diurnal nature of electricity usage. Energy is stored, usually at night when the load demand is low, and supplied back during the peak-load periods. It is possible to store energy in lead-acid batteries (other exotic

high-temperature batteries are being developed), in Super-conducting Magnetic Energy Storage (SMES) coils and in the inertia of flywheels. All these systems need power electronics interface, where the interface for the flywheel storage is shown in Fig. 15-9.

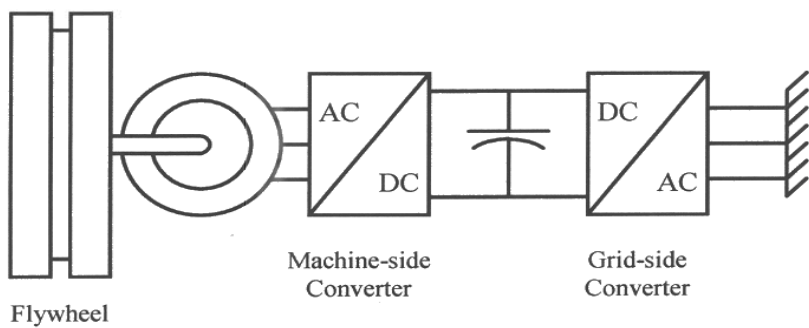


Figure 15-9 Flywheel storage system.

## 15-5 POWER ELECTRONIC LOADS

As discussed in Chapter 1, power electronics is playing a significant role in energy conservation, for example, as users discover the benefits of reduced energy consumption and better process control by operating electric drives at adjustable speeds. An adjustable-speed drive (ASD) is shown in Fig. 15-10 in a block diagram form. Power electronic loads of this type often use an interface with the utility that results in distorted line currents. These currents result in distorted voltage waveforms, affecting the neighboring loads. However, it is possible to design the utility interface (often called the power-factor-corrected front-end) that allows sinusoidal currents to be drawn from the grid. With the proliferation of power electronics loads, standards are being enforced that limit the amount of distortion in currents drawn.

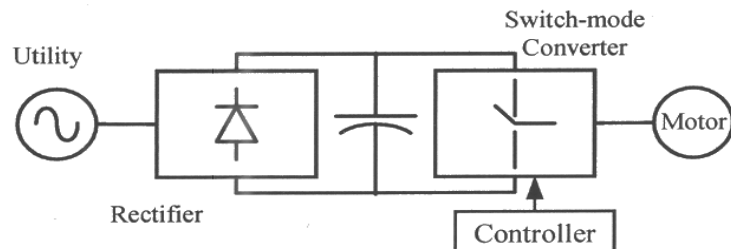


Figure 15-10 Adjustable-speed drive.

## 15-6 POWER QUALITY SOLUTIONS

Poor quality of power can imply any of the following: distorted voltage waveforms, unbalances, swells and sags in voltage and power outages, etc. This problem is exacerbated in a deregulated environment where utilities are forced to operate at marginal profits, resulting in inadequate maintenance of equipment. In this section, we will also see that power electronics can solve many of the power quality problems.

### 15-6-1 Dual Feeders

The continuity of service can be enhanced by dual power feeders to the load, where one acts as a backup to the other that is supplying the load as shown in Fig. 15-11. Using back-to-back connected thyristors, acting as a solid-state switch, it is possible to switch the load quickly, without interruption, from the main feeder to the backup feeder and back.

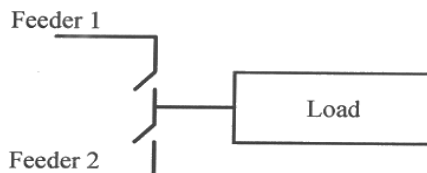


Figure 15-11 Dual-feeders.

### 15-6-2 Uninterruptible Power Supplies

Power outages, even for a few cycles, can be very disruptive to critical loads. To provide immunity from such outages, power-electronics-based uninterruptible power supplies (UPS) shown in Fig. 15-12 can be used, where the energy storage can be by means of batteries, SMES, flywheels or super-capacitors.

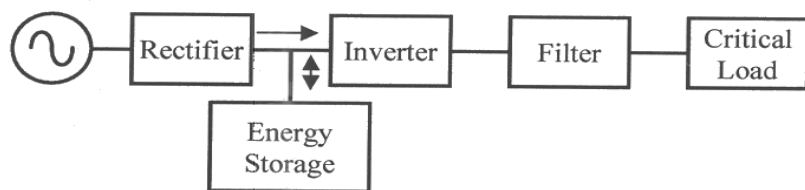


Figure 15-12 Uninterruptible power supplies.

### 15-6-3 Dynamic Voltage Restorers

Dynamic Voltage Restorers (DVR), shown in Fig. 15-13, can compensate for voltage sags or swells by injecting a voltage  $v_{inj}$  in series with that supplied by the utility.

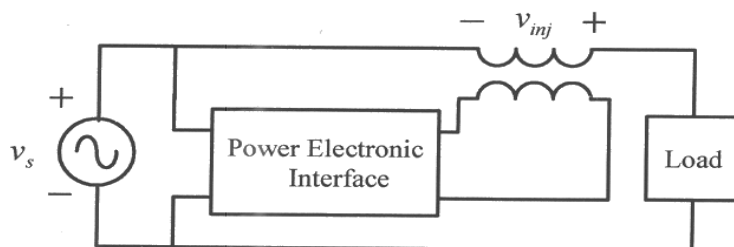


Figure 15-13 Dynamic voltage restorers.

## 15-7 TRANSMISSION AND DISTRIBUTION (T&D) APPLICATIONS

In the past, utilities operated as monopolies, where users had little or no option in selecting whom they can purchase power from. The recent trend, which seems

irreversible in spite of recent setbacks, is to deregulate where utilities must compete to sell power on an open market and the customers have a choice of selecting their power provider. In such an environment, utilities that were vertically integrated are now forced to split into generation companies that produce power, and transmission-line operators that maintain the transmission and distribution network for a fee.

In this deregulated environment, it is highly desirable to have the capability to dictate the flow of power on designated power lines, avoiding overloading of transmission lines and excessive power losses in them. In this section, we will look at some such options.

### 15-7-1 High Voltage DC (HVDC) and Medium Voltage DC (MVDC) Transmission

Direct current (DC) transmission represents the ultimate in flexibility, isolating two interconnected ac systems from the requirement of operating in synchronism or even at the same frequency. High voltage DC (HVDC) systems using thyristor-based converters have now been in operation for several decades. Lately, such systems at medium voltages have been proposed. Both of these types of systems are discussed below.

#### 15-7-1-1 High Voltage DC (HVDC) Transmission

Fig. 15-14 shows the block diagram of a HVDC transmission system, where power is transmitted over dc lines at high voltages in excess of 500 kV. First, the voltages in ac system 1 at the sending end are stepped up by means of a transformer. These voltages are rectified into dc by means of a thyristor-based converter, where the ac line voltages provide the commutation of current within the converter, such that ac currents drawn from system 1 turn into dc current on the other side of the converter. These currents are transmitted over the dc line where additional series inductance is added to ensure that the dc current is smooth, free of ripple as much as possible. At the receiving end, there are thyristor-based converters, which convert the dc current into ac currents and injects them into the ac system 2, through a step-down transformer. The roles of the sending and the receiving ends can be reversed by reversing the voltage polarity in the dc system.

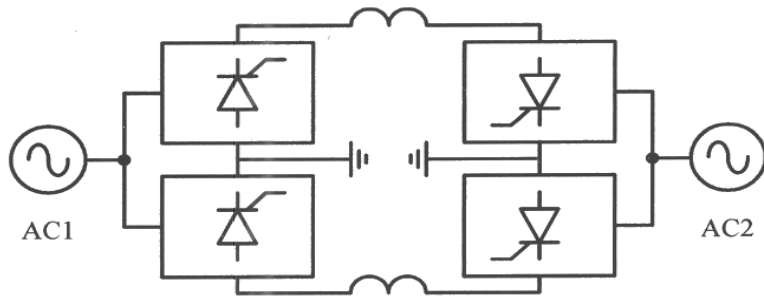


Figure 15-14 HVDC system block diagram (transformers are not shown).

At very high power levels in excess of 1,000 MW, use of thyristors, at least for now, represents the only reasonable choice.

## 15-7-1-2 Medium Voltage DC (MVDC) Transmission

At lower power levels, there are proposals to use medium voltages, in which case the block diagram of the system is as shown in Fig. 15-15. In such a system, the direction of power flow is reversed by changing the direction of current in the dc line.

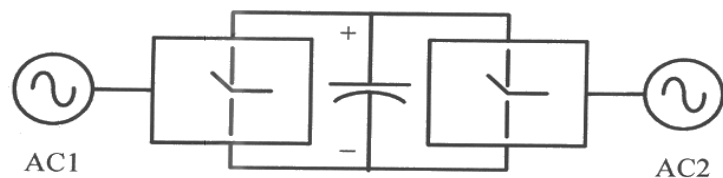


Figure 15-15 Block diagram for medium-voltage dc transmission systems.

## 15-7-2 Flexible AC Transmission Systems (FACTS) [2]

DC transmission systems discussed earlier are an excellent choice where large amount of power needs to be transmitted over long distances, or if the system stability is a serious issue. In existing ac transmission networks, limitation on constructing new power lines and their cost has led to other ways to increase power transmission capability without sacrificing the stability margin. These techniques may also help in directing the power flow to designated lines.

Power flow on a transmission line connecting two ac systems in Fig. 15-16 is given as

$$P = \frac{E_1 E_2}{X} \sin \delta \quad (15-1)$$

where  $E_1$  and  $E_2$  are the magnitudes of voltages at the two ends of the transmission line,  $X$  is the line reactance and  $\delta$  is the angle between the two bus voltages.

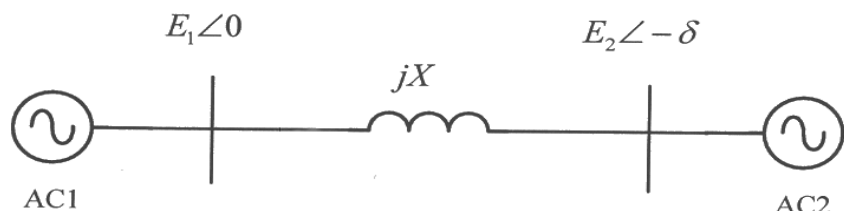


Figure 15-16 Power flow on a transmission line.

Eq. 15-1 shows that the power flow on a transmission line depends on three quantities: (1) the voltage magnitude  $E$ , (2) the line reactance  $X$ , and (3) the power angle  $\delta$ . Various devices which are based on rapidly controlling one or more of the above three quantities are discussed in the following sections:

### 15-7-2-1 Shunt-Connected Devices to Control the Bus Voltage Magnitude $E$

The reactive power compensation is very important and may even be necessary at high loadings to avoid voltage collapse. Shunt-connected devices can draw or supply reactive power from a bus, thus controlling the bus voltage, albeit in a limited range, based on the internal system reactance. Various forms of such devices are being used in different combinations. These include Thyristor-Controlled Reactors (TCR) shown in Fig. 15-17a, and Thyristor-Switched Capacitors (TSC) shown in Fig. 15-17b for Static Var Compensation (SVC). The advanced Static Var Compensator (STATCOM) shown in Fig. 15-17c can draw or supply reactive power.

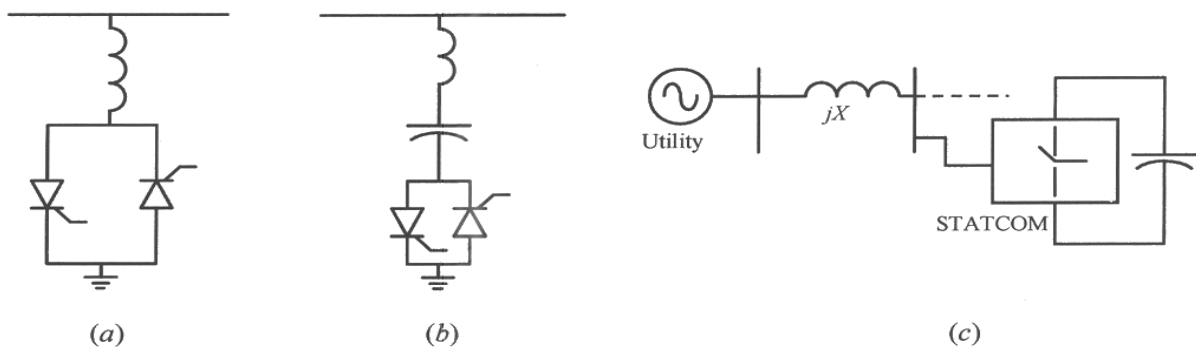


Figure 15-17 Shunt-connected devices for voltage control.

Shunt-compensation devices have the following limitations for controlling the flow of active power:

1. A large amount of reactive power compensation, depending on the system internal reactance, may be required to change the voltage magnitude. Of course, the voltage can only be changed in a limited range (utilities try to maintain bus voltages at their nominal values), which has a limited effect on the power transfer given by Eq. 15-1.
2. Most transmission systems consist of parallel paths or loops. Therefore, changing the voltage magnitude at a given bus changes the loading of all the lines connected to that bus, and there is no way to dictate the desired change of power flow on a given line.

### 15-7-2-2 Series-Connected Devices to Control the Effective Series Reactance $X$

These devices, connected in series with a transmission line, partially neutralize (or add to) the transmission line reactance. Therefore, they change the effective value of  $X$  in Eq. 15-1, thus allowing the active power flow  $P$  to be controlled. Various forms of such devices have been used. These include the Thyristor-Controlled Series Capacitor (TCSC) shown in Fig. 15-18.

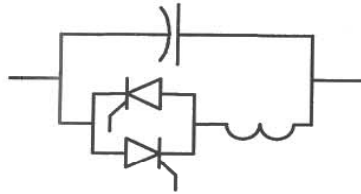


Figure 15-18 Thyristor-controlled series capacitor.

### 15-7-2-3 Static Phase Angle Control and Unified Power Flow Controller (UPFC)

Based on Eq. 15-1, a device connected at a bus in a substation, as shown in Fig. 15-19a, can influence power flow in three ways by:

1. controlling the voltage magnitude  $E$
2. changing the line reactance  $X$ , and/or
3. changing the power angle  $\delta$ .

Such a device called the Unified Power Flow Controller (UPFC) can affect power flow in any combination of the ways listed above. The block diagram of a UPFC is shown in Fig. 15-19a at one side of the transmission line. It consists of two voltage-source switch-mode converters. The first converter injects a voltage  $\bar{E}_3$  in series with the phase voltage such that

$$\bar{E}_1 + \bar{E}_3 = \bar{E}_2 \quad (15-2)$$

Therefore, by controlling the magnitude and the phase of the injected voltage  $\bar{E}_3$  within the circle shown in Fig. 15-19b, the magnitude and the phase of the bus voltage  $\bar{E}_2$  can be controlled. If a component of the injected voltage  $\bar{E}_3$  is made to be 90 degrees out-of-phase, for example leading with respect to the current phasor  $\bar{I}$ , then the transmission line reactance  $X$  is partially compensated.

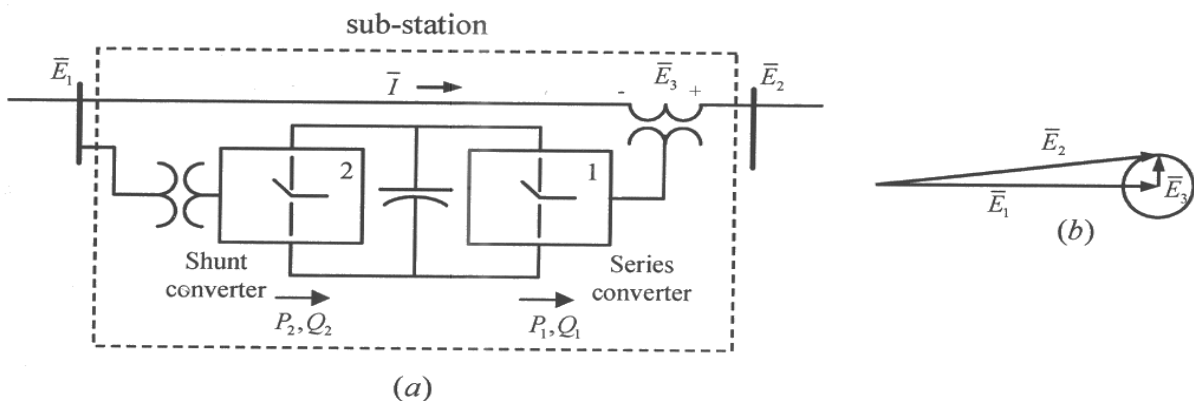


Figure 15-19 UPFC.

The second converter in a UPFC is needed for the following reason: since converter 1 injects a series voltage  $\bar{E}_3$ , it delivers real power  $P_1$ , and the reactive power  $Q_1$  to the transmission line (where  $P_1$  and  $Q_1$  can be either positive or negative):

$$P_1 = 3 \operatorname{Re}(\bar{E}_3 \bar{I}^*) \quad (15-3)$$

$$Q_1 = 3 \operatorname{Im}(\bar{E}_3 \bar{I}^*) \quad (15-4)$$

Since there is no steady state energy storage capability within UPFC, the power  $P_2$  into converter 2 must equal  $P_1$  if the losses are ignored:

$$P_2 = P_1 \quad (15-5)$$

However, the reactive power  $Q_2$  bears no relation to  $Q_1$ , and can be independently controlled within the voltage and current ratings of the converter 2:

$$Q_2 \neq Q_1 \quad (15-6)$$

By controlling  $Q_2$  to control the magnitude of the bus voltage  $\bar{E}_1$ , UPFC provides the same functionality as that of an advanced static var compensator STATCOM.

## REFERENCES

1. N. Mohan, T. M. Undeland, and W.P. Robbins, *Power Electronics: Converters, Applications and Design*, 3<sup>rd</sup> Edition, Wiley & Sons, New York, 2003.
2. N. G. Hingorani, and L. Gyugyi, *Understanding FACTS*, New York, IEEE Press, 2000.
3. N. Mohan, A. Jain, P. Jose and R. Ayyanar, "Teaching Utility Applications of Power Electronics in a First Course on Power Systems," submitted to the IEEE Transactions on Power Systems, Special Section on Power Engineering Education, 2003.

## PROBLEMS

- 15-1 Show the details and the average representation of converters in Fig. 15-7 for a wind-electric system.
- 15-2 Show the details and the average representation of converters in Fig. 15-8 for a photovoltaic system.
- 15-3 Show the details and the average representation of converters in Fig. 15-9 for a flywheel storage system.
- 15-4 Show the details and the average representation of converters in Fig. 15-10 for an adjustable-speed drive.
- 15-5 Show the details and the average representation of converters in Fig. 15-12 for a UPS.

- 15-6 Show the details and the average representation of converters in Fig. 15-13 for a DVR.
- 15-7 Show the details and the average representation of converters in Fig. 15-14 for an HVDC transmission system.
- 15-8 Show the details and the average representation of converters in Fig. 15-15 for an MVDC transmission system.
- 15-9 Show the details and the average representation of converter in Fig. 15-17c for a STATCOM.
- 15-10 Show the details and the average representation of converters in Fig. 15-19a for a UPFC system.

---

# DETAILED CHAPTER CONTENTS

---

## Chapter 1

### Power Electronics and Drives:

#### Enabling Technologies

- 1-1 Introduction to Power Electronics and Drives, 1-1
- 1-2 Applications and the Role of Power Electronics and Drives, 1-1
  - 1-2-1 Powering the Information Technology, 1-1
  - 1-2-2 Robotics and Flexible Production, 1-2
- 1-3 Energy and the Environment, 1-4
  - 1-3-1 Energy Conservation, 1-4
    - 1-3-1-1 Electric-Motor Driven Systems, 1-4
    - 1-3-1-2 Lighting, 1-5
    - 1-3-1-3 Transportation, 1-5
  - 1-3-2 Renewable Energy, 1-6
  - 1-3-3 Utility Applications of Power Electronics, 1-7
  - 1-3-4 Strategic Space and Defense Applications, 1-7
- 1-4 Need for High Efficiency and High Power Density, 1-8
- 1-5 Structure of Power Electronics Interface, 1-9
- 1-6 Switch-Mode Load-Side Converter, 1-10
  - 1-6-1 Switch-Mode Conversion: Switching Power-Pole as the Building Block, 1-11
  - 1-6-2 Pulse-Width Modulation (PWM) of the Switching Power-Pole (Constant  $f_s$ ), 1-12

1-6-3 Switching Power-Pole in A Buck DC-DC Converter: An Example, 1-13

1-7 Recent and Potential Advancements, 1-14

References, 1-15

Problems, 1-16

## Chapter 2

### Design of Switching Power-Poles

- 2-1 Power Transistors and Power Diodes, 2-1
- 2-2 Selection of Power Transistors, 2-1
  - 2-2-1 MOSFETs, 2-2
  - 2-2-2 IGBTs, 2-3
  - 2-2-3 Power-Integrated Modules and Intelligent-Power Modules, 2-4
- 2-2-4 Costs of MOSFETs and IGBTs, 2-4
- 2-3 Selection of Power Diodes, 2-4
- 2-4 Switching Characteristics and Power Losses in Power-Poles, 2-5
  - 2-4-1 Turn-on Characteristic, 2-6
  - 2-4-2 Turn-off Characteristic, 2-7
  - 2-4-3 Calculating Power Losses within the MOSFET (assuming an ideal diode), 2-8
    - 2-4-3-1 Conduction Loss, 2-8
    - 2-4-3-2 Switching Losses, 2-9
  - 2-4-4 Gate Driver Integrated Circuits (ICs) with built-In Fault Protection, 2-10
- 2-5 Justifying Switches and Diodes as Ideal, 2-11
- 2-6 Design Considerations, 2-11

2-6-1	Switching Frequency $f_s$ , 2-11
2-6-2	Selection of Transistors and Diodes, 2-12
2-6-3	Magnetic Components, 2-12
2-6-4	Capacitor Selection, 2-12
2-6-5	Thermal Design, 2-12
2-6-6	Design Tradeoffs, 2-14
2-7	The PWM Controller IC, 2-14
	References, 2-15
	Problems, 2-15
APPENDIX 2A	Diode Reverse Recovery and Power Losses, 2-16
2A-1	Diode Forward Loss, 2-16
2A-2	Diode Reverse Recovery Characteristic, 2-16
2A-3	Diode Switching Losses, 2-17

**Chapter 3**

**Switch-Mode DC-DC Converters:  
Switching Analysis, Topology  
Selection and Design**

3-1	DC-DC Converters, 3-1
3-2	Switching Power-Pole in DC Steady State, 3-1
3-3	Simplifying Assumptions, 3-4
3-4	Common Operating Principles, 3-4
3-5	Buck Converter Switching Analysis in DC Steady State, 3-4
3-6	Boost Converter Switching Analysis in DC Steady State, 3-7
3-7	Buck-Boost Converter Analysis in DC Steady State, 3-10
3-7-1	Other Buck-Boost Topologies, 3- 13
3-7-1-2	Cuk Converter, 3-14
3-8	Topology Selection [2], 3-15

3-9	Worst-Case Design, 3-16
3-10	Synchronous-Rectified Buck Converter for Very Low Output Voltages [3], 3-16
3-11	Interleaving of Converters [4], 3- 17
3-12	Regulation of DC-DC Converters by PWM, 3-17
3-13	Dynamic Average Representation of Converters in CCM, 3-18
3-14	Bi-Directional Switching Power- Pole, 3-21
3-15	Discontinuous-Conduction Mode (DCM), 3-22
	References, 3-24
	Problems, 3-24
	Appendix, 3-24
3A	Discontinuous-Conduction Mode (DCM) in DC-DC Converters, 3-24
3A-1	Output Voltages in DCM, 3-24
3A-1-1	Buck Converters in DCM, 3-24
3A-1-2	Boost and Buck-Boost Converters in DCM, 3-25
3A-2	Average Representation of DC- DC Converters in DCM, 3-26
3A-2-1	$v_k$ and $i_k$ for Buck and Buck- Boost Converters in DCM, 3-26
3A-2-2	$v_k$ and $i_k$ for Boost Converters in DCM, 3-28

**Chapter 4**

**Designing Feedback Controllers in  
Switch-Mode DC Power Supplies**

4-1	Introduction and Objectives of Feedback Control, 4-1
4-2	Review of Linear Control Theory, 4-2

- 4-2-1 Open-Loop Transfer Function  $G_L(s)$ , 4-3
- 4-2-2 Crossover Frequency  $f_c(s)$  of  $G_L(s)$ , 4-3
- 4-2-3 Phase and Gain Margins, 4-3
- 4-3 Linearization of Various Transfer Function Blocks, 4-5
  - 4-3-1 Linearizing the PWM Controller IC, 4-5
  - 4-3-2 Linearizing the Power Stage of DC-DC Converters in CCM, 4-6
  - 4-3-2-1 Using Computer Simulation to Obtain  $\tilde{v}_o / \tilde{d}$ , 4-9
- 4-4 Feedback Controller Design in Voltage-Mode Control, 4-11
- 4-5 Peak-Current Mode Control, 4-15
- References, 4-20
- Problems, 4-20

## Chapter 5

### Rectification of Utility Input Using Diode Rectifiers

- 5-1 Introduction, 5-1
- 5-2 Distortion and Power Factor, 5-1
  - 5-2-1 Rms Value of Distorted Current and the Total Harmonic Distortion (THD), 5-2
  - 5-2-2 The Displacement Power Factor (DPF) and Power Factor (PF), 5-5
  - 5-2-3 Deleterious Effects of Harmonic Distortion and a Poor Power Factor, 5-7
  - 5-2-3-1 Harmonic Guidelines, 5-7
- 5-3 Classifying the “Front-End” Of Power Electronic Systems, 5-9

- 5-4 Diode-Rectifier Bridge “Front-Ends”, 5-10
  - 5-4-1 The Single-Phase Diode-Rectifier Bridge, 5-13
    - 5-4-1-1 Effects of  $L_s$  and  $C_d$  on the Waveforms and the THD, 5-11
  - 5-4-2 Three-Phase Diode-Rectifier Bridge, 5-13
  - 5-4-3 Comparison of Single-Phase and Three-Phase Rectifiers, 5-15
- 5-5 Means to Avoid Transient Inrush Currents at Starting, 5-16
- 5-6 Front-Ends with Bi-Directional Power Flow, 5-16
- References, 5-16
- Problems, 5-16

## Chapter 6

### Power-Factor-Correction (PFC) Circuits and Designing the Feedback Controller

- 6-1 Introduction, 6-1
- 6-2 Operating Principle of Single-Phase PFCs, 6-1
- 6-3 Control of PFCs, 6-3
- 6-4 Designing the Inner Average-Current-Control Loop, 6-4
  - 6-4-1  $\tilde{d}(s) / \tilde{v}_c(s)$  for the PWM Controller, 6-5
  - 6-4-2  $\tilde{i}_L(s) / \tilde{d}(s)$  for the Boost Converter in the Power Stage, 6-5
  - 6-4-3 Designing the Current Controller  $G_i(s)$ , 6-5
- 6-5 Designing the Outer Voltage Loop, 6-6
- 6-6 Example of Single-Phase PFC Systems, 6-8

- 6-6-1 Design of the Current Loop, 6-8
- 6-6-2 Design of the Voltage Loop, 6-8
- 6-7 Simulation Results, 6-9
- 6-8 Feedforward of the Input Voltage, 6-9
- References, 6-10
- Problems, 6-11

## Chapter 7

### Magnetic Circuit Concepts

- 7-1 Ampere-Turns and Flux, 7-1
- 7-2 Inductance  $L$ , 7-2
- 7-2-1 Energy Storage due to Magnetic Fields, 7-3
- 7-3 Faraday's Law: Induced Voltage in a Coil due to Time-Rate of Change of Flux Linkage, 7-4
- 7-4 Leakage and Magnetizing Inductances, 7-5
- 7-4-1 Mutual Inductances, 7-7
- 7-5 Transformers, 7-7
- References, 7-9
- Problems, 7-9

## Chapter 8

### Switch-Mode DC Power Supplies

- 8-1 Application of Switch-Mode DC Power Supplies, 8-1
- 8-2 Need for Electrical Isolation, 8-1
- 8-3 Classification of Transformer-Isolated DC-DC Converters, 8-2
- 8-4 Flyback Converters, 8-2
- 8-5 Forward Converters, 8-5
- 8-5-1 Two-Switch Forward Converters, 8-6
- 8-6 Full-Bridge Converters, 8-7
- 8-6-1 Half-Bridge and Push-Pull Converters, 8-10

- 8-7 Practical Considerations in Transformer-Isolated Switch-Mode Power Supplies, 8-11
- References, 8-11
- Problems, 8-11

## Chapter 9

### Design of High-Frequency Inductors and Transformers

- 9-1 Introduction, 9-1
- 9-2 Basics of Magnetic Design, 9-1
- 9-3 Inductor and Transformer Construction, 9-1
- 9-4 Area-Product Method, 9-2
- 9-4-1 Core Window Area  $A_{window}$ , 9-2
- 9-4-2 Core Cross-Sectional Area  $A_{core}$ , 9-3
- 9-4-3 Core Area-Product  $A_p (= A_{core} A_{window})$ , 9-4
- 9-4-4 Design Procedure Based On Area-Product  $A_p$ , 9-5
- 9-5 Design Example of An Inductor, 9-6
- 9-6 Design Example of A Transformer For A Forward Converter, 9-7
- References, 9-8
- Problems, 9-8

## Chapter 10

### Soft-Switching in DC-DC Converters and Converters for Induction Heating and Compact Fluorescent Lamps

- 10-1 Introduction, 10-1
- 10-2 Hard-Switching in Switching Power-Poles, 10-1
- 10-3 Soft-Switching in Switching Power-Poles, 10-1

- 10-3-1 Zero Voltage Switching (ZVS), 10-3
- 10-3-2 Synchronous Buck Converter with ZVS, 10-3
- 10-3-3 Phase-Shift Modulated (PSM) DC-DC Converter, 10-6
- 10-4 Inverters for Induction Heating and Compact Fluorescent Lamps, 10-7
- References, 10-7
- Problems, 10-7

## Chapter 11

### Electric Motor Drives

- 11-1 Introduction, 11-1
- 11-2 Mechanical System Requirements, 11-2
- 11-2-1 Electrical Analogy, 11-4
- 11-3 Introduction to Electric Machines and the Basic Principles of Operation, 11-4
- 11-3-1 Electromagnetic Force, 11-5
- 11-3-2 Induced Emf, 11-7
- 11-3-3 Basic Structure, 11-7
- 11-4 DC Motors, 11-8
- 11-4-1 Structure of DC Machines, 11-8
- 11-4-2 Operating Principles of DC Machines, 11-9
- 11-4-3 DC-Machine Equivalent Circuit, 11-10
- 11-4-4 Torque-Speed Characteristics, 11-11
- 11-5 Permanent-Magnet AC Machines, 11-12
- 11-5-1 The Basic Structure of Permanent-Magnet Ac Machines, 11-13
- 11-5-2 Principle of Operation, 11-13

- 11-5-3 Mechanical System of PMAC Drives, 11-15
- 11-5-4 PMAC Machine Equivalent Circuit, 11-15
- 11-5-5 PMAC Torque-Speed Characteristics, 11-16
- 11-5-6 The Controller and the Power-Processing Unit (PPU), 11-17
- 11-6 Induction Machines, 11-17
- 11-6-1 Structure of Induction Machines, 11-8
- 11-6-2 The Principles of Induction Motor Operation, 11-18
- 11-6-3 Per-Phase Equivalent Circuit of Induction Machines, 11-20
- References, 11-22
- Problems, 11-22

## Chapter 12

### Synthesis of DC and Low-Frequency

### Sinusoidal AC Voltages for Motor

### Drives and UPS

- 12-1 Introduction, 12-1
- 12-2 Switching Power-Pole as the Building Block, 12-2
- 12-2-1 Pulse-Width-Modulation (PWM) of the Bi-Directional Switching Power-Pole, 12-2
- 12-2-3 Harmonics in The PWM Waveforms  $v_A$  and  $i_{dA}$ , 12-5
- 12-3 DC-Motor Drives, 12-5
- 12-4 AC-Motor Drives, 12-9
- 12-4-1 Space Vector Pulse Width Modulation, 12-13
- 12-5 Voltage-Link Structure with Bi-Directional Power Flow, 12-13
- 12-6 Uninterruptible Power Supplies (UPS), 12-15

12-6-1 Single-Phase UPS, 12-16

References, 12-19

Problems, 12-19

## Chapter 13

### Designing Feedback Controllers for Motor Drives

13-1 Introduction, 13-1

13-2 Control Objectives, 13-1

13-3 Cascade Control Structure, 13-3

13-4 Steps in Designing the Feedback Controller, 13-4

13-5 System Representation for Small-Signal Analysis, 13-4

13-5-1 The Average Representation of the Power-Processing Unit (PPU), 13-4

13-5-2 Modeling of the DC Machine and the Mechanical Load, 13-6

13-6 Controller Design, 13-7

13-6-1 PI Controllers, 13-7

13-7 Example of A Controller Design, 13-8

13-7-1 The Design of the Torque (Current) Control Loop, 13-9

13-7-2 The Design of the Speed Loop, 13-11

13-7-3 The Design of the Position Control Loop, 13-13

References, 13-14

Problems, 13-14

## Chapter 14

### Thyristor Converters

14-1 Introduction, 14-1

14-2 Thyristors (SCRs), 14-1

14-3 Single-Phase, Phase-Controlled Thyristor Converters, 14-2

14-3-1 The Effect of  $L_s$  on Current

Commutation, 14-5

14-4 Three-Phase, Full-Bridge Thyristor Converters, 14-6

14-5 Current-Link Systems, 14-8

Reference, 14-10

Problems, 14-10

## Chapter 15

### Utility Applications of Power Electronics

15-1 Introduction, 15-1

15-2 Power Semiconductor Devices and their Capabilities [1], 15-2

15-3 Categorizing Power Electronic Systems, 15-2

15-3-1 Solid-State Switches, 15-2

15-3-2 Converters as an Interface, 15-3

15-3-2-1 Voltage-Link Systems, 15-3

15-3-2-2 Current-Link Systems, 15-4

15-4 Distributed Generation (DG) Applications, 15-4

15-4-1 Wind-Electric Systems, 15-5

15-4-2 Photovoltaic (PV) Systems, 15-6

15-4-3 Fuel Cell Systems, 15-6

15-4-4 Micro-Turbines, 15-6

15-4-5 Energy Storage Systems, 15-6

15-5 Power Electronic Loads, 15-7

15-6 Power Quality Solutions, 15-8

15-6-1 Dual Feeders, 15-8

15-6-2 Uninterruptible Power Supplies, 15-8

15-6-3 Dynamic Voltage Restorers, 15-8

15-7 Transmission and Distribution (T&D) Applications, 15-9

- 15-7-1 High Voltage DC (HVDC) And Medium Voltage DC (MVDC) Transmission, 15-9
  - 15-7-1-1 High Voltage DC (HVDC) Transmission, 15-9
  - 15-7-1-2 Medium Voltage DC (MVDC) Transmission, 15-10
- 15-7-2 Flexible AC Transmission Systems (Facts), 15-10
  - 15-7-2-1 Shunt-Connected Devices to Control the Bus Voltage Magnitude  $E$  , 15-12

- 15-7-2-2 Series-Connected Devices to Control the Effective Series Reactance  $X$  , 15-12
- 15-7-2-3 Static Phase Angle Control and Unified Power Flow Controller (UPFC), 15-13
- References, 15-14
- Problems, 15-14